

The Roles of Ras in Controlling Cell Fate – A Yeast Model of Oncogenic Potential

Abstract:

The dynamic nature and diverse functionality of intracellular lipid droplets is associated with many cellular processes and signalling pathways, that collectively coordinate the maintenance of cellular health, adaptability, and survival. Lipid droplet regulation is intrinsically linked to the state of lipid metabolism within the intracellular environment, being essential in ensuring lipid levels in the cytosol are appropriately maintained, to prevent states of lipid starvation or lipotoxicity. The regulatory mediators of lipid droplet biogenesis and maintenance are poorly defined, alongside the full extent of interactions that are shared between lipid droplets and other organelles of the cell. The aims of this study were to investigate the link between the mitochondria and lipid droplets, specifically identifying how lipid droplet regulation was affected by the induction of mitochondrial dysfunction – by the loss of Cytochrome c oxidase (COX) function. The role of Ras2 and Yno1 signalling were also identified as points of interest to elicit the signalling pathways associated with lipid droplet regulation. Through the visualisation of cells using fluorescent microscopy and the additional analysis of the neutral lipid content of cells using flow cytometry, the levels of intracellular lipid droplets were assessed. Findings in this study suggest that mitochondrial dysfunction, induced by the loss of COX function, leads to lipid droplet dysregulation. Furthermore, Ras2 signalling appears to be essential in this regulation, promoting the increase in lipid droplets following exposure to the appropriate stimuli. Interestingly, the NADPH oxidase Yno1 also appears to have a role in the regulation of lipid droplets, while also interacting with Ras2 – thus suggesting that multiple layers of regulation, involving both Yno1 and Ras2 signalling, exist to appropriately regulate levels of intracellular lipid droplet. Detailing these intracellular signalling pathways that regulate lipid droplets is key in understanding the depth of functionality associated with lipid droplets in *S. cerevisiae*. Developing this understanding may help us to understand the pathophysiology of diseases associated with both mitochondrial dysfunction and lipid droplet dysregulation as well as providing new avenues to explore for the treatment of such condition.

**School of Bioscience
University of Kent**

**MSc Cell Biology
Research Project
(November 2021)**

Supervisor: Dr Campbell Gourlay

Word Count/Pages: 34,362/132



Declaration

There is no part of this thesis that has been submitted in support of an application for any degree or qualification at the University of Kent, or any other university or institute of learning.

Jamie Thomas

Acknowledgements

I would like to firstly thank my supervisor, Dr Campbell Gourlay, for providing the opportunity to undertake this project, alongside providing support and guidance throughout its completion. Secondly, I would like to thank the Gourlay Lab, particularly Jack Davis, who guided my research journey from day one, offering knowledge and moral support throughout. I would also like to collectively thank my friends and family for the moral support they provided throughout this year. Finally, I would like to thank the University of Kent for providing the facilities and equipment that have allowed me to complete this project.

Jamie T

Table of Contents

	Declaration	2
	Acknowledgements	3
	Figures	6
	Abbreviations	8
	Abstract	9
1.0	Chapter 1: Introduction	
1.1	<i>S. cerevisiae</i> as a Model Organism	11
1.2	The Study of Mitochondria	12
1.2.1	Mitochondrial Structure	13
1.2.2	<i>S. cerevisiae</i> Mitochondria	15
1.2.3	Mitochondrial Function	18
1.2.4	Intracellular ROS Production	22
1.2.5	Free Radical Theory of Aging (FRTA)	25
1.2.6	Ras Dependent ROS Production via YNO1 NADPH Oxidase	26
1.3	Ras Superfamily	28
1.3.1	Ras Structure and Expression	30
1.3.2	Ras Post-Translational Modifications	32
1.3.3	Ras Regulation	35
1.3.4	Ras Signalling Pathway Overview	37
1.4	Lipid Metabolism and Lipid Droplet Regulation	41
1.4.1	Lipid Droplet Structure	42
1.4.2	Lipid Droplet Formation	43
1.4.3	The Roles of Lipid Droplets	46
1.4.4	Lipid Droplet Regulation via Mitochondria and ER Interactions	48
1.5	Aims of Study	51
2.0	Chapter 2: Materials and Methods	
2.1	Yeast Strains and Growth Conditions	53
2.1.1	Water Used in Study	54
2.2	Biochemical Methods	55
2.2.1	Whole Cell Protein Extraction	55
2.2.2	Polyacrylamide Gel Electrophoresis	55
2.2.3	Semi-Dry Transfer of Protein to a PVDF Membrane	56
2.2.4	Immunoblotting	57
2.2.5	Enhanced Chemiluminescence (ECL) Detection	58
2.2.6	PVDF Membrane Stripping	59
2.3	Cell Biology Techniques	59
2.3.1	Yeast Strain Growth Assay	59
2.3.2	Cell Counting (Haemocytometer)	60
2.3.3	Colony Forming Unit (CFU) Viability Assay	61
2.4	Microscopy and Flow Cytometry	61

2.4.1	Sample Preparation	61
2.4.1.1	LD540 Staining	62
2.4.1.2	Bodipy 493/503 and Propidium Iodide (PI) Staining	62
2.4.2	Microscope Slide Preparation	63
2.4.3	Fluorescent Microscopy	63
2.4.4	Cell Diameter Measurement	64
2.4.5	Flow Cytometry	64
2.5	Statistical Analysis	64
3.0	Chapter 3: Results	
3.1.1	Part 1: Introduction	
3.1.2	Assessing the level of histone 4 (H4) acetylation within cells with partial or full loss of COX function.	67
3.1.3	Effects of KAc supplementation on growth of <i>S. cerevisiae</i> cells with impaired or loss of COX function.	69
3.1.4	Effects of KAc supplementation on the viability of <i>S. cerevisiae</i> cells with impaired or loss of COX function.	71
3.1.5	Conclusions	72
3.2.1	Part 2: Introduction	
3.2.2	Investigating the effect that increased levels of mitochondrial dysfunction have on the growth of <i>S. cerevisiae</i> cells, under standard growth conditions.	74
3.2.3	Investigating the effect that increased levels of mitochondrial dysfunction have on the viability of <i>S. cerevisiae</i> cells, under standard growth conditions.	76
3.2.4	Investigating the effects of partial and full loss of COX function on levels of intracellular lipid droplets.	77
3.2.5	Analysis of growth in WT and <i>ras2</i> mutants, under standard growth conditions.	80
3.2.6	Analysis of viability in WT and <i>ras2</i> mutants, under standard growth conditions.	82
3.2.7	Assessing level of intracellular Lipid Droplets in $\Delta ras2$ and <i>ras2-ala18, val19</i> cells.	83
3.2.8	Optimisation of Bodipy 493/503 Stain Lipid Droplet Staining.	86
3.2.9	Assessing level of Intracellular Lipid Droplets in $\Delta ras2$ and <i>ras2-ala18, val19</i> cells, following the addition of heat and oxidative stressors.	87
3.2.10	Investigating the effects of partial and full loss of COX function on levels of intracellular lipid droplets, following the addition of heat and oxidative stressors.	91
4.0	Chapter 4: Discussion	96
	Future Work	105

Figures

Figure 1: <i>Structure of the Mitochondria.</i>	14
Figure 2: <i>Schematic diagram of the ETC of the <i>S. cerevisiae</i> mitochondria.</i>	15
Figure 3: <i>Overview of mitochondrial protein import machinery.</i>	17
Figure 4: <i>Schematic diagram of the ETC of human mitochondria.</i>	18
Figure 5: <i>Chemical reaction that produces hydrogen peroxide within cells.</i>	22
Figure 6: <i>Impact of redox balance on cellular activity.</i>	23
Figure 7: <i>Hypothesised model detailing the intracellular signalling that leads to an increase in intracellular ROS following loss of COX function in the mitochondria.</i>	27
Figure 8: <i>Human Ras Superfamily.</i>	29
Figure 9: <i>Schematic diagram of prenylation, proteolysis and carboxyl methylation of Ras proteins.</i>	32
Figure 10: <i>Schematic diagram of the palmitoylation of Ras proteins.</i>	34
Figure 11: <i>Overview of the regulation of Ras activity.</i>	35
Figure 12: <i>Range of GEF, GAP and effectors associates with Ras signalling in humans.</i>	36
Figure 13: <i>Signalling pathway associated with <i>ras1/2</i> activation in <i>S. cerevisiae</i>.</i>	38
Figure 14: <i>Schematic diagram showing the signalling pathway generated following the activation of Ras proteins, via tyrosine kinase receptors, in humans.</i>	39
Figure 15: <i>Schematic diagram detailing the basic structure of lipid droplets.</i>	42
Figure 16: <i>Schematic diagram showing the process of lipid droplet biogenesis.</i>	43
Figure 17: <i>Schematic diagram showing the interactions between lipid droplet, the mitochondria, and the ER.</i>	50
Figure 18: <i>Western blot images showing the levels of H4 acetylation.</i>	67
Figure 19: <i>Graph showing the average fluorescent intensity of anti-H4 acetylation bands from western blots.</i>	68
Figure 20: <i>Growth analysis of <i>S. cerevisiae</i> cells, with and without the supplementation of KAc.</i>	70
Figure 21: <i>Graph showing the average number of CFU of <i>S. cerevisiae</i> cells, with and without the supplementation of KAc.</i>	71
Figure 22: <i>Growth analysis of <i>S. cerevisiae</i> cells.</i>	74
Figure 23: <i>Growth analysis of <i>S. cerevisiae</i> cell.</i>	75
Figure 24: <i>Graph showing the average number of CFU of <i>S. cerevisiae</i> cells.</i>	76
Figure 25: <i>Fluorescent microscopy images of <i>S. cerevisiae</i> cells, following staining with LD540.</i>	77
Figure 26: <i>Graph showing the average number of intracellular lipid droplets in <i>S. cerevisiae</i> cells.</i>	78
Figure 27: <i>Average Fluorescence intensity of stained intracellular neutral lipid in <i>S. cerevisiae</i> cells.</i>	79
Figure 28: <i>Growth analysis of <i>S. cerevisiae</i> cells.</i>	80

Figure 29: <i>Graph showing the average cell diameter of S. cerevisiae cells.</i>	81
Figure 30: <i>Graph showing the average number of CFU of S. cerevisiae cells.</i>	82
Figure 31: <i>Fluorescent microscopy images of S. cerevisiae cells, following staining with LD540.</i>	83
Figure 32: <i>Graph showing the average number of intracellular lipid droplets in S. cerevisiae cells.</i>	84
Figure 33: <i>Average Fluorescence intensity of stained intracellular neutral lipid in S. cerevisiae cells.</i>	85
Figure 34: <i>Histograms showing the fluorescent intensity of Bodipy 493/503 stained cells.</i>	86
Figure 35: <i>Graph showing the fluorescent intensity of the cells stained with Bodipy 493/503.</i>	87
Figure 36: <i>Fluorescent microscopy images of S. cerevisiae cells, following staining with Bodipy 493/503, following the introduction of heat and oxidative stressors.</i>	88
Figure 37: <i>Graph showing the average number of intracellular lipid droplets in S. cerevisiae cells, following the introduction of heat and oxidative stressors.</i>	89
Figure 38: <i>Average Fluorescence intensity of stained intracellular neutral lipid in S. cerevisiae cells, following the introduction of heat and oxidative stressors.</i>	90
Figure 39: <i>Fluorescent microscopy images of S. cerevisiae cells, following staining with Bodipy 493/503, following the introduction of heat and oxidative stressors.</i>	92
Figure 40: <i>Fluorescent microscopy images of S. cerevisiae cells, following staining with Bodipy 493/503, following the introduction of heat and oxidative stressors.</i>	92
Figure 41: <i>Graph showing the average number of intracellular lipid droplets in S. cerevisiae cells, following the introduction of heat and oxidative stressors.</i>	93
Figure 42: <i>Average Fluorescence intensity of stained intracellular neutral lipid in S. cerevisiae cells, following the introduction of heat and oxidative stressors.</i>	94
Figure 43: <i>Diagram detailing the sensors, signalling pathway components and effect induced by specific stressors.</i>	102

Abbreviations

<i>S. cerevisiae</i>	<i>Saccharomyces cerevisiae</i>
DNA	Deoxyribonucleic Acid
RNA	Ribonucleic Acid
mtDNA	Mitochondrial DNA
OM	Outer Membrane
IM	Inner Membrane
IMS	Intermembrane Space
PC	Phosphatidylcholine
PE	Phosphatidylethanolamine
PG	Phosphatidylglycerol
PS	Phosphatidylserine
PI	Phosphatidylinositol
PA	Phosphatidic Acid
CL	Cardiolipin
ETC	Electron Transport Chain
COX	Cytochrome C Oxidase
TCA	Tricarboxylic Acid
NAD	Nicotinamide Adenine Dinucleotide
FAD	Flavin Adenine Dinucleotide
ATP	Adenosine Triphosphate
ROS	Reactive Oxygen Species
SOD1	Super Oxide Dismutase 1
SOD2	Super Oxide Dismutase 2
FTRA	Free Radical Theory of Aging
MFTRA	Mitochondrial Free Radical Theory of Aging
ERAD	Endoplasmic Reticulum associated Degradation
GTP	Guanosine Triphosphate
GDP	Guanosine Diphosphate
RCE1	Ras Converting Enzyme 1
ICMT	Isoprenylcysteine Carboxyl Methylation
cAMP	cyclic Adenosine Monophosphate
PKA	Protein Kinase A
PTM	Post Translational Modifications
GEF	Guanine-nucleotide Exchange Factor
GAP	GTPase Activating Protein
LD	Lipid Droplets
DAG	Diacylglycerol
TAG	Triacylglycerol
SE	Sterol Esters
FA	Fatty Acids

Abstract

The dynamic nature and diverse functionality of intracellular lipid droplets is associated with many cellular processes and signalling pathways, that collectively coordinate the maintenance of cellular health, adaptability, and survival. Lipid droplet regulation is intrinsically linked to the state of lipid metabolism within the intracellular environment, being essential in ensuring lipid levels in the cytosol are appropriately maintained, to prevent states of lipid starvation or lipotoxicity. The regulatory mediators of lipid droplet biogenesis and maintenance are poorly defined, alongside the full extent of interactions that are shared between lipid droplets and other organelles of the cell. The aims of this study were to investigate the link between the mitochondria and lipid droplets, specifically identifying how lipid droplet regulation was affected by the induction of mitochondrial dysfunction – by the loss of Cytochrome c oxidase (COX) function. The role of Ras2 and Yno1 signalling were also identified as points of interest to elicit the signalling pathways associated with lipid droplet regulation. Through the visualisation of cells using fluorescent microscopy and the additional analysis of the neutral lipid content of cells using flow cytometry, the levels of intracellular lipid droplets were assessed. Findings in this study suggest that mitochondrial dysfunction, induced by the loss of COX function, leads to lipid droplet dysregulation. Furthermore, Ras2 signalling appears to be essential in this regulation, promoting the increase in lipid droplets following exposure to the appropriate stimuli. Interestingly, the NADPH oxidase Yno1 also appears to have a role in the regulation of lipid droplets, while also interacting with Ras2 – thus suggesting that multiple layers of regulation, involving both Yno1 and Ras2 signalling, exist to appropriately regulate levels of intracellular lipid droplet. Detailing these intracellular signalling pathways that regulate lipid droplets is key in understanding the depth of functionality associated with lipid droplets in *S. cerevisiae*. Developing this understanding may help us to understand the pathophysiology of diseases associated with both mitochondrial dysfunction and lipid droplet dysregulation as well as providing new avenues to explore for the treatment of such condition.

Chapter 1:
Introduction

1.1 *Saccharomyces cerevisiae* as a Model Organism

Eukaryotic organisms are frequently exploited, as model organisms, in numerous areas of research to further biological discoveries. Use of these organisms allow experimental and ethical constraints to be overcome, while still obtaining results that are significant in advancing research. For model organisms to be used effectively, the biological process being investigated must be well-characterised, the organism must be easy to manipulate experimentally, and a quantitative and qualitative metric should exist to compare the different organisms, to ensure findings are applicable. Commonly used eukaryotic model organisms include *Saccharomyces cerevisiae*, *Schizosaccharomyces pombe*, *Drosophila melanogaster* and *Caenorhabditis elegans* [1].

The unicellular eukaryote, *Saccharomyces cerevisiae* (*S. cerevisiae*), has been widely utilised as a model eukaryote to study conserved processes within higher eukaryotes. To date, *S. cerevisiae* has been fundamental in the investigation of processes associated with aging [2], regulation of gene expression [3][4], the cell cycle [5], metabolism [6][7], apoptosis [8], and human disease – 17% of yeast genes are identified as members of orthologous gene families associated with human disease, conversely, 30% of known genes associated with human disease have yeast orthologs [9][10]. The combination of a relatively short doubling time (1.25-2 hours at 30°C) and an ability to be manipulated genetically, in both haploid and diploid forms, makes this organism a desirable experimental system [1]. Genetic manipulation of *S. cerevisiae* is made possible by the extensive range of molecular tools available, including a fully sequenced genome, published in 1996 and updated in 2014 – revealing a genome size of 12,068 kilobases, comprising approximately 5885 protein encoding genes, 140 ribosomal RNA genes, 40 nuclear RNA genes and 275 transfer RNA genes [11][12]. Other resources include a comprehensive collection of open reading frame (ORF) deletion strains – including GFP-fused chimera proteins – and information related to all yeast genes via the *Saccharomyces* Genome Database (SGD) – (www.yeastgenome.org/)[13][14][15].

1.2 The Study of Mitochondria

Mitochondria are versatile and dynamic membrane-bound organelles that perform essential roles within numerous cellular processes, as well as acting as a component in a variety of intricate intracellular signalling pathways [16]. This diverse functionality places the mitochondria at the foundation of the cell's ability to adapt, maintain, and survive, within its local environment. For these reasons, it is understood that mitochondrial health is intrinsically linked with cellular health – which is further illustrated by the recurrent observation that when mitochondrial function is impaired or lost, there is a significant decline in cellular health. Although a considerable number of research studies have been focused on the mitochondria, the full extent of all its roles within the cell is still unknown, meaning the mitochondria remains a point of interest in many research studies to date. Furthermore, the underlying mechanisms associated with mitochondrial dysfunction remain relatively unknown. Developing a greater understanding of mitochondrial function/dysfunction may be beneficial in identifying the underlying pathologies of numerous chronic noncommunicable disease within higher eukaryotes, that have been linked to the state of mitochondrial health [17][18]. Diseases which are shown to afflict a variety of organs and tissues, while being accompanied by a high morbidity and mortality rate [19].

For over 60-years, *S. cerevisiae* has been used as a genetic system in the study of mitochondria, which has been aided by a well-characterised mitochondrial genome – that can be manipulated experimentally, tolerate loss of mitochondria DNA (mtDNA) and withstand mutations that induce loss of mitochondria function – alongside a well-characterised proteome [20][21]. Mass spectrometry analysis has identified ~850 proteins and an estimated 1000 distinct protein species within the yeast mitochondria, which was similarly described during the analysis of 14 different murine tissue samples in an independent study – indicating similarities in mitochondria composition across these eukaryotes, bridging the gap between lower and higher eukaryotes [22][23][24]. Notably, mammalian cells diverge from this showing ~1000 estimated proteins within their mitochondria – likely resulting from increased tissue diversity [25].

1.2.1 Mitochondrial Structure

To facilitate its extensive range of functions, the mitochondria possess a relatively complex structure (Figure 1). This structure consists of an outer membrane (OM) – that forms a barrier between the cytoplasm and the inner mitochondrial compartments, an inner membrane (IM) – that encases the mitochondrial matrix, and the intermembrane space (IMS) which is located between the OM and IM [26]. The IM and OM both contain a variety of lipids including phosphatidylcholine (PC), phosphatidylethanolamine (PE), phosphatidylglycerol (PG), phosphatidylserine (PS), phosphatidylinositol (PI), phosphatidic acid (PA) and cardiolipin (CL) – with PG and CL being exclusively found within mitochondrial membranes [27]. PC and PE are the most abundant phospholipids, contributing 40% and 30% of total mitochondrial phospholipids, respectively. While PA and PS contribute 5%, and CL makes up for approximately 15% of total mitochondrial phospholipids – low levels of sphingolipids and cholesterol are also present in the mitochondrial membranes [28][29]. Alongside these lipids, the mitochondrial membranes possess many proteins that are required for regulating transport and the rate of local biochemical reactions. Notably, the IM has a higher concentration of proteins, when compared to the OM, alongside a larger proportion of PI and CL [27].

In appearance, the IM is a highly folded, invaginated structure that gives rise to sub-structures, known as cristae. These structures increase the surface area of the membrane, allowing for more enzymatic and transport proteins to be present – increasing the capacity of metabolic activity hosted within the IMS and the matrix. Notably, a higher level of transport proteins required within the IM, to facilitate the efficient transport of molecules, due to the impermeable nature of the IM – only allowing the movement of small molecules (e.g., CO₂, H₂O and O₂) across the membrane [26][28]. By contrast, the OM is semi-permeable, allowing the movement of molecules like ions to move freely across the membrane, via porins. The OM continues to diverge from the IM by possessing a characteristically smooth structure that protects the organelle from the intracellular environment, while also facilitating interaction with other cellular components.

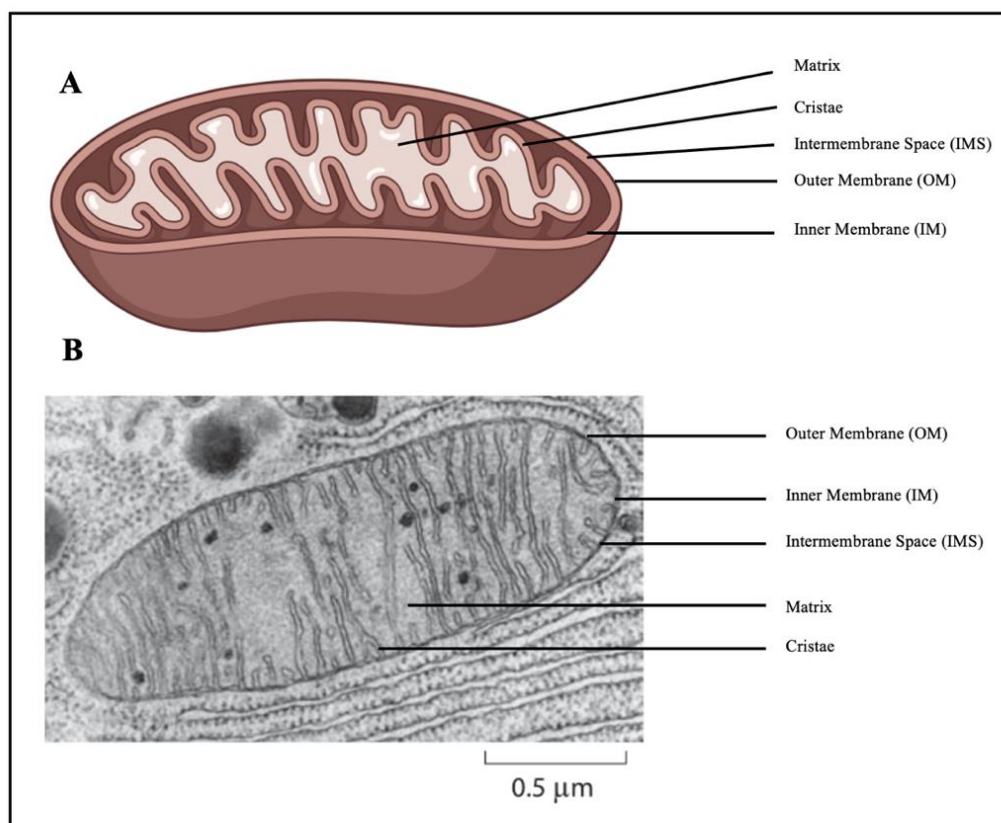


Figure 1: Structure of the mitochondria. (A) Labelled schematic diagram of the mitochondria. (B) Labelled scanning electron microscopy image of a mitochondria from the pancreas of a bat. Both the diagram and image highlight the major components of the mitochondria, including: the matrix, cristae, intermembrane space, intermembrane space, inner membrane, and the outer membrane – image taken from Fawett.D.E., et al 1966.

The morphology of the mitochondria is extremely dynamic, which is illustrated by the different morphological forms that the organelles can acquire. This is influenced by continuous mitochondria transport, fragmentation, fusion, and fission events, throughout the lifespan of a cell, in response to fluctuating changes of the intracellular environment [31]. The dynamic nature of the mitochondrial structure is beneficial as it directly influences the organelles' ability to function. This has been highlighted through experimental studies that showed that the reduction of mitochondrial fission protein activity leads to the formation of more elongated mitochondrial networks. This allowed cells to be more metabolically active than those with smaller, fragmented mitochondria – even when total mitochondria remain the same [32]. Alternatively, inhibition of mitochondrial fusion, increases mitochondrial fragmentation, which results in a reduction of both the rate of oxygen consumption and mitochondrial membrane potential [33]. This plasticity in morphology is therefore intrinsically linked with the mitochondria's metabolic capabilities and adaptability.

1.2.2 Mitochondria Genome and Proteome of *S. cerevisiae*

Sequencing of the mitochondrial genome of *S. cerevisiae*, in 1998, revealed a genome size of approximately 75,000 bases containing 35 genes – contributing to approximately 15% of cellular DNA content [21][34]. This differs considerably from the mitochondria genome of humans, which have been shown to contain 16,569 bases and 37 genes that in turn encode 2 rRNA, 22 tRNA and 13 proteins [35]. The major divergence in genomic content between human and yeast, apart from genes encoding the subunits for complex I – which in yeast is replaced by two types of NADH dehydrogenases (Figure 2) – is found in the ribosomal protein of the subunit Var1 and the Atp9 subunit of ATP synthase [20]. While the remaining mtDNA shows significant conservation between yeast and humans [20]. The size of the mtDNA is limited, which results in most genes that encode mitochondrial proteins being required to reside within the nucleus. Interestingly, experimental studies have shown that transfer of genes from the nucleus towards the mitochondria is very favourable, however the reason behind the lack of full genetic transfer is unknown [36][37].

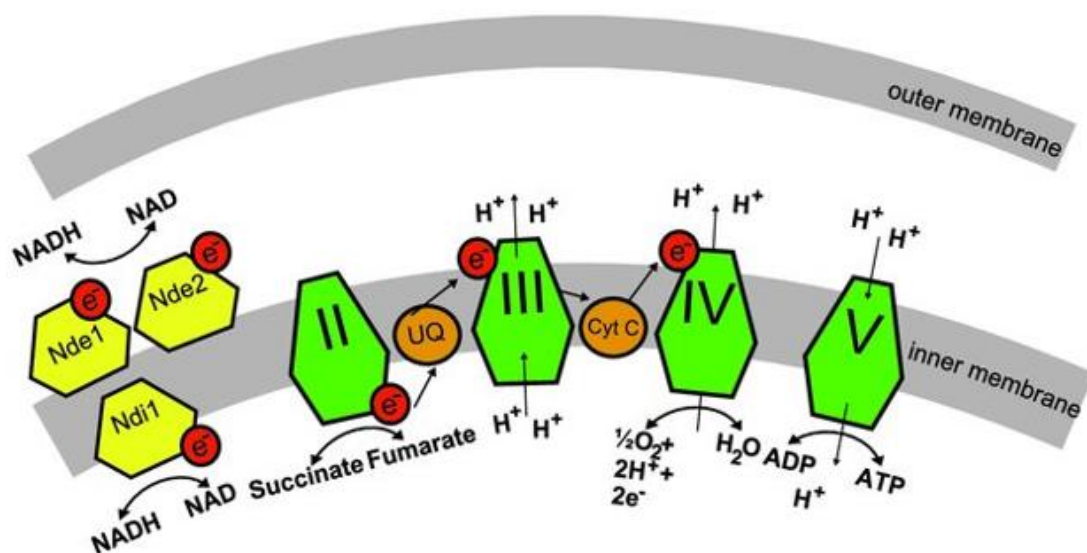


Figure 2: Schematic diagram of the electron transport chain (ETC) within the mitochondria of *S. cerevisiae*. The diagram highlights the presence of NADH dehydrogenase enzymes, that take the place of complex I typically seen in the mammalian mitochondria, alongside the remaining respiratory complexes of the ETC (II-V). The diagram also shows the movement of electron through the ETC, alongside the products of reactions within the ETC – Figure taken from Rintala.E. 2010.

Unlike the genome of the nucleus, the mitochondrial genome lacks protective histones and effective DNA repair machinery, alongside its replication being independent from the cell cycle, which makes the mtDNA more susceptible to mutations [38][39]. The mitochondrial genome contributes a range of proteins that typically take the form of subunits for mitochondria respiratory protein complexes and other proteins associated with transport and the metabolic activity of the mitochondria [40]. Regarding this proteome, recent advancements in technologies, including mass spectrometry, have aided the characterisation of proteins and their compartmental localisation. In 2003, the isolation and analysis of mitochondria of *S. cerevisiae* identified 749 unique proteins [41]. This was expanded on in 2006, identifying a further 102 proteins and then in 2017 a total of 1205 proteins were identified [42][43]. Of these proteins, 15% are thought to contribute directly to energy metabolism, highlighting the integral role the mitochondria have in energy homeostasis [40].

Although the mitochondria possess its own genetic machinery, that regulate transcription and translation of the mitochondria genome, only 8 proteins are synthesised within the mitochondria [44]. These proteins include the subunits of complex III (Cytb), complex IV (Cox1, Cox2, Cox3), complex V (Atp6, Atp8, Atp9) and a ribosomal subunit (Var1) [45]. In addition to the 8 proteins, the 35 genes of the mtDNA is responsible for encoding large and small rRNAs (Rnl and Rns), 24 tRNAs, and an RNA component of the mitochondrial RNase P (RnpB) [21][34]. The remaining 1197 proteins are encoded by the nuclear genome and synthesised by cytoplasmic ribosomes, before being imported into the mitochondria (Figure 3). Proteins synthesised within the cytoplasm, destined for the mitochondria, typically take the form of N-terminal cleavable extensions (pre-sequences), that consist of 15-18 amino acids and form positively charged amphipathic α -helices [46]. These pre-sequences are targeted to the mitochondria by targeting signals and then imported into the mitochondria via pre-sequence pathways, which utilise pores within receptors in the translocase of the inner membrane (TOM complexes) [47]. Further transport through the IMM is facilitated by pores within the receptors of the translocase of the inner membrane 23 (TIM23) – utilising the membrane potential of the IMM. Further translocation to the matrix is driven by the pre-sequence-associated motor (PAM), which utilises ATP-hydrolysis, via the Hsp70 subunit (Ssc1) [48][49]. Within the matrix the pre-sequences are cleaved by peptidases to

produce active proteins. Some of the cleaved pre sequence proteins retain targeting signal, which when translocated into the TIM23 pore, leads to the translocation, arrest and subsequent insertion of the protein into the IMM or release into the IMS. Alternatively, pathways for insertion into membranes involve the partial translation of the protein within the matrix, before being inserted into the membrane by OXA translocase/invertase complexes [50][51]. Other proteins without cleavable sequences can contain multiple targeting signals within the protein sequences that ensures the protein travels to the appropriate sub-mitochondrial compartment [20].

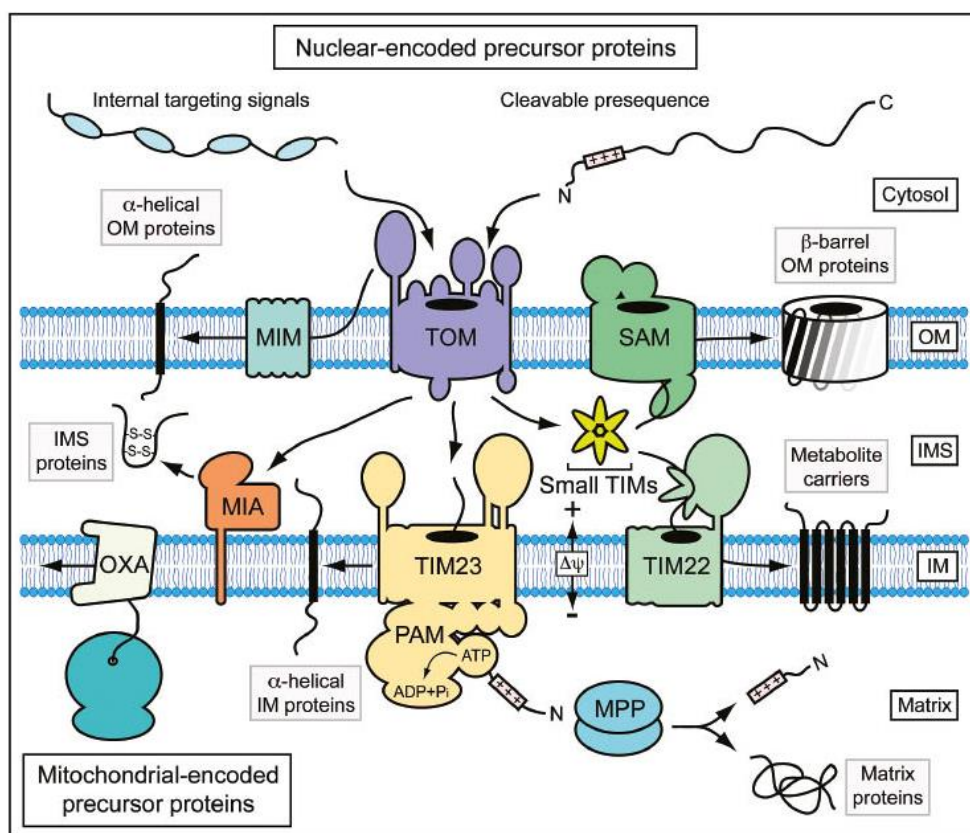


Figure 3: Overview of mitochondrial protein import machinery. The machinery ensures that proteins destined for the mitochondria localise in the necessary location to facilitate the proteins function. The large majority of mitochondrial proteins are synthesised in the cytosol and then imported into the outer membrane, by translocases. Further sorting of precursor proteins are then coordinated by mitochondrial machinery to ensure precursor proteins are delivered to the correct intramitochondrial compartment. The mitochondrial IMS import, and assembly (MIA) machinery facilitates protein import and oxidation by inserting disulphide bonds into the protein structure. Pre sequence translocation of the inner membrane (TIM23) are responsible for sorting proteins into the inner membrane or into the matrix, further aided by pre sequence translocase-associated motors (PAM). Mitochondrial processing peptidase (MPP) is responsible for cleaving the amino-terminal pre sequences, while small TIM chaperones in the IMS distribute β-barrel precursors to the sorting and assembly machinery (SAM) of the outer membrane and non-cleavable precursors of multi-spanning inner membrane proteins to the carrier translocase of the IM (TIM22). Protein translocation by TIM23 and TIM22 are driven by membrane potential. Notably, some α-helical outer membrane proteins can be directed inserted into the outer membrane by mitochondrial import (MIM) complexes. The remaining oxidase assembly (OXA) translocase are responsible for exporting mitochondrial-encoded proteins into the IM – Figure taken from Strub.S.P., Stiller.S.B. 2016.

1.2.3 Mitochondria Function

The mitochondria have a range of complex and intricate roles within cells centred around many different cellular processes and signalling pathways. This myriad of functions attributed to the mitochondria, include the generation of chemical energy in the form of 5'-adenosine triphosphate (ATP), synthesis of amino acids [52], synthesis of lipids and steroids [53], regulation of calcium compartmentalisation [54], cell redox homeostasis [55] and the synthesis of iron-sulphur clusters and haem [56]. Partaking in these functions, and therefore being an integral component in the supply of various biological molecules, further solidifies the essential role that the mitochondria have with regards to the adaptability, maintenance, and survival of cells.

Energy requirements in cells fluctuate throughout an organism's lifespan. With the main form of chemical energy being ATP, and with the mitochondria being the major source of ATP within the cell, the mitochondria are at the forefront of coordinating and maintaining energy metabolism and homeostasis. The production of chemical energy, via aerobic respiration, is the dominant role of the mitochondria, a process that couples the oxidation of carbohydrate fuel sources (e.g., glucose) with the generation of ATP [57].

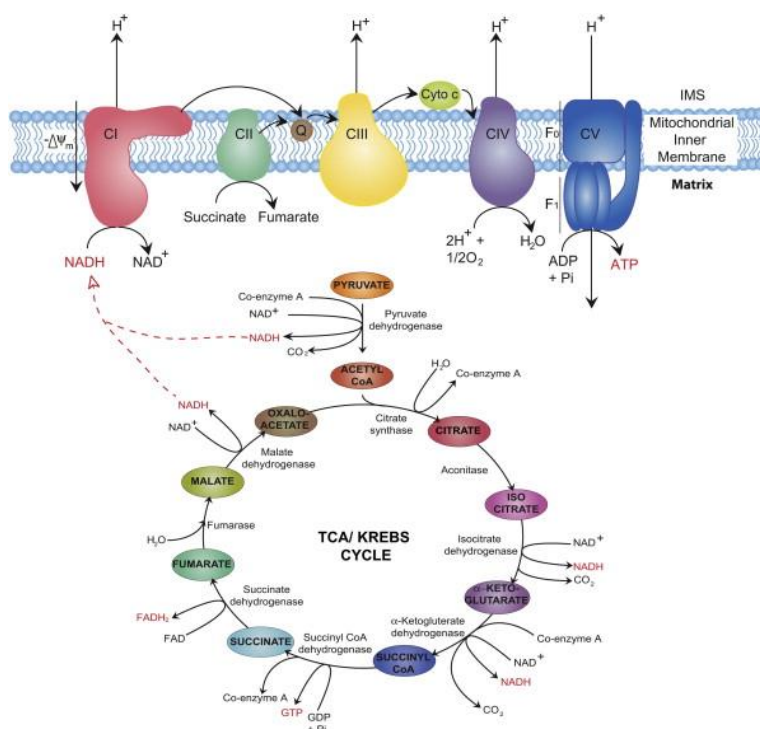


Figure 4: Schematic diagram showing the structure of the ETC within human mitochondria. Alongside the tricarboxylic acid (TCA) cycle that occurs within the mitochondrial matrix – Figure taken from Laura.D., Thomas.S. 2012.

Carbohydrate fuels enter the mitochondria in the form of pyruvate, produced following glycolysis, which is then converted into Acetyl-CoA – by pyruvate dehydrogenase [57]. Acetyl-CoA is the organic molecule that is entered into the tricarboxylic acid (TCA) cycle – that takes place within the mitochondrial matrix (Figure 4). During the TCA cycle, two-carbon acetyl groups, obtained from acetyl-CoA, are transferred to the four-carbon molecule oxaloacetate – forming the six-carbon molecule, citrate. A further seven enzymatic steps, that aim to oxidise citrate back to oxaloacetate, then take place to form a repeating cyclic reaction. The excess carbon molecules produced by the TCA cycle are excreted in the form of carbon dioxide (CO₂), while the electrons harvested from this reaction are passed to local cofactors: nicotinamide adenine dinucleotide (NADH) and flavin adenine dinucleotide (FADH₂) [57]. The electrons liberated by the cofactors can then be incorporated into the mitochondrial electron transport chain (ETC) (Figure 2/4), which facilitates the final stage of cellular respiration – oxidative phosphorylation – which produces more than 90% of cellular energy [58][59].

The ETC, also known as the respiratory chain, consists of respiratory protein complexes (complex I-IV) embedded in the IMM, which work in unison to utilise the energy of harvested electrons to generate ATP [57]. Mitochondrial ETC's show significant conservation between animals, plants, and fungi, however divergences are still observed [20]. In mammalian cells, these respiratory complexes include NADH: ubiquinone oxidoreductase, succinate: ubiquinone oxidoreductase, ubiquinol: cytochrome c oxidase oxidoreductase and cytochrome c oxidase [57]. *S. cerevisiae* diverge from these higher eukaryotes as they lack complex I and instead possess several peripheral membrane NADH dehydrogenases [20]. The collective action of the of the respiratory complexes and the electrons provided by the NADH and FADH₂ cofactors, pump protons from the matrix to the IMS, which is considered energetically unfavourable, to generate a potential difference across the IMM, which is utilised by the final respiratory complex (complex V) [58].

Following the TCA cycle, two electrons are transferred from the NADH and FADH₂ cofactors to complex I or complex II, these electrons then pass along the complex via a series of iron sulphur clusters, until it reaches the lipid soluble redox carrier – coenzyme Q [60]. Notably, complex II does not pump any protons from the mitochondrial matrix to the IMS, this complex is also unique to the other respiratory complexes by being encoded entirely by nuclear DNA. Following reduction by complex I or II, coenzyme Q can freely diffuse through the IMM to donate electrons to complex III – the smallest of the ETC complexes. Complex III (Cytochrome c reductase) is responsible for oxidising coenzyme Q and passing the liberated electrons to complex IV – Cytochrome c oxidase. Two protons obtained from the oxidation of coenzyme Q are then deposited in the IMS, while two other protons are translocated to the mitochondrial matrix [60]. At complex IV, the electrons continue to pump a total of four protons from the mitochondrial matrix into the IMS. Alongside, aiding the generation of H₂O molecules from available O₂ molecules, by providing the required electrons and protons. In total, four molecules of Cytochrome c oxidase donate one electron to the iron/copper active site of local enzymes that catalyses the production of H₂O molecules [59].

The final complex within the ETC is complex V, more commonly known as ATP synthase. This complex utilises the electrostatic ion gradients, and the subsequent discharge of the proton motive force, to generate ATP, by catalysing the addition of inorganic phosphate (iP) to ADP – via an energetically favourable reaction [61]. Approximately 2-5 protons are required to pass through ATP synthase during the production of one ATP molecule [61]. Notably, it is more difficult to gauge the number of NADH or FADH₂ molecules required for the generation of each ATP molecules, as protons can leak across the mitochondrial membranes – dissipating the energy as heat [61]. Further examples of the inefficiency associated with this biochemical process can be observed during ‘uncoupling’, which occurs when the removal of protons from the IMS fails to utilise ATP synthase and therefore fails to contribute to ATP synthesis. Electrons can also leak from the respiratory complexes, leading to a reduction of energy within the ETC – these electrons can then interact with local oxygen molecules to produce superoxide, a potent reactive oxygen species [61].

As previously mentioned, other functions of the mitochondria include amino acid synthesis, maintaining lipid homeostasis/metabolism, and the generation of iron sulphur clusters and heme. Regarding protein synthesis, the mitochondria form an essential component in the synthetic pathways of amino acids formed from pyruvate and α -ketoglutarate [62]. The amino acids synthesised from pyruvate include alanine and the branched chain amino acids: leucine, valine, and isoleucine [62]. In *S. cerevisiae* the entire synthetic pathway for isoleucine and valine is localised within the mitochondria, however the final stages can also occur within the cytoplasm. Amino acids synthesised from α -ketoglutarate, include glutamate, proline, arginine, and glutamine – the most abundant amino acids within cells [62].

Regarding lipid metabolism and homeostasis, the mitochondria are solely responsible for the synthesis of PE, CL, and several intermediate phospholipids [63]. Yeast mitochondria have also been attributed to the biosynthesis of fatty acids, via the production of octanoyl-ACP – a precursor required to synthesise lipoic acid, which is required for the regular function of pyruvate dehydrogenase, α -ketoglutarate dehydrogenase and the glycine cleavage system. However, to date, the full extent of the role that the mitochondria have in the synthesis of fatty acids remains relatively unknown. Another essential function of the mitochondria is centred on iron-sulphur cluster biogenesis. Iron sulphur clusters are versatile co-factors with functions in numerous cellular processes [64]. In yeast, the mitochondria are involved in both the biogenesis and assembly of mitochondrial, cytoplasmic, and nuclear iron-sulphur clusters, highlighting the mitochondria's integral role in this process. The mitochondria also play a significant role in the synthesis of heme. As the mitochondrial matrix acts as the primary sites for the reaction – the cytoplasm is the other possible location for heme synthesis [65]. These functions, although essential, only highlight a few the vast range of functions attributed to the mitochondria – further highlighting the essential role the mitochondria have in coordinating cellular activity.

1.2.4 Intracellular ROS Production

Reactive oxygen species (ROS) are highly reactive molecules formed from O₂ molecules. These can take the form of peroxides, superoxide, hydroxyl radical, singlet oxygen and alpha-oxygen molecules. The generation of ROS molecules typically begins with the reductions of O₂ to produce superoxide – which is the precursor for the majority of the other ROS molecules [66]. Within cells, at physiological pH, superoxide is converted to hydrogen peroxide – the most abundant ROS molecule – by a reaction catalysed by copper-zinc superoxide dismutase (SOD1) and manganese superoxide dismutase (SOD2) – located within the cytoplasm/IMS and the mitochondrial matrix, respectively (Figure 5) [67].

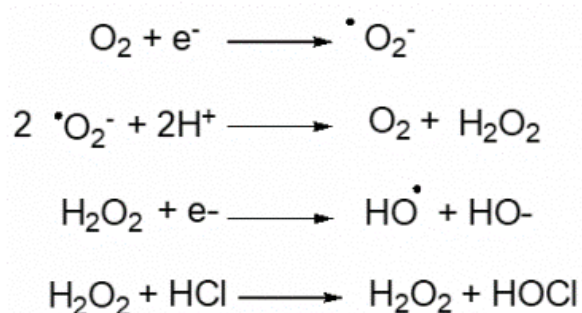


Figure 5: Chemical reaction that produces hydrogen peroxide within cells. Highlighting the initial reduction of oxygen, followed by the reaction with local hydrogen ions, to produce hydrogen peroxide. The diagram also details the further reduction of hydrogen peroxide to produce hydroxy radicals which can occur in the presence of transient metals – Fenton reaction – Diagram taken from Ayer.A., Gourlay.C.W. 2014.

Exposure to ROS is a byproduct of normal metabolism, in aerobic organisms. Contribution of ROS in these instances can alter the redox balance within the intracellular environment, which in turn can have major effects on cell function, through the regulation of numerous signalling pathways [68]. Throughout a cell's lifespan ROS is continuously produced through the action of multiple enzymes and cellular processes, including oxidative phosphorylation by the ETC, fatty acid β-oxidation, the endoplasmic reticulum protein disulphide resolution system and NADPH oxidases. Notably, a characteristic phenotype associated with mitochondrial dysfunction is the accumulation of cellular damage, attributed to a significant increase in intracellular ROS levels [67]. The increased intracellular concentration of ROS and altered redox homeostasis has separately been associated with cellular senescence, diseases in higher eukaryotes and the progression of aging [69][70]. However, contrastingly an increase in ROS has also been shown to lead to an increase in stress resistance and longevity in certain model organisms, highlighting the mysterious relationship associated with ROS and cellular health [71].

The role that ROS plays within cells is varied and dependent on the type and concentration of the specific ROS molecules present. The most abundant and well-known ROS molecule is hydrogen peroxide, which is a relatively stable molecule, unlike most ROS molecules, which allows the ROS to be present in higher concentrations within cells [67]. This is important as hydrogen peroxide has been identified as a potent signalling molecule, that is capable of oxidising targets (e.g., thiol esters) to elicit structural and functional changes in macromolecules that subsequently influence different cellular processes, including regulating cell division and stress response pathways [68]. However, when the concentration of ROS increases cells aim to detoxify and repair while simultaneously decreasing cellular replication to promote cell survival. When intracellular ROS concentrations continue to increase apoptosis is induced [72] (Figure 5).

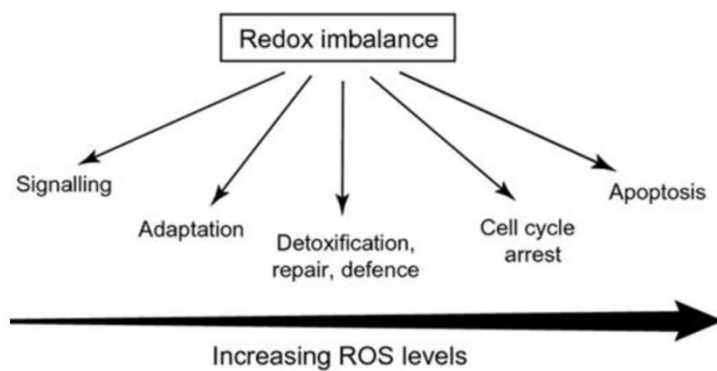


Figure 6: Diagram highlighting the impact of redox balance on cellular activity and health, relative to the concentration of intracellular ROS – Diagram taken from Ayer.A., Gourlay.C.W. 2014.

To combat the negative implications associated with increases in intracellular ROS concentrations, cells possess numerous intracellular antioxidant mechanisms to protect against the detrimental effects of high intracellular ROS concentrations. These include catalases – in *S. cerevisiae* encoded by *CTA1* and *CTT1* genes – and thiol peroxidases, which catalyse the breakdown of H_2O_2 to H_2O and O_2 [67]. Yeast cells possess 8 thiol peroxidases (5 peroxiredoxins Tsa1, Tsa2, Ahp1, Dot5, Prx1) (3 GSH – Gpx1, Gpx2, Gpx3), which have antioxidant function, but also contain catalytic cysteine residues that are frequently oxidised by hydrogen peroxide to sulfenic acid – the oxidised enzymes then oxidise regulatory proteins resulting in gene regulatory responses, providing another avenue for hydrogen peroxide to act as a signalling molecule [73]. Non-enzymatic protection also exists in the form of glutathione and ascorbic acid being present. It is the result of these pro-oxidant processes and antioxidant levels that reflect the state of cellular ROS levels within the intracellular environment [67].

In the ETC electron leakage primarily from complex III, and complex II/IV to a lesser extent, facilitate the thermodynamically favourable one-electron reduction of oxygen molecules, leading to the production of a superoxide molecule ($O\bullet$) [67]. This production of superoxide in the mitochondria is dependent on the protonmotive force, O_2 concentrations and the ratio of redox donors-acceptor pairs (e.g., NADH/NAD⁺ and CoQH₂/CoQ) [67]. The superoxide molecules produced utilising electrons from complex III are released into the IMS and matrix, while electrons utilised from complex II/IV generate superoxide molecules that typically reside within the mitochondrial matrix, exclusively [67]. The production of ROS via the β -oxidation of fatty acids, primarily within peroxisomes, is another intracellular source of ROS – specifically hydrogen peroxide. The role of fatty acid β -oxidation is the initial breakdown of long chain or methyl branched fatty acids, to later act as substrates for other metabolic activities. Specifically, the enzyme acyl-CoA oxidase, which oxidises acyl-CoA, is responsible for transferring the hydrogen to local oxygen molecules to produce the hydrogen peroxide. Most of the hydrogen peroxide produced within the peroxisomes is then detoxified by Cta1 [74].

The endoplasmic reticulum protein disulphide resolution system is another source of intracellular ROS. Specifically, during the generation of disulphide bonds ROS is produced or alternatively, ROS can be produced during protein misfolding, following depletions in reduced glutathione. ROS can also be produced within the intracellular environment by NADPH oxidase enzymes. These integral membrane enzymes oxidise local NADPH molecules, to facilitate their involvement in additional metabolic processes. During the oxidation of NADPH local oxygen molecules are utilised and reduced as a biproduct of the reaction. Collectively, the production of ROS through these reactions and processes contributes to the tightly regulated redox levels within the intracellular environment. Regulation of ROS is essential within many organisms, with a large majority of organisms experiencing many negative implications associated with increases in intracellular ROS.

1.2.5 Free Radical Theory of Aging (FRTA)

Originally described in the 1950s, the FRTA proposed that the progression of aging, is the result of the accumulation of oxidative damage, induced by an increase in intracellular ROS [75]. This proposal was based on similarities observed between cellular damage as a result of irradiation and that which occurs naturally – both of which were thought to be caused by the presence of free radicals – specifically $\text{OH}\cdot$ and HO_2 [75]. This theory has garnered support from numerous studies that have demonstrated a relationship between the generation of ROS, oxidative damage, and aging. Further findings, linking the reduction of ROS with an increase in lifespan, across various model organisms, as well as showing that an increase in ROS can shorten an organism's lifespan have continued to support this theory [75][76].

In 1972, the FRTA was further refined with the mitochondria becoming a focal point of interest, with the mitochondria being thought to be the major source of free radicals that cause the oxidative damage within cells. This new hypothesised theory was referred to as the Mitochondrial Free Radical Theory of Aging (MFRTA) [77]. This hypothesis is based on the knowledge, that the mitochondria produced ROS as a byproduct of cellular respiration. It was considered that the ROS could then leak from the organelle and damage macromolecules of the cell – including DNA, lipids, and proteins. Alongside this, the ROS is thought to damage the internal structures of the mitochondria and the mtDNA, which in turn exacerbates the production of ROS [76].

However, many findings of research studies have conflicted with this theory. Notably, studies on increasing longevity, via the genetic manipulation of mitochondrial ROS production and antioxidant activity, have garnered mixed results. During studies, in 2005, it was found that the overexpression of the antioxidant mitochondrial targeted catalase, increased longevity in murine models (4.5-5.5-month median increase and 4.5-month maximum increase – relative to WT), alongside reducing cardiac pathologies/myopathy, reducing intracellular H_2O_2 concentrations in cardiac cells and reducing mtDNA damage in skeletal cells [78]. However, in 2009, studies found that the overexpression of other intracellular antioxidants – CuZnSOD and mitochondria-localised MnSOD – had no significant effect

on extending longevity, compared to WT [79]. To further fuel the confusion among theorists, it was also observed, in a study using *C. elegans*, that increases in intracellular ROS production is associated with an increase in lifespan, relative to WT [80]. This conflict of findings has led to uncertainty among many regarding the FRTA and more specifically the MFRTA. Leading scientists to investigate ROS production within the cell in greater depth, to identify the true major source of intracellular ROS.

1.2.6 Ras Dependant ROS Production via Yno1 NADPH Oxidase

In studies using *S. cerevisiae* as a model organism, it was identified that in cells lacking Cytochrome c oxidase (COX) function the mitochondria were not the major source of ROS, but instead act as a signalling platform that promoted non-mitochondrial increases in intracellular ROS [81]. This required the migration of Ras2 towards the dysfunctional mitochondria, alongside its GEF – Cdc25, which is required for Ras2 activation. From the surface of the mitochondria an aberrant signalling pathway (Figure 7) was initiated that suppressed the endoplasmic reticulum associated degradation (ERAD) pathway, which is essential in the regulation of protein quality control and homeostasis. This in turn led to a significant increase in the level of the ER-localised NADPH oxidase, called Yno1. NADPH oxidases are a class of enzyme that characteristically consist of 6/7 transmembrane helices that coordinate two heme molecules via four highly conserved histidine's. These proteins catalyse electron transfer from NADPH to FADH, then from FADH to the two heme groups within the protein structure, before finally transferring the electrons to local oxygen molecules, to produce superoxide [81]. Interestingly, alongside its interaction with NADPH and FADH, Yno1 signalling has also been shown to regulate the actin cytoskeleton, highlighted by cells lacking Yno1 being hypersensitive to inhibitors of the actin cytoskeleton. Specifically, Yno1 signalling is thought to regulate the nucleation and elongation of F-actin cables, which is essential in coordinating and facilitating the dynamic nature of the actin cytoskeleton [82].

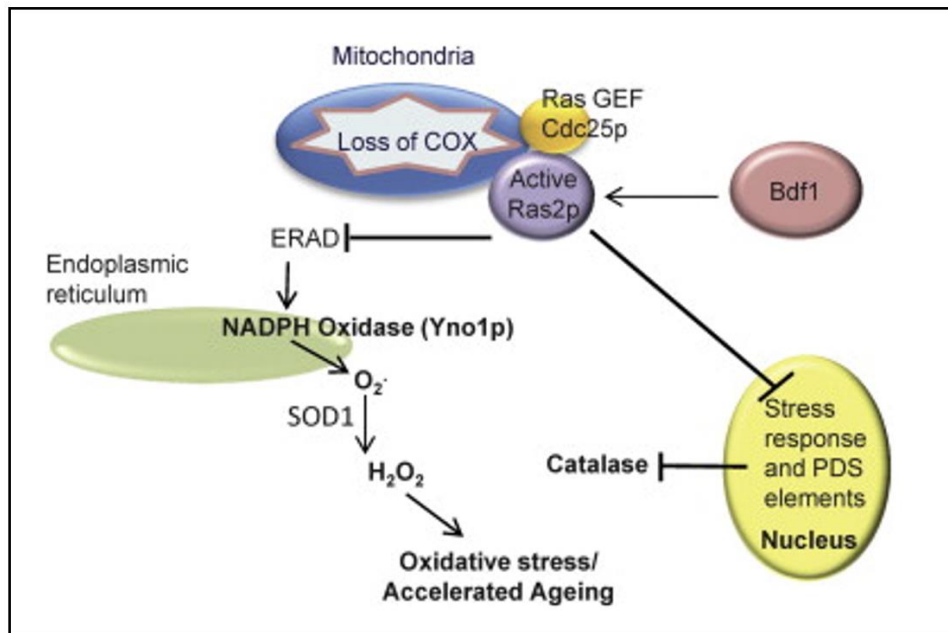


Figure 7: Schematic diagram showing the hypothesised model that leads to an increase in intracellular ROS concentrations, following loss of mitochondrial function induced by loss of *cox4* function. In this model, Ras2 translocates and becomes active on the surface of the dysfunctional mitochondria, aided by its localised GEF – Cdc25. Upon activation Ras2 suppresses the ER-associated degradation (ERAD) pathway, leading to an increase in the NADPH oxidase enzyme, called Yno1. This enzyme then produces superoxide, which is subsequently converted into hydrogen peroxide by superoxide dismutase 1, Sod1. The Ras2 signalling also suppresses PDS elements to reduce intracellular antioxidants – Figure taken from Leadsham.J.E., Sander.G. 2013.

The ROS produced by Yno1 in *S. cerevisiae* typically acts as a signalling molecule – that interacts with proteins localised to the ER and plasma membrane (e.g., yeast casein kinases) – as it is converted to hydrogen peroxide by the action of superoxide dismutase 1, Sod1 [83]. However, the aberrant Ras2 signalling, associated with the loss of COX activity, also suppressed specific genes associated with the oxidative stress response and PDS elements. This combination of effects led to the generation of a pro-ROS environment that was detrimental to cellular health and reduced cell viability. Notably, an additional protein, Bdf1, which is a bromo-domain containing protein that is homologous to human Brd3 – which is associated with chromatin and the TFIID transcription factors that regulate RNA polymerase II activity – was proposed to be essential in the localisation of Ras2 to the mitochondria and in the initiation of pro-ROS signalling [84].

Interestingly, K-Ras within humans has been observed to be targeted to the mitochondria upon phosphorylation by protein kinase C – which is an event that leads to apoptosis within these cells [85]. A number of Ras2-derived phosphopeptides have been identified – that can act as a target for kinase activity – which could provide avenues for additional regulatory levels of phosphorylation that could be associated with inducing localisation to endomembranes [86]. By understanding the mechanisms behind Ras2 localisation and the signalling pathway generated by the active Ras2, a greater understanding of the process within mammalian cells could be gained and utilised in the future, alongside understanding the fundamental rules of life associated with *S. cerevisiae*.

1.3 Ras Superfamily

The Ras superfamily is a large group of small monomeric guanosine triphosphate hydrolase (GTPase) proteins (20-40 kDa). GTPases characteristically exhibit a relatively high affinity for GDP/GTP, alongside possessing a relatively low intrinsic GTP hydrolase activity and GDP/GTP exchanging activity – which is associated with their active (GTP-bound) and inactive (GDP-bound) states [87] [88]. These proteins have conserved structures, containing 30-55% similarities within their primary structure, alongside sharing biochemical mechanisms related to their function [89]. In humans, this superfamily comprises 167 members (Figure 6), which have evolutionally conserved orthologs found in numerous other eukaryotes, including *Drosophila*, *C. elegans*, *S. cerevisiae*, *S. pombe*, *Dictyostelium* and plants [90]. Although this superfamily of proteins exhibits many structural and biochemical similarities, significant differences can be observed related to their posttranslational modifications, subcellular localisation, and downstream regulators/effectors [91]. Of the large Ras superfamily, there are five distinct branches, based on protein sequence and function, these include: Ras, Rho, Rab, Arf and Ran [89].

S. cerevisiae has been utilised in studies focused on cell signalling pathway components, with the small GTPase proteins of the Ras superfamily being a prime example. The study of these proteins has led to an increased understanding of their roles as key regulators of cellular biology. Research studies, using *S. cerevisiae*, also interestingly led to the discovery of additional proteins and processes associated with the Ras counterparts in humans [93]. The identification of significant conservation in sequence and function between yeast and human Ras isoforms has aided these studies, even with divergences existing between the Ras isoforms downstream signalling pathways [93]. For these reasons, *S. cerevisiae* was selected as the model organism for this research study, which is focused on investigating aberrant Ras signalling that is initiated from the surface of dysfunctional mitochondria – which in turn generates a pro-ROS environment within the cell that in turn reduces cell viability [81].

1.3.1 Ras Structure and Expression

Ras proteins possess a distinct folded structure that contain six β -strands and five α -helices. Within this structure, a highly conserved N-terminus resides that hosts the G domain (166aa/20KDa), which is comprised of groups of short stretches of amino acids – known as G boxes (G1 to G5) – that can interact with guanine nucleotides and phosphates [94][95]. To further aid nucleotide binding, the Ras proteins also bind magnesium ions, which when incorporated into the Ras protein's structure, localises in the active site [95]. However, it is the G boxes that prove to be the most essential component of the Ras proteins, when considering guanine nucleotide and phosphate binding. The G1 motif (P-loop) of the G boxes, is responsible for interacting with the β -phosphate of both GDP and GTP, while the G2 motif (switch I) interacts with the terminal phosphate (γ -phosphate) of GTP and the divalent magnesium ion in the active site, via a threonine 35 residue [96]. The G3 motif (switch II) has a distinct DXXGQ sequence, in which notably D – aspartate 57 is required for guanine binding and Q – glutamine 61 is essential for GTP hydrolysis [90] [95].

Finally, the G4 and G5 motifs contain LVGNKxDL and SAK motifs, respectively, and both are responsible for further aiding the interaction between the Ras protein and the guanine of GDP/GTP [90] [95]. Notably, it is the switch I and switch II motifs that regulate the conformational change of the protein between the active and inactive conformations – which is directly related to the binding affinity of the protein [95]. Comparing the N-terminus of mammalian and yeast Ras proteins significant evolutionary conservation can be observed - approximately 58% of amino acid residues are conserved [95]. The Ras proteins also contain a distinct hypervariable C-terminus that comprises the CAAX motif, a four amino acid sequence, consisting of a C – cysteine, two A – aliphatic amino acids and X – a C-terminal amino acid [97]. The C-terminal region shows less conservation across yeast and mammalian cells, as the C-terminus is required to undergo post-translational modifications to facilitate protein trafficking, which is linked the generation of different signalling pathways – which hosts the most divergences between yeast and mammalian Ras [93].

In *S. cerevisiae*, there are two genes: *RAS1* and *RAS2*, which are in chromosome XV and XIV, respectively [98] [99]. Notably the Ras1 gene is a paralog of the Ras2 gene, having originally arisen from whole genome duplication [98]. These yeast genes encode two proteins: Ras1 (36kDa) and Ras2 (40kDa), which are homologous to human Ras proteins [100]. Ras1 (309aa) and Ras2 (322aa) are responsible for regulating signalling pathways associated with coordinating many intracellular processes, including sporulation, the nitrogen starvation response and filamentous growth [100] [101]. The functions of Ras1 and Ras2 are interchangeable, with differences between the proteins only being observed in the protein's expression [102]. The levels of *RAS1* mRNA, and the associated Ras1 synthesis, are significantly reduced during the mid-logarithmic growth phase and during growth on non-fermentable carbon sources [100]. Contrastingly, *RAS2* mRNA levels, and associated Ras2 synthesis, are high throughout all phase of growth and when grown on both fermentable and non-fermentable carbon sources [100]. Notably, the Ras proteins within *S. cerevisiae* have been shown to have compensatory roles when one of the Ras genes are deleted – thus further demonstrating the extent in which there is a crossover of function.

1.3.2 Post-translational Modifications (PTM) of Ras Proteins

The activity and sub-cellular localisation of Ras is reliant on the proteins C-terminal region being processed, following protein synthesis. This means that PTM provide an additional level of regulation, by determining the subcellular microdomain in which the protein localises, which in turn determines the available effectors and regulators, that can coordinate downstream signalling pathways [100]. The PTM that take place include prenylation, proteolysis, carboxyl methylation (Figure 9), and palmitoylation (Figure 10) [103]. These PTM are similarly observed in both yeast and mammalian cells, with only minor alterations [100].

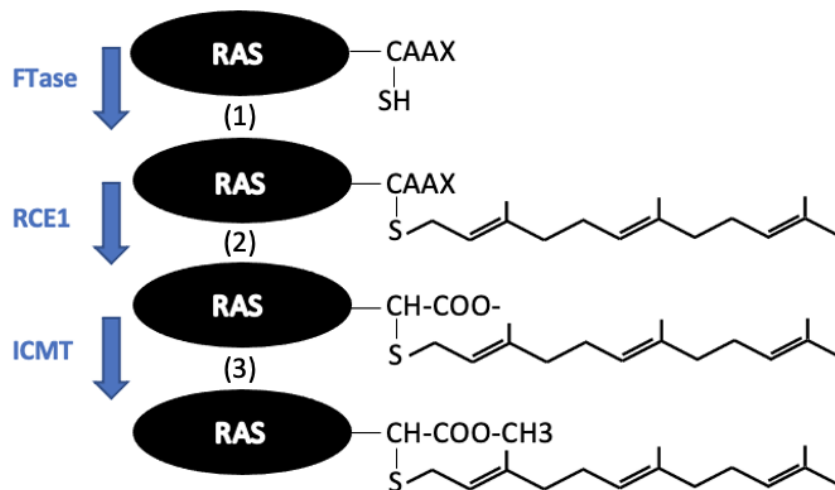


Figure 9: Schematic diagram showing the Ras post-translational modification. (1) prenylation, (2) proteolysis and (3) carboxyl methylation. FTase – Farnesyltransferase. RCE1 – Ras Converting Enzyme. ICMT – Isoprenylcysteine Carboxyl Methyltransferase.

Prior to prenylation, the newly synthesised Ras protein has a methionine residue removed from its N-terminus, this is thought to occur co-translationally, to ensure that a proline residue solely remains [104]. Prenylation, first observed in 1990, then takes place in which the cysteine residue of the CAAX motif is targeted by cytoplasmic prenyltransferase enzymes – farnesyltransferase (FTase) or geranylgeranyltransferase type 1 (GGTase 1) [105] [106]. In humans, the spliced variant SMGGDs, a guanine nucleotide exchange factor, can bind to unprenylated Ras which retards prenylation, offering an extra level of regulation. The recruitment of FTase or GGTase1 is dependent on the amino acid present in the ‘X’ position of the CAAX motif. The presence of serine or methionine provides the

substrate for FTase, which catalyses the addition of a 15-carbon farnesyl lipid to the protein, via a stable thioester to sulfhydryl groups of the cysteine residue [107]. Alternatively, the presence of leucine in the 'X' position, provides the substrate for GGTase1 which catalyses the addition of a 20-carbon polyisoprene lipid, also via a stable thioester to a sulfhydryl group on the cysteine residue [107]. The activity of GGTase1 is typically associated with the Rho family GTPases and the γ -subunit of heterotrimeric G proteins. While FTase activity is associated with all Ras proteins. This PTM provides the protein with a relatively weak affinity for cellular membranes, allowing the Ras to translocate, from the cytosol, towards the cytoplasmic face of the endoplasmic reticulum (ER).

When localised at the ER, proteolysis of the Ras protein can occur, which is a reaction that is responsible for the proteolytic removal of the 'AAX' amino acids from the CAAX motif. This reaction is catalysed by the ER-localised transmembrane endoprotease, ras-converting enzyme 1 (RCE1) [108]. Resulting in the generation of a prenyl-cysteine as the new C-terminus of the Ras protein [108]. The prenyl-cysteine then becomes the target of carboxyl methylation, a reversible reaction catalysed by the enzyme isoprenylcysteine carboxyl methyltransferase (ICMT) – a 26 KDa integral transmembrane protein, encoded by the *STE14* gene [108]. This PTM is thought to have an important role in the signalling activity of Ras [109]. This modification also facilitates the translocation of Ras from the ER to the Golgi apparatus [109].

The previously mentioned PTM collectively remodel the C-terminus of Ras, converting it from a hydrophilic region to a hydrophobic region that can insert into the cell membranes. Modifications to the CAAX motif therefore act as a primary signal for Ras localisation, however, an additional 'secondary' signal is required to complete protein localisation. This secondary signal takes the form of the final PTM, palmitoylation (Figure 10), which is a reaction catalysed by palmitoyl acyltransferase enzymes [108]. Palmitoylation is a reversible reaction that involves the covalent attachment of palmitic acid – usually obtained from Palmitic-CoA – to a cysteine, serine, or threonine residues, within the hypervariable region of the Ras protein, via a labile thioester [108] The aim of this modification is to trap the Ras protein in the membrane of the Golgi apparatus, from where it is then trafficked, via

vesicular transport, to the cellular membrane [109]. Once localised to a membrane (plasma membrane or endomembrane), the Ras isoforms are not dispersed randomly, but grouped in sub domains – clustering of Ras proteins at the plasma membrane seems to be related to galectins (galectin 1 and 3) and cholesterol content [109]. Notably, the half-life of palmitic acid is considerably shorter than the half-life of Ras, meaning translocation mechanisms, to and from the Golgi apparatus are required to facilitate the reattachment of palmitic acid to the Ras protein – to ensure continued Ras function [109].

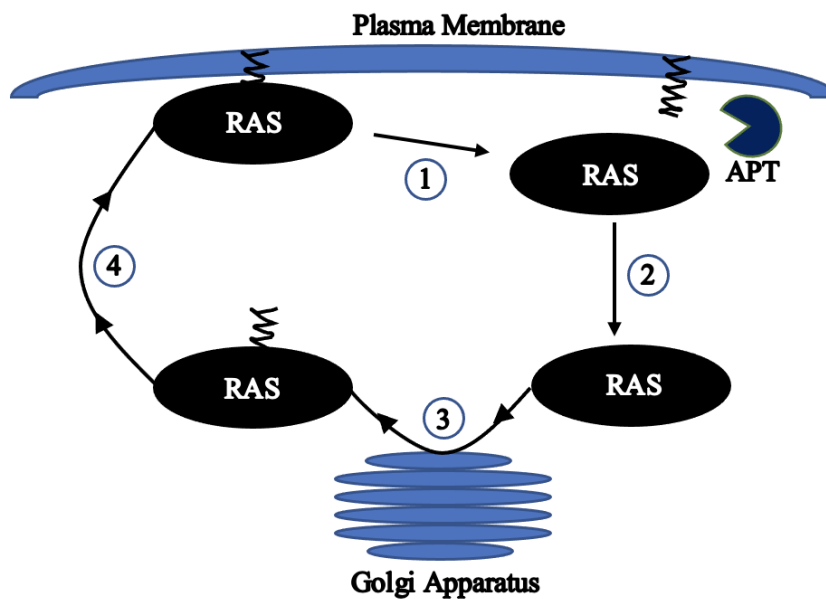


Figure 10: Schematic diagram of the movement of Ras within cells. Showing the (1) de-palmitoylation, (2) translocation to the Golgi apparatus, (3) palmitoylation and (4) translocation to the plasma membrane.

In humans, ‘Harvey rat sarcoma virus’-Ras (H-Ras) has two cysteine residues, Cys 181 and Cys 184, which can accept palmitic acid, while N-Ras – first identified in neuroblastoma cells - and ‘Kirsten rat sarcoma virus’-Ras (K-Ras) isoform 4A only have one cysteine residues available, Cys 181 and Cys 180, respectively [110]. Contrastingly, the other K-Ras isoform, 4B, is not palmitoylated, instead the protein contains a polybasic region (stretch of lysine residues) that enable electrostatic interactions with negatively charged plasma membrane phospholipids [110]. This also causes the protein to be excluded from Golgi-dependent trafficking, K-Ras4B is instead transported to the required subcellular location by chaperone proteins [110]. Additional modifications to Ras have also been observed, including phosphorylation, acylation and diacylation. Like the core PTM, these modifications can also influence

Ras function, localisation, and activity. Phosphorylation has become a point of interest in research studies after the identification of many targets – typically serine, threonine, and tyrosine residues – within mammalian cells, or exclusively serine residues in yeast cells [110]. Notably, the phosphorylation of Ras serine targets within yeast have been shown to induce the translocation of Ras to the plasma membrane [109]. While in mammalian cells, H-Ras has been shown to be modulated by phosphorylation – experimental evidence suggests that the phosphorylation of serine 181 results in the rapid translocation of K-Ras from the plasma membrane to the endomembranes [110]. This further highlights the important role that PTM have in Ras regulation.

1.3.3 Ras Regulation:

As previously mentioned, there are many levels of regulation that ensure that the activity of ras is tightly regulated, to ensure that the associated cellular activities are co-ordinated appropriately, to prevent aberrant Ras signalling that could induce detrimental effects on cellular health. Besides the regulatory mechanisms that have already been discussed, alongside additional feedback mechanisms that utilise downstream products of Ras signalling, the primary form of regulation for Ras proteins is co-ordinated by several regulatory proteins. These proteins can be divided into two major categories: guanine-nucleotide exchange factors (GEF) and GTPase activating proteins (GAP) – (Figure 11).

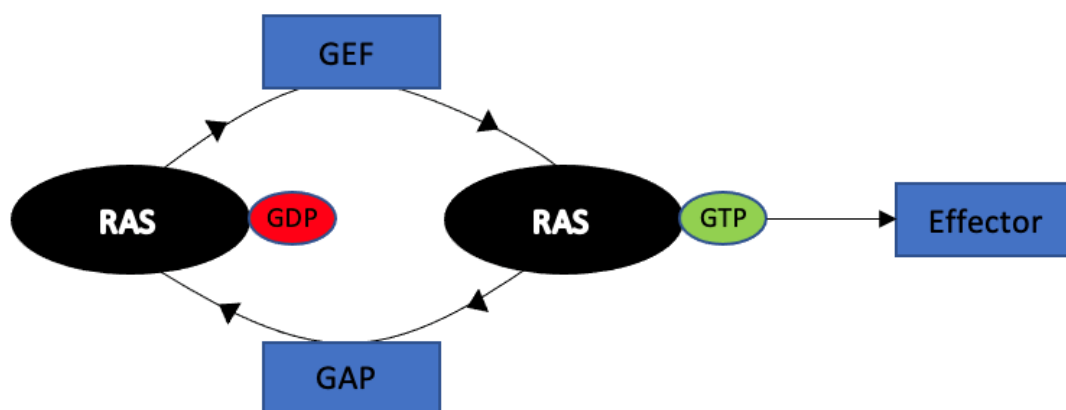


Figure 11: Schematic diagram showing an overview of the regulation of Ras activity. The inactive, guanosine diphosphate (GDP)-bound ras is converted to an active form with guanosine triphosphate (GTP) bound, through the action of guanine nucleotide exchange factors (GEF). Allowing ras to then interact with downstream effectors. The active GTP-bound form of ras is then converted back to the inactive form by the action of GTPase activating proteins (GAP).

Guanine-nucleotide exchange factors (GEF) are proteins or protein domains that promote the dissociation of tightly bound guanine nucleotides – guanosine diphosphate (GDP) – from monomeric GTPase proteins [111]. The release of the tightly bound nucleotides facilitates the exchange of these nucleotides for free cytosolic guanosine triphosphate (GTP), which activates the GTPase. The GEF is required to accelerate the exchange of GDP for GTP, which is a relatively slow process in the absence of GEF [112]. The action of GEF can be highly specific, with a single GEF activating a single GTPase, while other GEFs can activate multiple GTPases [113]. For this reason, the GEF are often themselves regulated, by adaptor proteins in response to upstream signals and by autoinhibitory mechanisms. In *S. cerevisiae*, GEFs include Cdc25 and Sdc25 [100]. While mammalian GEFs include Grf and mSos (Figure 12) [112].

Contrastingly, GTPase activating proteins (GAP) promote the GTPase activity of Ras proteins, and other GTPases within the Ras superfamily. The action of GAP promotes increased GTPase activity, inducing GTP hydrolysis within the GTPases – which typically have very slow intrinsic GTPase activity. The majority of GAP’s target GTP to promote involvement, as a substrate, for nucleophilic attack, lowering the transition state energy of the hydrolysis reaction – thus increasing the rate of reaction [111]. GAP are able to interact with GTPases, in a highly specific manner, to promote the hydrolysis of GTP to GDP, which in turn induces a conformational change that ensures the GTPases switches from an active GTP-bound formation to an inactive GDP-bound formation [114]. In *S. cerevisiae*, the two GAP present are Ira1 and Ira2 [100]. While in mammalian cells, GAP include p120GAP (Figure 12) [111].

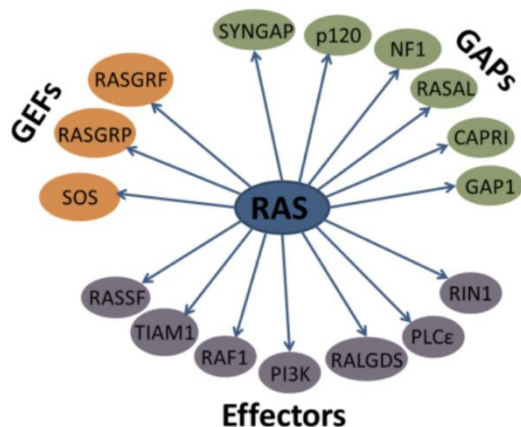


Figure 12: Schematic diagram showing the range of GEF’s, GAP’s and effectors that influence the activity and downstream signalling pathways of Ras isoforms within humans – Figure taken from Simanshu.D.K., Nissley.D.V. 2017.

1.3.4 Ras Signalling Pathway Overview

Ras proteins, in human and yeast, are essential for many cellular processes including regulating cellular growth, morphogenesis, progression of the cell cycle, proliferation, regulation of the stress response and aging [92] [100]. These proteins are clearly important in maintaining the appropriate activity of cells, which is highlighted in *S. cerevisiae* as when *RAS1* and *RAS2* are deleted cells become nonviable. Similarly, when just *RAS2* is deleted, the mutants become nonviable when grown on nonfermentable carbon sources – as under this condition the cells would be defective in both Ras1 and Ras2 on nonfermentable carbon sources [101][102]. This therefore highlights the cells dependence on the appropriate activity of Ras signalling.

Upon activation, Ras1 and Ras2 routinely activate the downstream effector adenylylase – encoded by the gene *CYR1* – located within the plasma membrane – the primary location in which Ras activity is localised (Figure 13) [100]. Notably, Cyr1 does not have transmembrane domains, like human adenylylase, instead displaying characteristics similar to sAC. Adenylylase is a large protein (2,026aa) that possesses four distinct domains: An N-terminus, a middle repetitive domain, catalytic domain, and a C-terminus [102]. The middle repetitive domain is comprised of a repeating 23-residue amphipathic leucine-rich motif (LRR domain – 674-1300aa), which acts as the primary site of Ras interactions [102]. The N-terminus region (81aa) of the LRR domain (676-756aa) has also been identified as a Ras association domain (RAD) that is also capable of interacting with Ras proteins [102]. When activated, adenylylase synthesises cyclic adenosine monophosphate (cAMP) from cytosolic ATP molecules. An increase in intracellular cAMP concentrations facilitates the interaction of cAMP with Bcy1 proteins – regulatory subunits of protein kinase A (PKA) [100]. Following the activation of PKA, three primary catalytic subunits, that exhibit cAMP-dependant protein kinase activity, are activated. These three subunits – encoded by *TPK1*, *TPK2*, and *TPK3* – catalyses the phosphorylation of substrates that regulate a variety of cellular functions [100]. The PKA catalytic subunits share overlapping functions; however, they have diverging regulatory functions – an example being the regulatory role of the Tpk1 subunit in branched chain amino acid biosynthesis, mitochondrial DNA

stability and mitochondrial iron homeostasis, contrasted to Tpk2 regulatory role in iron uptake, trehalase synthesis and water homeostasis [100] [115].

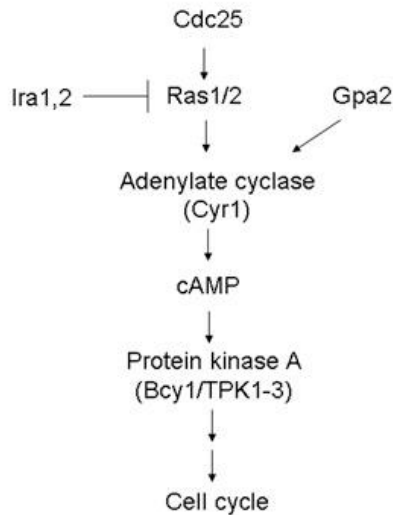


Figure 13: Diagram detailing the signalling pathway generated by the activation of Ras1/2 within *S. cerevisiae*. Highlighting the GEF's and GAP's present, alongside the downstream effectors and the associated cellular responses that are elicited by the Ras signalling – Figure taken from Tamanai.F. 2011.

As so many cellular processes are dependent on the appropriate activity of PKA, the intracellular levels of cAMP must be tightly regulated. This regulation takes the form of negative feedback loops, that utilise the activity of phosphodiesterase proteins, which catalyse the degradation of intracellular cAMP concentrations [116]. Within *S. cerevisiae*, two cAMP phosphodiesterase enzymes are present, one of which is a low-affinity phosphodiesterase – encoded by *PDE1*– while the other is a high-affinity phosphodiesterase – encoded by *PDE2* [116]. The phosphodiesterase proteins encoded by *PDE1* and *PDE2* have unrelated primary sequences [116]. The production of cAMP is also regulated by members of the heterotrimeric Gα proteins family called Gpa2 – encoded by *GPR1* – which is structurally related to seven transmembrane GPCR, whose ligands are fermentable sugars (e.g., glucose) [100]. This regulatory pathway runs in parallel to the Ras pathway.

Although human and yeast Ras proteins show significant levels of conservation across sequence, structure, post-translational modifications and regulators, the proteins show considerable divergences related to effectors and signalling pathways. The primary role of human Ras is the transduction of pro-survival signals from the external environment to the intracellular compartments of the cell. This action is best observed through the activation of tyrosine kinase receptors (TKR) – the most well-studied being

the epidermal growth factor receptor (EGFR) (Figure 14) [117]. Ligand binding to the EGFR induces dimerization, that activates the catalytic domain of the receptor, this subsequently leads to auto-phosphorylation events that facilitate the full activation of the receptor. The phosphorylated intracellular carboxyl-terminal domain of the receptor then acts as a beacon, to which GEFs localise – thus promoting Ras signalling within this intracellular micro-domain. Local Ras proteins can then bind to the receptor and become activated, enabling the Ras protein to then activate at least 20 distinct downstream effectors. These effectors include the rapidly-accelerated fibrosarcoma (RAF) kinases, phosphatidylinositol 3-kinase (PI3K), RAL guanine nucleotide dissociation stimulators (RALGDS), RIN1, Af6, Nore1, PLC (epsilon), PKC and T lymphoma invasion and metastasis-inducing 1 (Tiam 1) – alongside many others [118].

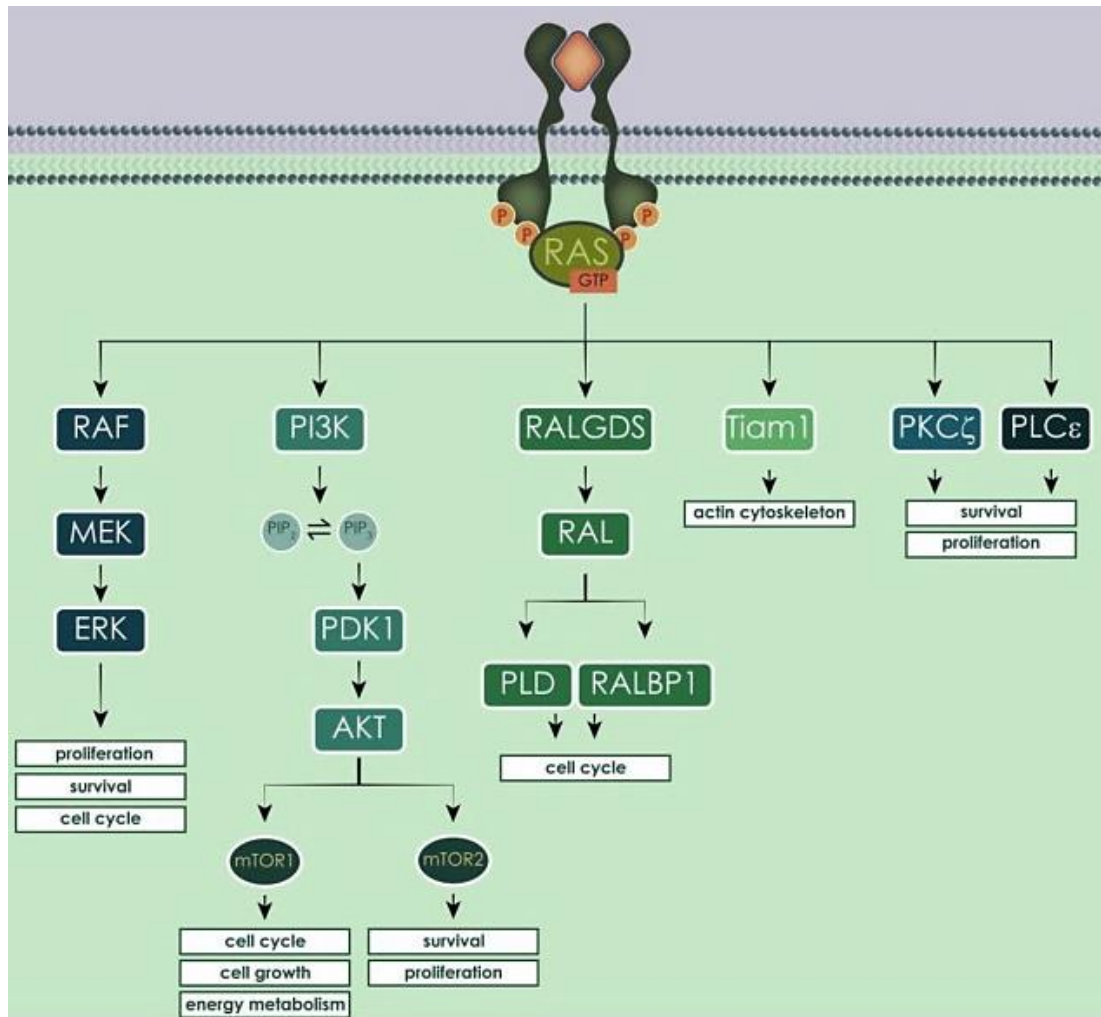


Figure 14: Schematic diagram showing the diverging signalling pathways generated following the activation of Ras proteins via the well-characterised tyrosine kinase receptors activation. Alongside the signalling pathways, the intracellular process that are being coordinated are also shown – Figure taken from Wee.P., Wang.Z. 2017.

The activation of these effectors can lead to further diversification of the signalling pathways. Facilitating the branching and incorporation of additional downstream effectors associated with numerous other cellular processes. For example, RAF kinases phosphorylate and subsequently activate MAPK/ERK kinases (MEK), this then leads to the activation – via phosphorylation – of extracellular signal-regulated kinase (ERK - also known as MAPK). ERK is then responsible for the regulation of several transcription factors that indirectly control cell cycle progression, proliferation and survival [118] [119]. Another example of Ras signalling diversification, via an effector, is observable through the activation of PI3K which promotes the production of phosphatidylinositol-3,4-triphosphate (PIP3) via the reversible phosphorylation of phosphatidylinositol-4,5-diphosphate (PIP2). PIP3 then activates phosphatidylinositol dependent kinase 1 (Pdk1), which is responsible for recruiting AKT to the plasma membrane. AKT, localised at the plasma membrane, can activate another downstream effector, mammalian target of rapamycin (mTOR). mTOR is capable of forming two distinct protein complexes, mTOR complex 1 (mTORC1) and mTOR complex 2 (mTORC2). mTORC1 primarily promotes the transcription of genes associated with cell growth, cell cycle progression and energy metabolism. While mTORC2 continues to phosphorylate AKT to promote cell survival and proliferation, through telomerase activity enhancement, inhibition of apoptosis and inactivation of pro-apoptotic factors [118].

These examples highlight the magnitude of divergence that is capable from a single Ras signalling pathways, which in turn highlights how integrated Ras signalling is in the coordination of normal cell function – in both yeast and mammalian cells. With mammalian Ras isoforms being responsible for transducing signals from the extracellular matrix to promote cell survival, similarly to yeast Ras that transduce signals in response to nutritional conditions of the extracellular and intracellular environment (e.g., glucose availability) to facilitate cell adaption and survival. Both yeast and mammalian Ras are therefore directly and indirectly associated with maintaining and regulating numerous aspects of cellular health, including energy metabolism and homeostasis, iron metabolisms and homeostasis, protein homeostasis and lipid metabolism and homeostasis – alongside many others.

1.4 Lipid Metabolism and Lipid Droplet Regulation

Lipids are organic substances that are soluble in nonpolar, organic solvents. The diversity of structure, and associated function, of lipids within cells allows lipids to be characterised and divided into 8 distinct groups, including: fatty acids, glycolipids, glycerophospholipids, sterols/sterol derivatives, sphingolipids, prenol lipids, glycolipids, and polyketides [120][121]. These lipids are synthesised throughout the cell, by a variety of organelles including the endoplasmic reticulum, Golgi apparatus and the mitochondria – however, interestingly some of these organelles have relatively low concentrations of lipids, indicating the presence of lipid transport mechanisms [122-126]. This is concurrent with the fact that lipids are associated with the function of many other organelles within the cell, directly and indirectly, linking lipid metabolism and homeostasis with numerous different cellular processes. Specific functions attributed to lipids, within cells, include acting as a cellular energy source, building blocks for cellular structures, mediators of membrane fusion and apoptosis, and acting as components within many cell signalling pathways [127]. Due to the significant role that lipids have within cells; it is essential that there are a number of mechanisms and organelles present to tightly regulate intracellular lipid concentrations. Failure to control lipid metabolism and maintain lipid homeostasis can induce cellular damage and cell death – lipotoxicity. This is highlighted by clinical evidence that suggests a significant link between the loss of lipid homeostasis and the development of numerous noncommunicable diseases (e.g., obesity and cancer) within higher eukaryotes [128][129]. A key organelle, within eukaryotes, that is responsible for the storage of non-polar lipids in a neutral, non-toxic, and biologically inert form, are lipid droplets (LD) [130]. Lipid droplets are membrane bound organelles, located within the cytoplasm, and in rare cases within the nucleus, of prokaryotic and eukaryotic cells, that through their primary function regulate lipid metabolism and homeostasis. Although as understanding of these organelles increases, the wider range of functions being uncovered also increases (e.g., role in protein quality control) [127]. For these reasons, LD have remained a focal point of many research studies to uncover the full scope of functionality attributed to LD, alongside their role in aiding cell maintenance, adaptability and survival.

1.4.1 Lipid Droplet Structure

Following their discovery in the 1880s and being the focal point of many research studies in the 1990s and 2000s, the understanding of LD has developed rapidly, particularly regarding the structure and function of the organelle [131]. Lipid droplets (Figure 14) are primarily composed of a neutral lipid core (oil phase), that comprises triacylglycerols (TAG) and sterol esters (SE) in equal proportions. This is encased by a phospholipid monolayer, which itself has integral and peripheral proteins distributed throughout [131].

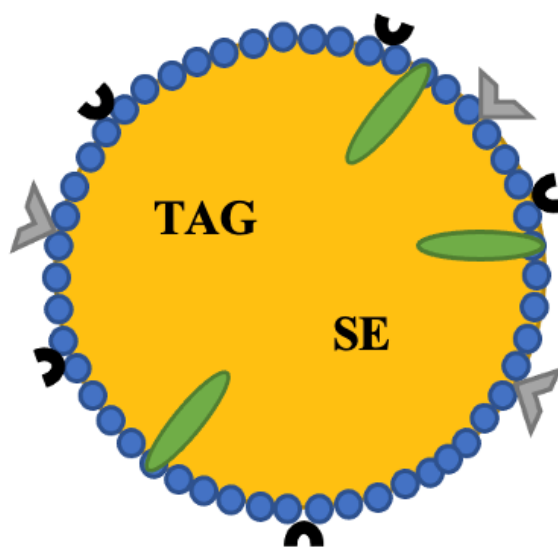


Figure 15: Schematic diagram detailing the basic structure of a lipid droplets. The diagram includes the (Blue) phospholipid monolayer, which possesses a variety of (Grey/Black) lipid proteins and (Green) unesterified sterols. The centre of the lipid droplet is a (Yellow) hydrophobic core, containing triacylglycerol (TAG) and sterol esters (SE).

The TAG and SE, that form the hydrophobic core of the lipid droplets, are organised in a formation that generates a densely packed TAG centre, surrounded by multiple layers of SE [132]. TAG is composed of 3 fatty acid chains that are attached to a glycerol backbone, via an ester bond. While SE comprise a sterol, group esterified with a fatty acid [132]. The phospholipid monolayer of lipid droplets, within *S. cerevisiae*, is composed of approximately 56% phosphatidylcholine (PC), 21% phosphatidylinositol (PI) and 17% phosphatidylethanolamine (PE), alongside lower concentrations of glycerophospholipids (e.g., lyso-PC and lyso-PE) [133] [134]. The proteins embedded within this phospholipid monolayer facilitate interactions with organelles including the mitochondria, ER, peroxisomes, and vacuoles. It is also thought that these proteins are essential in many undiscovered and hypothesised functions of LD [131]. The main proteins present in the phospholipid monolayer include enzymes for TAG and SE synthesis, membrane trafficking proteins, signalling molecules and lipases [131].

The dynamic nature of LD is essential to cellular maintenance and adaptability. Within *S. cerevisiae*, the LD range in size, being between 0.3-0.4 micrometres in diameter – although sizes of 1 micrometre have been observed [135]. However, when compared to mammalian cells, this is relatively small, as mammalian LD are significantly larger, but still extremely variable in nature [135]. Alongside this, the quantity of proteins in the phospholipid monolayer also differs, between *S. cerevisiae* and mammalian cells, with mammalian cells having between 100-150 proteins, compared to 35-40 proteins present in *S. cerevisiae* LD [131].

1.4.2 Lipid Droplets Formation

The biogenesis of lipid droplets is strongly linked with the endoplasmic reticulum (ER), which provides a hydrophobic environment with hydrophilic motifs with the aqueous milieu cytosol [136]. Regarding the specific mechanisms associated with lipid droplet biogenesis, there are a few hypothesised models – the most popular of which describes the upregulation of neutral lipids synthesis within the phospholipid bilayer of the ER, followed by bulging of the ER membrane and the formation of a ‘lens’ before the eventual budding of the lipid droplet from the ER and the release into the cytoplasm (Figure 15) [131][137][138].

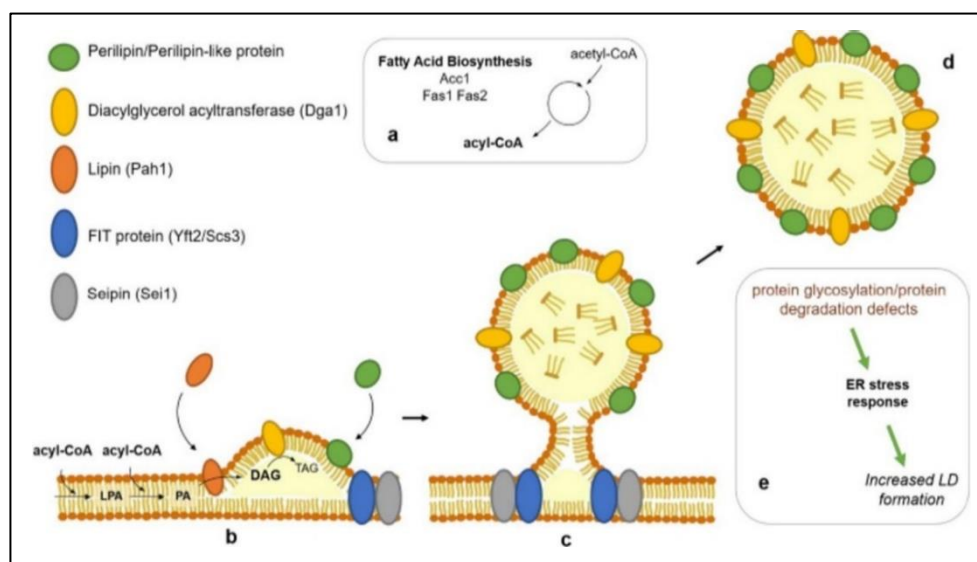


Figure 16: Schematic diagram showing the process of lipid droplet biogenesis. Highlighting the ER and lipid droplet proteins involved in the process – Figure taken from Wilfling.F., Haas.J.T. 2014.

The initial synthesis of neutral lipids, commonly TAG and SE, within the phospholipid bilayer of the ER, is controlled by four ER-associated enzymes. The enzymes responsible for TAG synthesis are diacylglycerol acyltransferases – DGAT1 and DGAT2 in mammalian cells; Dga1p and Lro1p in yeast cells [139-141]. While the enzymes required for SE synthesis are Acyl-CoA: cholesterol O-acyltransferases – ACAT1 and ACAT2 in mammalian cell; Are1 and Are2 in yeast cells [139]. It has been observed that cells that lack these enzymes required for neutral lipid synthesis are devoid of LD – highlighting their essential role in LD biogenesis [131]. Additionally, these mutants display increased sizes and significantly larger quantities of free intracellular neutral lipids. Notably, the expression of any of these enzymes individually can facilitate LD biogenesis, indicating that LD formation can be induced by either TAG and/or SE synthesis [131]. At low concentrations, neutral lipids are distributed evenly between the leaflets of the ER bilayer, among the acyl chains – sequestered from the polar heads of the phospholipids. However, as neutral lipid concentrations increase and are continually sequestered, the neutral lipids laterally diffuse and coalesce – causing the ER membrane to bulge and curve [131]. Coalescence of the neutral lipids expends less energy than what would be expended during lipid-phospholipid interactions, thus making coalescence energetically favourable [142]. This continues, alongside the energetically favourable process of neutral lipids de-mixing – ensuring neutral lipids do not interact with the phospholipid membrane and/or local proteins – which subsequently leads to the ‘lens’ being formed (30-60 nm in diameter) [142].

Continuous bulging of the ‘lens’ structure induces budding of the lipid droplet from the ER membrane – which seems to be a process that is dependent on the composition of the phospholipid membrane of the ER [131]. Although the composition of the phospholipid membrane is thought to regulate LD budding – through geometric interactions – the surface tension at the contact site between the aqueous cytosol and the ER also has a significant role in generating the spherical shape of the LD and controlling the directionality of the process [131]. The specific composition of phospholipids and presence of proteins can also influence directionality, via disruption of the surface tension, which enables the proteins to ensure the release of LD from the cytosolic face of the ER – however LD have been observed within the lumen of the ER [131][136]. Within the ER membrane, fat storage-inducing transmembrane

(FIT) proteins are present that facilitate – via an unknown mechanism – the budding of LD. Two highly related FIT proteins are present within mammalian cells, FIT1 and FIT2, while yeast cells exclusively express Fit2-related proteins [143]. LD budding in yeast is also aided by Pln1 proteins, which are structurally and functionally related to mammalian perilipins [131]. The Pln1 proteins are recruited from the cytosol to the LD phospholipid monolayer, during the early stages of LD biogenesis. It is this early recruitment, alongside cells lacking Pln1 showing delayed LD budding, that suggests Pln1 has an essential role in LD budding [131]. It has also been considered that the Pln1 protein has a stabilising role during LD budding, which seems to be dependent on the presence of TAG [131]. Another ER-associated protein that is involved in LD budding is seipin, which is thought to be essential in generating the morphology of the LD and controlling the proteins and lipid content of the LD [144]. It was through research studies, in yeast cells, using seipin mutants that an additional protein, Pex30, was identified to also share and contribute to some of the functions of seipin [145]. The united function of these proteins highlights the complex and intricate interactions that are required to facilitate LD budding.

Following LD budding, the LD can expand and grow through three distinct mechanisms: droplet-droplet fusion, transfer of TAG via ER membrane bridges or through unregulated TAG synthesis from the LD phospholipid monolayer [146]. During this growth and expansion of the LD, phospholipid synthesis can be unregulated to maintain phospholipid homeostasis and to minimise interfacial energy between the aqueous environment of the cytosol against the non-polar environment, within the lipid droplet core. Following growth and expansion, LD fission from the ER occurs, allowing the LD to freely translocate to its desired location within the cell, aided by diffusion gradients and the proteins within the phospholipid monolayer [131]. The breakdown of intracellular lipid droplets is essential in utilising the sequestered neutral lipids, for energy metabolism and lipid metabolism. Cytosolic and LD-resident lipases are responsible for the breakdown of lipid droplets to release, and make available, the neutral lipids within. This activity is tightly regulated by the lipid droplets and a number of external factors, to ensure the lipid droplets do not act in an aberrant fashion [131].

1.4.3 The Roles of Lipid Droplets

As previously stated, the main and most documented role of lipid droplets is the storage of excess fatty acids, in the form of TAG and SE – within their neutral lipid core. This is essential in preventing the build-up of fatty acids that can induce lipotoxicity when intracellular concentrations are great enough. The cytotoxic effects exuded by high intracellular concentrations of fatty acids include mitochondrial dysfunction, loss of cell wall integrity and decreased membrane formation, alongside many others - all equating to a decline in cellular health [147][148]. Experimentally evidence has supported this role, as yeast cells that are supplemented with oleic acid have significantly higher numbers of lipid droplets within their cytosol [149]. In contrast, the lipid droplets can also provide additional neutral lipids to the intracellular environment when intracellular lipid and fatty acid concentrations are depleted. This is regularly observed during the stationary phase of growth, during times of nitrogen starvation and when lipid metabolism is disrupted [131].

Lipid droplets also have a significant role in regulating energy metabolism. This is made possible by the relatively large amount of energy stored within the neutral lipids – encased within the lipid droplets core. Following lipolysis, the released neutral lipids offer a high-energy substrate that can be harvested for energy via β -oxidation [150]. This alternative form of chemical energy production is required when environmental conditions are altered (e.g., lack of fermentable carbon sources), this therefore ensures that cells can adapt to the fluctuating intra/extra-cellular environment. The neutral lipids, within the lipid droplet, can also act as precursor molecules for numerous biological compounds that form intracellular structures (e.g., phospholipids). The neutral lipid TAG can be used to generate molecules of DAG, following lipolysis, which itself can act as a common precursor molecule for phospholipids, such as PC [151]. This therefore highlights a role for lipid droplets in the generation of phospholipid membranes, which is essential in maintaining cell integrity and fluidity. Linked to this function, is the role that lipid droplets also have in contributing to the cell wall of yeast. Like the plasma membrane, the cell wall is required to separate the intracellular environment from the extracellular environment, this places the cell wall at the forefront of cellular components that are regularly exposed to stressors.

For this reason, the cell wall must be extremely versatile, capable of undergoing remodelling events that replenish and restore the cell wall regularly – in a similar respect to intracellular membranes [152]. For this to occur, a continuous supply of resources is required which can be provided by local lipid droplets. Specifically, through the release of TAG to produce DAG, which can then be used to produce glycosylphosphatidylinositol-modified (GPI) proteins [153]. Additional roles have also been linked to lipid droplets in regulating cell wall adaptability and stability – highlighting the depth of functionality attributed to the organelle. Lipid droplets are also thought to have an essential role in preventing oxidative damage. In many experimental studies, it has been observed that cells exposed to greater oxidative stress have higher concentrations of intracellular lipid droplets [154][155]. This may be caused by lipid droplets providing additional lipids, that can be used to repair intracellular structures that are more susceptible to oxidative damage (e.g., cellular membranes), however it has also been considered that the lipid droplets may act as reservoirs that sequester reactive oxygen species – thus preventing excessive intracellular oxidative damage [132-133].

Being linked with the ER throughout the lifespan of a cell it can be assumed that some of the function attributed to the lipid droplets are linked to the ER - one being protecting against ER stress and the associated imbalances of ER-protein folding capacity, calcium uptake and lipid homeostasis [156]. This can take the form of storing potential toxic proteins, generated during metabolic stress – aiding their removal via autophagy, alongside regulating lipid homeostasis that can be significantly disrupted by ER stress [156]. Experimental evidence has also linked lipid droplet function with autophagy in general, being needed to form auto-phagosomes, studies in yeast that have defective lipid droplet biogenesis pathways observed concurrent defective macro-autophagy mechanisms, alongside higher concentrations of aberrant proteins within their cytosol [157]. This combined function of maintaining lipid homeostasis, with regards to excess lipids, and protein homeostasis feeds into the larger function of protecting the cell against ER stress.

The dynamic nature of lipid droplets, through the active sequestering and mobilisation of neutral lipids ensures the cells needs are continuously met, through the varying environmental conditions that the cell is exposed to. The full extent of functionality attributed to the lipid droplets is still unknown which provides additional need to investigate not only the individual role the lipid droplets have within the cell, but also how this influences the wider perspective of cellular health.

1.4.4 Lipid Droplet Regulation via Mitochondrial and ER Interactions

The ubiquitous lipid droplets in the cytoplasm are regulated by many intracellular factors. A key regulator of the lipid droplets, that also facilitates a large proportion of their intracellular function is the interactions between lipid droplets and the major intracellular organelles. These organelles include the ER, mitochondria, plasma membrane, vacuoles, Golgi apparatus and endosomes [158]. The interaction with these organelles contributes significantly to the dynamic nature of lipid droplets, with the ER and mitochondria appearing to engage in some of the most significant interactions.

Interactions between lipid droplets and the ER were first observed in the 1980s [159]. Since then, the understanding of these interactions has increased. In yeast, lipid droplets remain directly associated with the ER throughout the lifespan of a cell, while mammals have been shown to have two populations, one which remains at the ER and one that migrates away [160][161]. The physical interaction between lipid droplets and ER are poorly understood, but it is thought to involve the Arf1-COPI complex. As previously described, the ER is involved in the biogenesis of lipid droplets, alongside regulating the stability of the small organelle through protein and lipid trafficking, response to ER stress and through the activity of the ER-associated degradation (ERAD) pathway. Regarding trafficking, proteins from the ER are targeted to lipid droplets to facilitate their generation and to embed within their phospholipid monolayer. These proteins include the DAG acyltransferase, Dga1, which was first observed in 2011 [162]. Due to this enzymes function, this interaction is not only necessary for lipid droplet biogenesis, but also lipid droplet growth [163]. Bridges between the ER and lipid droplets also facilitate the transfer of phospholipids and neutral lipids between the two organelles – enabling a tighter regulation of cytosolic and ER lipid content.

ER stress, independent from the classical stress response pathway, has been shown to be correlated with an increase in intracellular lipid droplet concentrations. As observed in yeast cells treated with tunicamycin or brefeldin A (inducers of ER stress) [164]. These effects are thought to reroute substrates (e.g., phosphatidic acid and DAG) for the synthesis of neutral lipids to provide a protective mechanism that prevents misfolded protein aggregation by aiding the ERAD pathway [165]. The ERAD pathway comprises numerous proteins that function in unison to maintain quality of proteins within the cell. Interestingly, there are a number of ERAD proteins that are colocalised to the ER and lipid droplets, including derlin-1, UBXD2, UBXD8, p97/VCP, and AUP1 [166][167][168].

The interactions between the ER and lipid droplets facilitate the degradation of specific proteins, most notably HMG-CoA reductase and poorly lipidated apolipoprotein B-100 [169][170]. HMG-CoA reductase, destined for degradation, copurifies with isolated lipid droplets in the presence of cholesterol, to aid the action of the ERAD pathway [170], while Apolipoprotein B-100 has been shown to accumulate around lipid droplets when degradation is inhibited – suggesting degradation is associated with the lipid droplets [169]. The importance of the interaction between the ER and lipid droplets, with regards to the ERAD pathway, was further demonstrated by inhibiting neutral lipid synthesis with triacin C – acyl-CoA synthetase inhibitor – which resulted in reduced concentration of lipid droplets and a slower rate of degradation via the ERAD pathway. Notably, the deletion of *Aup1*, a protein within the ERAD pathway, induced a reduction of lipid droplets – further highlighting the link between the organelles [171]. These findings have been identified in higher eukaryotes, while studies with yeast have suggested that the suppression of lipid droplet biogenesis had no effect on the ERAD pathway, suggesting the mechanisms of the ERAD pathway differ, however it is still plausible that both systems share common droplet elements [172].

The interactions between lipid droplets and the mitochondria are also essential in regulating the activity of both the lipid droplets and mitochondria. These junctions between the lipid droplets and mitochondria are dependent on *PLIN5* [173], which has been shown to act as a key barrier to lipolysis. This has been demonstrated by deletion of *PLIN5* in animals inducing rapid loss of neutral lipids upon fasting, while

overexpression of *PLIN5* results in increased levels of neutral lipids [174]. Close interactions have been observed in a variety of cells including adipocytes, myotubes and oocytes [175]. The dynamic nature of both the lipid droplets and mitochondria are reflected in the junctions that are formed between the two organelles. It is believed that the lipid droplet-mitochondria interactions facilitate the direct flow of fatty acids, from the lipid droplet core, into the matrix of the mitochondria, to provide a substrate for β -oxidation within the mitochondria. Notably, the discovery of fatty acid reacylation enzymes within the mitochondria suggests two-way trafficking of lipids may exist [176]. The lipid droplet-mitochondria interactions are particularly beneficial during starvation.

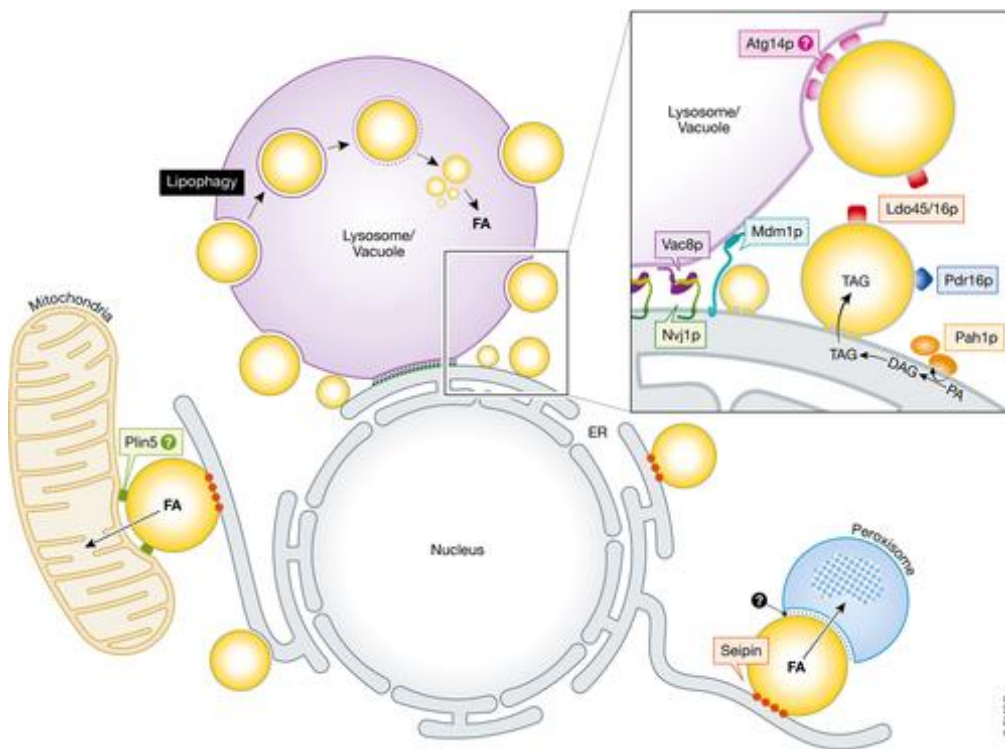


Figure 17: Schematic diagram showing the interaction between lipid droplet, the mitochondria and the ER – diagram taken from Henne, W.M., Reese, M.L. et al 2018.

Due to the significant interactions between the lipid droplets, ER and mitochondria, any structural or functional changes to any of these organelles would have significant effects on the other organelles, which can then indirectly affect overall cellular health, by altering the state of health associated with the individual organelles.

1.5 Study Objectives

The detrimental effects of mitochondrial dysfunction on cellular health have already been detailed and linked to the development and progress of degenerative diseases within multicellular organism, including neurodegeneration (e.g., Alzheimer's disease and Parkinson's disease). However, the state of lipid metabolism and homeostasis, alongside the directly and indirectly associated cellular processes, has yet to be described and could lead to a greater understanding of intracellular mechanisms and pathways associated with mitochondrial dysfunction. The aims of this study therefore include:

- 1) Analyse the state of lipid metabolism and homeostasis, through the observation of intracellular lipid droplets.**
- 2) Investigate if lipid droplet biogenesis is Ras signalling dependent or independent.**
- 3) Investigate the role that NADPH oxidase (Yno1) has within the biogenesis and regulation of lipid droplets.**

Chapter 2:

Materials and Methods

2.1 Yeast Strains and Growth Conditions

Unless stated otherwise, all experiments conducted utilised *S. cerevisiae* strain BY4741, and respective mutant strains (Table 1). All media used was autoclaved, in a Prestige Medical bench-top autoclave, at 121°C, 15 lb/sq.in for 11 minutes. Overnight cultures were grown in yeast extract, peptone, dextrose (YPD) media (1% Bacto Yeast Extract [Difco], 2% Bactopeptone [Difco], 2% Glucose [Fisher Scientific]) in a 30°C rotary incubator – rotating at 180 RPM. All strains used in this study were maintained on YPD agar plates (1% Yeast Extract [Difco], 2% Bactopeptone [Difco], 2% Glucose [Fisher Scientific], 20% Oxoid Technical Agar No.3). pAG347/pAG354 transformants were maintained on SD-URA/LEU plates (0.675% Nitrogen Base w/o Amino Acids [Formedium], 0.193% Synthetic Dropout Kaiser Media w/o Uracil and Leucine [Formedium], 2% Glucose [Fisher Scientific], 20% Oxoid Technical Agar No.3). While pAG347/pAG354 transformant overnights were grown in SD-URA/LEU media (0.675% Nitrogen Base w/o Amino Acids [Formedium], 0.193% Synthetic Dropout Kaiser Media w/o Uracil and Leucine [Formedium], 2% Glucose [Fisher Scientific]) in a 30°C rotary incubator – rotating at 180 rpm.

Table 1: Origin and genotype for *S. cerevisiae* strains, used in this study.

Strain	Genotype	Origin
CGY424 – Wild Type	Mata <i>his3Δ1 leu2Δ met15Δ ura3Δ</i>	Horizon Discovery™ Yeast Knockout Collection
CGY862b – <i>cox4D1</i>	Mata <i>his3Δ1 leu2Δ met15Δ ura3Δ cox4d-1::HIS3</i>	Leadsham et al 2013
CGY862d – <i>cox4D2</i>	Mata <i>his3Δ1 leu2Δ met15Δ ura3Δ cox4d-2::HIS3</i>	Leadsham et al 2013
CGY638 – <i>Δcox4</i>	Mata <i>his3Δ1 leu2Δ met15Δ ura3Δ Δcox4:: HIS</i>	Leadsham et al 2013

CGY907 – Δcox4/Δras2	Mata <i>his3ΔI leu2Δ</i> <i>met15Δ ura3Δ</i> <i>Δcox4Δras2::HIS</i>	Leadsham et al 2013
CGY926 – Δras2	Mata <i>his3ΔI leu2Δ</i> <i>met15Δ ura3Δ</i> <i>Δras2::HIS</i>	Leadsham et al 2013
CGY908 – Δcox4/Δyno1	Mata <i>his3ΔI leu2Δ</i> <i>met15Δ ura3Δ</i> <i>Δyno1::KanMx</i> <i>Δcox4::HIS</i>	Leadsham et al 2013
CGY903 – Δyno1	Mata <i>his3ΔI leu2Δ</i> <i>met15Δ ura3Δ</i> <i>Δyno1::KanMx</i>	Leadsham et al 2013
(KAY836) WT	Mata <i>ura 3-52 leu 2</i> <i>his4-539</i>	Heeran et al 2004
(KAY836) RAS2	<i>Δras2::leu2</i> Mata <i>ura</i> <i>3-52 leu 2 his4-539</i>	Heeran et al 2004
(KAY836) RAS2 – ala18, val19	<i>his3ΔI leu2Δ met15Δ</i> <i>ura3Δ met15Δ RAS2</i> <i>(ala18, val19)</i>	Heeran et al 2004

2.1.1 Water Used in Study

Water used throughout this study was pure deionised water (dH₂O). This was produced by a Thermo Scientific Barnstead NanoPure Diamond Water System and then sterilised further by autoclaving.

2.2 Biochemical Methods

2.2.1 Whole Cell Protein Extraction

Overnight cultures of each strain were grown in 3 mL of YPD media under standard growth conditions and subsequently used to inoculate 3 mL of fresh YPD media and YPD media with potassium acetate (1% Bacto Yeast Extract [Difco], 2% Bactopeptone [Difco], 2% Glucose [Fisher Scientific], 1% w/v Potassium Acetate [Sigma]) at an OD600 of 0.1. Cells were then grown for 24 hours, to ensure cells had entered the stationary phase of growth. After 24 hours of growth, 1×10^8 were harvested by acquiring a new OD600 reading for each sample, using an Eppendorf Biospectrometer, to calculate the number of cells from this value, to ensure an appropriate dilution of cell can be made to achieve the desired cell number. The harvested cells were then transferred to microcentrifuge tubes [Eppendorf] and centrifuged at 4000 rpm for 5 minutes. The supernatant was then discarded, and the pelleted cells were resuspended in 200 μ L of lysis buffer (0.05 M EDTA, 0.1 M NaOH, 2% w/v SDS, 2% v/v β -mercaptoethanol), and incubated at 90°C for 10 minutes. Following incubation, 5 μ L of 4 M acetic acid was added to the samples and then samples were vortexed for 30 seconds, before being incubated for another 10 minutes, at 90°C. After the 10 minutes of incubation, 50 μ L of loading buffer (50% Glycerol, 0.25 M Tris-HCL pH 6.8, 0.05% Bromophenol Blue) was added to the samples. The samples were then centrifuged for 1 minute at 13,000 rpm in a bench microcentrifuge, prior to loading into the polyacrylamide gel.

2.2.2 Polyacrylamide Gel Electrophoresis (PAGE)

Each SDS-PAGE gel was composed of a standard 5% acrylamide stacking gel (126 mM Tris pH 8.8, 0.1% SDS, 12% Acrylamide (29:1), 0.15% Ammonium Persulphate, 0.07% TEMED) and a 7.5-12% resolving gel (240 mM Tris pH 6.8, 0.1% SDS, 4.3% Acrylamide (29:1), 0.23% Ammonium Persulphate, 0.07% TEMED) - ammonium persulphate was dissolved in water at 10% (w/v). The SDS-PAGE gels were mixed within sterile 50ml falcon tubes and then cast in 0.75 mm glass cassettes [BioRad]. The resolving gel was poured into the glass cassette, to the height of 4 cm below the top of the cassette, and then allowed to set for 30 minutes. 1 mL of isopropanol was added to the top of the

resolving gel to prevent gel exposure to the air. After 30 minutes, the isopropanol was discarded, and the stacking gel was poured in excess to fill the remaining space in the glass cassette and remove residual isopropanol. To the top of the cassette, an appropriately sized plastic comb was added to form the wells within the SDS-PAGE gel. The stacking gel was left to set for 1 hour. When the stacking gel had set, the SDS-PAGE gels contained within the glass cassettes were inserted into the protein gel tank and sealed against the central column. Following this, 1 x SDS Running buffer (0.3% (w/v) Tris-HCL, 1.44% (w/v) Glycine, 0.15% (w/v) SDS) was added to the protein gel tank to cover the SDS-PAGE gels – care was taken to avoid the accumulation of air bubbles. The plastic comb was then removed from the SDS-PAGE gel. To the first well, 5 μ L of a protein standard protein ladder (ColorPlus Marker p7709S, New England BioLabs) was loaded, followed by 10 μ L of supernatant of the samples being loaded into the subsequent wells. Any wells that remained empty after sample loading were loaded with 10 μ l of loading buffer (50% Glycerol, 0.25 M Tris-HCL pH 6.8, 0.05% Bromophenol Blue) to ensure the gel ran evenly. Electrodes of the protein gel tank were then connected to a power pack [BioRad] and a voltage of 95 V was applied for 20 minutes. When the protein front had entered the resolving gel, the voltage was increased to 135 V and ran for approximately 90 minutes, or until the protein samples had migrated and separated within the resolving gel – careful notice was taken to ensure the protein samples didn't migrate past the edge of the gel. The protein gel tank was then disconnected from the power pack, 1 x SDS Running Buffer was discarded, and the glass cassettes were removed for the gel to be used in the proceeding semi-dry transfer, for the western blot procedure.

2.2.3 Semi-Dry Transfer of Proteins to PVDF Membrane

The polyacrylamide gel containing the protein samples was removed from the glass cassettes and placed in transfer buffer (0.0058% v/v Tris Base, 0.0029% w/v Glycine, 0.00004% w/v SDS, 20% v/v Methanol). Four pieces of Whatman's extra thick blotting paper [Thermo Fisher] was then cut into 8x9cm pieces and soaked in transfer buffer. Alongside this, an 8 x 9 cm piece of Polyvinylidene difluoride membrane (PVDF) [Roche] was cut and wet with methanol, before also being placed in transfer buffer. Following 20 minutes in transfer buffer, two pieces of thick blotting paper were placed

on the anode plate of a Trans-Blot Semi-Dry Transfer Cell [BioRad], a roller was then used to remove any air bubbles present. The PVDF membrane was then placed on top of the two pieces of blotting paper, followed by the resolving layer of the polyacrylamide gel – with the stacking layer being discarded. The two remaining pieces of blotting paper were then added, and a roller was used to remove any air bubbles. The cathode plate was then clipped and locked in place over the anode plate, before being connected to the power pack. A voltage of 25 V was applied for 30 minutes, after which the PVDF membrane was removed and used for the immunoblotting procedure, while other contents were discarded

2.2.4 Immunoblotting

Following completion of the semi-dry transfer, the PVDF membrane was transferred to a 50 mL falcon tube and 10 mL of blocking solution (5% w/v Dried Skimmed Milk [Oxoid], PBS/T (Phosphate Buffered Saline, 0.2% Tween 20 [Sigma])) was added, the 50 mL falcon tube was then placed on a roller mixer [Stuart] for 45 minutes at room temperature. Following this incubation, the PVDF membrane was briefly washed twice with PBS/T, before being transferred to a fresh 50 mL falcon tube containing 10 mL of blocking solution and the appropriate concentration of primary antibody (Table 4). The 50 mL falcon tube, containing the PVDF membrane, was then placed on a roller mixer for 1 hour at room temperature. The PVDF membrane was then removed from the 50 mL falcon tube and briefly rinsed twice with PBS/T, before being incubated with PBS/T and washed via shaking for 15 minutes, at room temperature. This wash step was then followed by another two 5-minute wash steps with fresh PBS/T. The PVDF membrane was then transferred to a new 50 mL falcon tube containing 10 mL of blocking solution and the appropriate concentration of secondary antibody conjugated to Horse-Radish Peroxidase (Table 4). The 50 mL falcon tube containing the PVDF membrane was then placed on a roller mixer for 30 minutes, at room temperature. The PVDF membrane was then removed from the falcon tube and briefly rinsed with PBS/T, before commencing a 15-minute washing step with fresh PBS/T, on a roller mixer at room temperature. This was then followed by an additional two 5-minute wash steps with fresh PBS/T. The PVDF membrane was then placed in sterile 1 x PBS, in preparation for protein detection with enhanced chemiluminescence (ECL).

Table 4: Antibodies Used in this Study

Antibody	Dilution	Source
Rabbit Anti-Histone H4 (Acetylated) – Primary Antibody for the detection of H4 – acetylation	1:800	Bio-Rad, product number AHP418
Rabbit Anti-Pgk1p – Primary Antibody for the detection of Pgk1p (Loading Control)	1:5000	Supplied by Professor Mick Tuite
Anti-Rabbit IgG HRP – Secondary Antibody for the detection of H4 – acetylation and Pgk1p	1:3000	Sigma Aldrich, product number A3415

2.2.5 ECL (Enhanced Chemiluminescence) Detection

Following immunoblotting, the PVDF membrane was placed in a clean polyethylene terephthalate box, with the remaining PBS being discarded. ECL solution 1 (1 mL Luminol 250 mM (3-aminophthalhydrazide [FLUKA]), 0.44 mL p-coumaric acid 90 mM [Sigma], 10 mL 1 M Tris-HCL pH 8.5, Water to 100 mL) and ECL solution 2 (64 µL 30% Hydrogen Peroxide, 10mL 1 M Tris-HCL pH 8.5, Water to 100 mL) (Table 5) were then mixed in a 1:1 ratio and added to the PVDF membrane. After 1 minute of incubation at room temperature and constant shaking, the ECL solutions was discarded and the PVDF membrane was placed on a stage in the SYNGENE G: BOX Gel Doc System, in which luminescence was detected to visualise the western blots. The GeneSys Software (Version 1.6.5.0) was used to analyse the western blots and a Synoptics 6 MP camera was used to capture images. To calculate the band intensity relative to Pgk1p loading control, densitometry was preformed using ImageJ (Version 1.51n). The intensity values obtained were then divided by the WT value to normalise to the control.

Table 5: ECL Solution Recipes

Name	Recipe
Solution 1	1 mL luminol 250 mM (3-aminophthalhydrazide from FLUKA No. 09253) 0.44 mL p-coumaric acid 90 mM (Sigma No C9008) 10 mL 1 M Tris.HCL (pH 8.5) Water to 100 mL
Solution 2	64 μ L 30% Hydrogen Peroxide 10 mL 1 M Tris.HCL (pH8.5) Water to 100 mL

2.2.6 PVDF Membrane Stripping

Following probing with specific antibodies, the PVDF membrane could be stripped to re-probe with additional antibodies (e.g., loading control). To strip the PVDF membrane, the membrane was transferred to a 50 mL falcon tube and washed briefly with PBS/T. 10 mL of Restore PLUS Western Blot Stripping Buffer [Thermo Scientific] was then added to the 50ml falcon tube, containing the PVDF membrane, and the 50 mL falcon tube was then placed on a roller mixer for 15 minutes, at room temperature. Following this incubation, the stripping buffer was discarded and the PVDF membrane was washed briefly with PBS/T. The PVDF membrane was then ready to re-block with blocking solution before re-probing with the appropriate antibody.

2.3 Cell Biology Techniques

2.3.1 Yeast Strain Growth Assays

Overnight cultures of each strain were grown in 3 mL of YPD media, under standard growth conditions, and subsequently used to inoculate 1 mL of fresh YPD media or YPD media with potassium acetate (1% Bacto Yeast Extract [Difco], 2% Bactopeptone [Difco], 2% Glucose [Fisher Scientific], 1% v/w Potassium Acetate [Sigma]) to an OD600 reading of 0.1, with 3 technical replicates, in a sterile 24-well plate [Greiner]. The plate was then sealed with parafilm [Bemis]. Growth of yeast strains was then measured using a BMG LABTECH SPECTROstar Nano Plate Reader. The BMG LABTECH SPECTROstar Nano Plate Reader script was set to run within a set of defined parameters (Table 6) to

measure the growth rates of the strains. Three biological replicates and three technical replicates were included for each strain.

Table 6: Growth Curve Setting Parameters

Parameter	Setting
Excitation	600 nm
Shaking Frequency	400 rpm
Shaking Mode	Double Orbital
Addition Shaking Time	120 Seconds
Temperature	30°C

Analysis and processing of data generated by the BMG LABTECH SPECTROstar Nano Plate Reader, was analysed using the BMG LABTECH MARS data analysis software. This data was then exported to Microsoft Excel for further analysis. From the biological and technical repeats, the doubling time, maximum rate of growth, lag times and final OD for each strain was calculated.

2.3.2 Cell Counting (Haemocytometer)

To perform a relatively accurate cell count, a haemocytometer was used. An overnight culture was diluted to 1/10 in sterile microcentrifuge tubes [Eppendorf]. The samples were then vortexed thoroughly and 10 μ L of the sample was loaded onto the haemocytometer. A light microscope [Nikon] was then used to count the cells, using a magnification 40x. Care was taken to ensure artifacts were not counted and that only mother cells were counted. Only cells present within or on the bottom or left-hand line of the box were counted. When possible, a minimum of 300 cells were counted in the four squares of the haemocytometer avoiding counting cell that were out of the squares. The number of cells observed were then counted and multiplied by dilution factor, and then the value can be converted from μ L to mL. The value can then be divided by 100 to calculate the number of cells in the original culture, then divided again by 100 to calculate cells.ml in the diluted culture. This value can then be used to calculate the required amount of culture to plate 300 cells. Three biological replicates and three technical replicates were included for each strain.

2.3.3 Colony Forming Unit (CFU) Viability Assay

Overnight cultures of each strain were grown in 5 mL of YPD media, under standard growth conditions and then subsequently used to inoculate 3 mL of fresh YPD media or YPD media with potassium acetate (1% Bacto Yeast Extract [Difco], 2% Bactopeptone [Difco], 2% Glucose [Fisher Scientific], 1% v/w Potassium Acetate [Sigma]), at an OD600 reading of 0.1, the cells were then grown for 24 hours. After 24 hours of growth, a 1:100 dilution was made to each strain (10 μ L cell culture, 990 μ L dH₂O) within a sterile 1.5 mL microcentrifuge tube [Eppendorf]. The samples were then vortexed thoroughly and a 1:10,000 dilution was created from the previously diluted sample (10 μ L diluted cell culture, 990 μ L dH₂O) and transferred into a fresh sterile 1.5 mL microcentrifuge tube. 10 μ L of the 1:100 dilution was then applied to a haemocytometer. Based on the number of cells counted, the volume of the 1:10,000 sample dilution required to plate 300 cells was calculated. This volume was then plated transferred to YPD agar plates and streaked thoroughly. The YPD agar plates were then left to dry, before being incubated at 30°C for 48 hours. Each cell should lead to the growth of 1 colony forming unit (CFU) – with 300 CFU's indicating 100% cell viability. Following the incubation, the percentage viability was then determined by dividing the number of observed CFU's by the number of expected CFU's and multiplying by 100. For each strain three biological replicates were used, which included three technical replicates.

2.4 Microscopy and Flow Cytometry

2.4.1 Sample Preparation

Strains were grown overnight in 3 mL the appropriate media under standard growth conditions and subsequently used to inoculate 3 mL of fresh media at an OD600 of 0.1. These cells were then grown under standard growth conditions for 24 hours. The cultures were then divided into 1 mL aliquots and were either treated or left untreated (Table 7), in preparation for cell staining.

Table 7: Treatment of cells prior to staining and flow cytometry analysis

Treatment	Concentration	Duration of Treatment
No Treatment (Control)	N/A	N/A
37°C (Heat Stress)	N/A	2 Hours
H ₂ O ₂ (Oxidative Stress)	0.1 mM	2 Hours
Cu ₂ SO ₄	0.1 mM	2 Hours

2.4.1.1 LD540 Staining of Lipid Droplets

The lipophilic dye, LD540, was used to stain lipid droplets. Following the 24 hours of growth, cultures were divided into 200 µL aliquots and transferred into 1.5 mL micro centrifuge tubes [Eppendorf]. Samples were then centrifuged for 1 minute at 10,000 rpm and the supernatant was discarded. Pelleted cells were then re-suspended in 200 µL of 1 x phosphate buffered saline (PBS) (10x PBS pH 7.4- 8% NaCl, 0.2% potassium chloride [KCl], 1.44% Sodium phosphate dibasic [Na₂HPO₄], 0.24% Potassium phosphate dibasic [KH₂PO₄], before being centrifuged – with the previous step being repeated. With the pelleted cells now re-suspended, 0.2 µL of 0.5 mg/mL LD540 was added to the sample – taking care to prevent photo bleaching. Samples were then centrifuged for 1 minute at 10,000 rpm and left to stand for 1 minute. The supernatants were then discarded, and the pelleted cells were re-suspended in 50 µL of 1 x PBS.

2.4.1.2 Bodipy and Propidium Iodide (PI) Staining

The combination of the Bodipy and propidium iodide stains are used to identify lipid droplets and necrotic cell population, respectively. Following 24 hours of growth, 3 x 10⁷ cells were harvested and re-suspended in 1 mL of PBS, in a fresh 15 mL falcon tube. The re-suspended cells were then treated as appropriate (Table 7). Following treatment, samples were centrifuged at 4000 rpm for 5 minutes with the supernatant being discarded. The remaining cells were then re-suspended in either 1 mL of 4 µM of Bodipy or 1 mL of fresh PBS, depending on whether the cells are an experimental sample or negative control, respectively. The samples were then incubated at 30°C for 15 minutes, taking care to prevent

photo bleaching. After 15 minutes, the samples were then centrifuged again for 5 minutes at 4000 rpm, with the supernatant being discarded. Pelleted cells were then re-suspended in 4mg/ml of propidium iodide, before being centrifuged again for 5 minutes at 4000 rpm. The supernatant was then discarded, and the samples were re-suspended in 50 μ L of PBS. A positive control was used for PI staining of each strain, in which cells were heated at 90°C for 10 minutes to ensure cell necrosis would be observable. The samples were then analysed in the same manner as previous samples.

2.4.2 Microscopy Slide Preparation

Samples were vortexed thoroughly, to ensure even distribution of cells, before 2 μ L of the sample was pipetted onto a clean microscope slide [Thermo Scientific]. To the microscope slide, a 22 mm by 22 mm cover slip [Fisher Scientific] was carefully lowered onto the microscope slide to ensure the sample was covered and no air bubbles were present. No additional sealants were required to fix the cover slip to the slide.

2.4.3 Fluorescence Microscopy

An Olympus IX81 inverted microscope, coupled with an Olympus 100x objective lens, was used to observe cells. To aid observations, Olympus Immoil – F30CC immersion oil was applied to the lens. A CoolLED pE4000 illumination system provided the light source and images were captured using an Andor's Zyla 4.2 PLUS sCMOS camera, coupled with Metamorph microscope control and analysis software. The fluorescent excitation of the stains, used during cell preparation, were observable in different fluorescent channels. LD540 with an excitation/emission wavelength of 543 nm is observable in the RFP channel, Bodipy with an excitation/emission wavelength of 493 nm and 503 nm, respectively. GFP-tagged proteins with an excitation/emission wavelength of 488/512 nm is observable in the GFP channel. For each strain, three biological replicates were conducted, and five technical replicates were utilised to obtain the images. A single bright field image was taken for each technical replicate, while Z-stack images were taken for the fluorescent microscopy for each technical replicate

– which were later compressed into a single image, based on maximum fluorescence. Images were then processed and analysed in ImageJ FIJI.

2.4.4 Cell Diameter Measurements

The global scale for the image was set for the images taken with a 100x objective lens, specifically defined by the specification of the camera and microscope used. Randomly selected cells, across images of the biological and technical replicates, were then selected for measurement in ImageJ. A line was then drawn across the widest part of the selected cell and the measure function was used to obtain a value in micrometres. 150 cells were counted for each strain, across three biological replicates and 5 technical replicates, allowing an average cell diameter for each strain to be calculated and analysed.

2.4.5 Flow Cytometry Analysis

Following sample preparation (Section: 2.6.1), a 1:20 dilution of sample to PBS was loaded into each well in a 96-well plate [Grenier]. The plate was then loaded into the benchtop flow cytometer [BD Accuri C6 Plus]. A total of 10,000 cells were analysed per sample within defined parameters based on forward scatter and side scatter profiles, alongside an addition parameter in which only singlet cells were analysed. Data was then transferred to Microsoft Excel for further analysis. Three biological replicates and three technical replicates were included for each strain.

2.5 Statistical Analysis

Unless stated otherwise, all data was analysed using Minitab software utilising ANOVA's to assess variance, in unison with post hoc Tukey tests to test for statistical significance. Prior to analysis the distribution of data was identified utilising Minitab software, so the most appropriate statistical tests could be used. Standard deviation of the data sets was also used to generate error bars, alongside being used when standardising data, using Z-scores.

Chapter 3:

Results

3.1.1 Part 1: Introduction

Based on unpublished data from the Gourlay Lab, a proposed link was described that coupled the intracellular levels of acetyl-CoA with the modification of histones and subsequently, the initiation of the Ras-dependent ROS production pathway, involving NADPH oxidase, Yno1. In the unpublished study, acetyl-CoA is described as an acetyl donor that can, amongst other targets, acetylate lysine residues of histones of the DNA. These histone modifications disrupt the electrostatic interactions between the histone and the DNA strands. The reduction in electrostatic interactions allows the DNA strands to unravel, facilitating additional interactions with transcriptional machinery.

We hypothesised that a reduction of acetyl-CoA, induced by the loss of mitochondrial function, may alter the pattern of histone acetylation and that this may in turn lead to changes in transcription that promote ROS accumulation. This is suggested as a bromodomain-containing protein, that binds to acetylated histones, called Bdf1, is essential for ROS accumulation in cells lacking COX function [81]. In cells lacking COX function, Bdf1 translocates from the nucleus to the mitochondria, suggesting a communicatory link between the mitochondria and nucleus. Interestingly, the addition of potassium acetate (KAc), which can increase intracellular concentrations of Acetyl-CoA, has been shown to reduce or delay increases in intracellular ROS levels, within cells lacking COX function, further supporting the proposed link. Therefore, the initial experiments in this study were aimed at identifying how the levels of histone 4 (H4) acetylation was affected by loss of COX function in the mitochondria, in order to determine if the level of histone acetylation, was linked to both intracellular acetyl-CoA concentrations and the initiation of the Ras-dependent ROS production via the NADPH oxidase Yno1. The initial experiments were also intended to detail the mechanisms of action of KAc, regarding inducing the reduction of intracellular ROS, while also determining if the supplementation of KAc had any significant effect of growth and/or viability of cells with loss of COX function.

3.1.2 Assessing the level of Histone 4 (H4) Acetylation within cells with partial or full loss of COX function.

Western blot analysis was used to identify and quantify the levels of acetylation to H4 across cells with varying levels of mitochondrial dysfunction – WT, *cox4D1*, *cox4D2* and Δ *cox4* strains – using an anti-acetylated H4 antibody probe (Figure 18). The *cox4D1* and *cox4D2* strains were generated by destabilising *cox4* mRNA – this was achieved by inserting a 3' prime extension into the untranslated region of *cox4* mRNA which induced mRNA destabilisation and more rapid degradation of the mRNA, leading to an altered basal Cox4 protein level [81]. *cox4D1* exhibits a 60% reduction of Cox4 protein, while *cox4D2* exhibited a 96% reduction in Cox4 protein. Δ *cox4* is the full gene deletion. These alterations in Cox4 directly inhibit oxidative phosphorylation, therefore altering the metabolic activity of the mitochondria – inducing mitochondrial dysfunction. The strains were grown in standard YPD media and YPD media supplemented with Kac. The aim of which was to initially determine if the level of H4 acetylation were altered in cells with mitochondrial dysfunction, alongside determining whether the phenotype, if present, could be rescued by the addition of KAc.

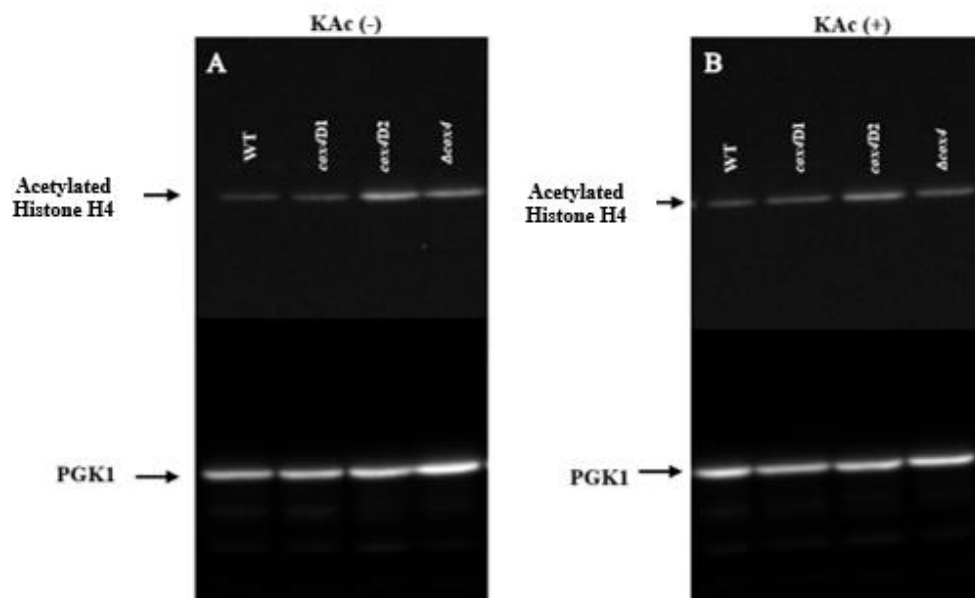


Figure 18: Western blot image showing the level of H4 acetylation in WT, *cox4D1*, *cox4D2* and Δ *cox4* cells. A) Samples of WT, *cox4D1*, *cox4D2* and Δ *cox4* cells were visualised in stationary phase, after 24 hours of growth in YPD media, to detect levels of H4 acetylation. B) Samples of WT, *cox4D1*, *cox4D2* and Δ *cox4* cells were visualised in stationary phase, after 24 hours of growth in YPD media supplemented with KAc, to detect levels of H4 acetylation. Both western blots were probed with a Pgc1 antibody loading control to allow results to be normalised.

Visualisation of the western blot (Figure 18) indicated that H4 acetylation was increased in cells with mitochondrial dysfunction greater than 96%, relative to wild type and in the absence of KAc. However, there appears to be a reduction in H4 acetylation in the Δcox4 cells, compared to the cox4D2 cells. Comparatively, the addition of KAc appeared to reduce the level of H4 acetylation across all cells. As KAc can act as a substrate to generate Acetyl-CoA the reduction of H4 acetylation observed suggests that intracellular levels of Acetyl-CoA had no significant effect on these specific histone modifications. To confirm these findings, and overcome the subjectivity of the western blot images, densitometry was used to measure the fluorescent intensity of the western blot bands (Figure 19). This data was then analysed following normalisation based on a P_{gk1} loading control.

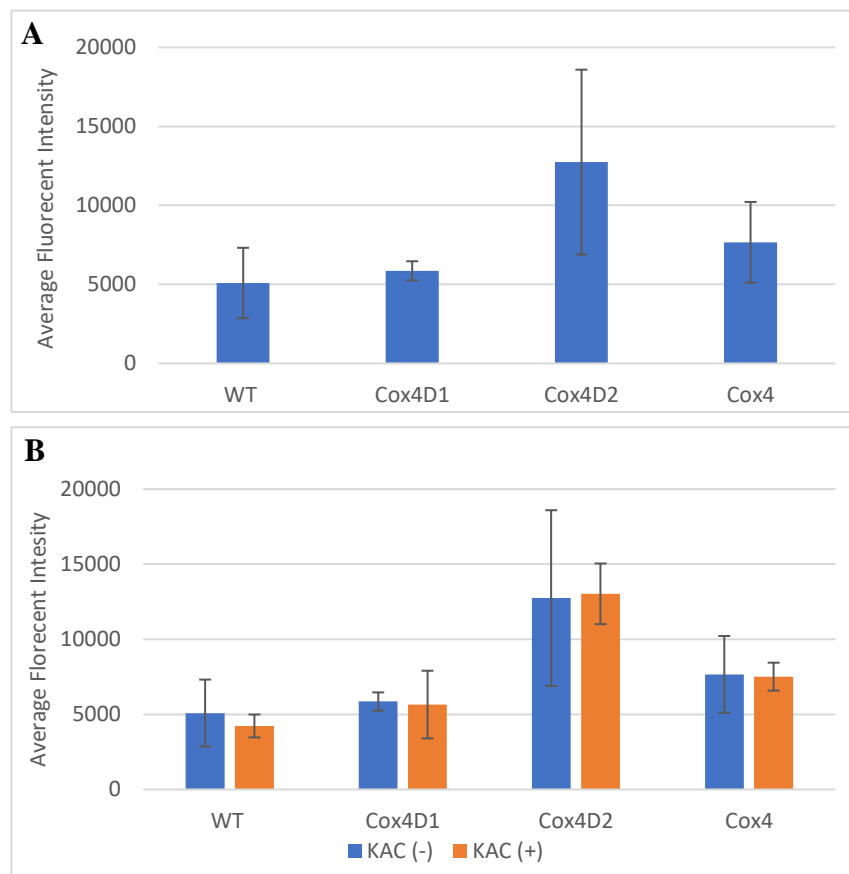
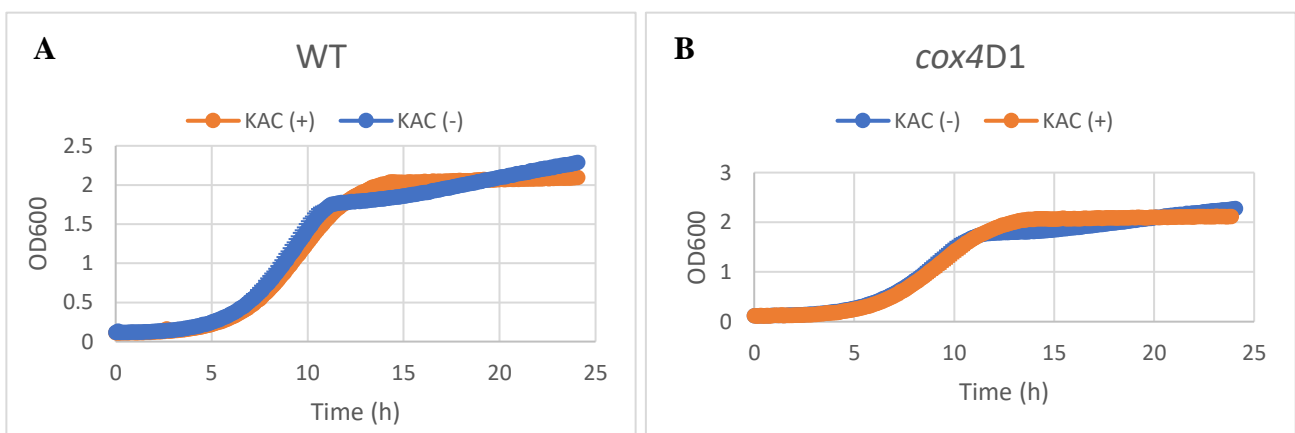


Figure 19: Graph showing the average fluorescent intensity of anti-H4 acetylation bands visualised during western blot analysis, in WT, cox4D1 , cox4D2 and Δcox4 cells, with and without KAc supplementation. (A) Strains without KAc (B) Comparison of the strains with and without KAc. Data are means \pm SEM of three biological replicates. Error bars represent the standard deviation of the data set. A one-way ANOVA with a post hoc Tukey analysis was performed on the data set in Figure 19A, while a two-way ANOVA was used for the analysis of data in Figure 19B.

The average fluorescent intensity of the western blot bands (Figure 19) highlighted no significant increase in fluorescence for any of the strains, in the absence of KAc. The strains with greater levels of mitochondrial dysfunction (*cox4D2* and Δ *cox4*) appeared to show increased fluorescence, however the spread of data prevented significance from being determined. With regards to the comparison of the KAc treated and untreated cells, no significant difference could be observed in the treated strains, relative to untreated strains. This finding in concurrence with the western blot images, suggest that increasing intracellular levels of Acetyl-CoA via supplementation with KAc does not reduce H4 acetylation in cells with mitochondrial dysfunction.

3.1.3 Effects of KAc supplementation on growth of *S. cerevisiae* cells with impaired or loss of COX function.

With KAc having no significant effect on rescuing H4 acetylation in cells with mitochondrial dysfunction and with it being shown in unpublished data from the Gourlay lab that intracellular ROS concentration are decreased by KAc supplementation, we wished to determine if KAc supplementation alter the growth of our strains. The purpose of this was to give some indication into how significant this reduction in ROS was on growth capabilities of our strains. The growth of WT, *cox4D1*, *cox4D2* and Δ *cox4* cells was analysed over a 24-hour period in YPD media and YPD media supplemented with KAc (Figure 20).



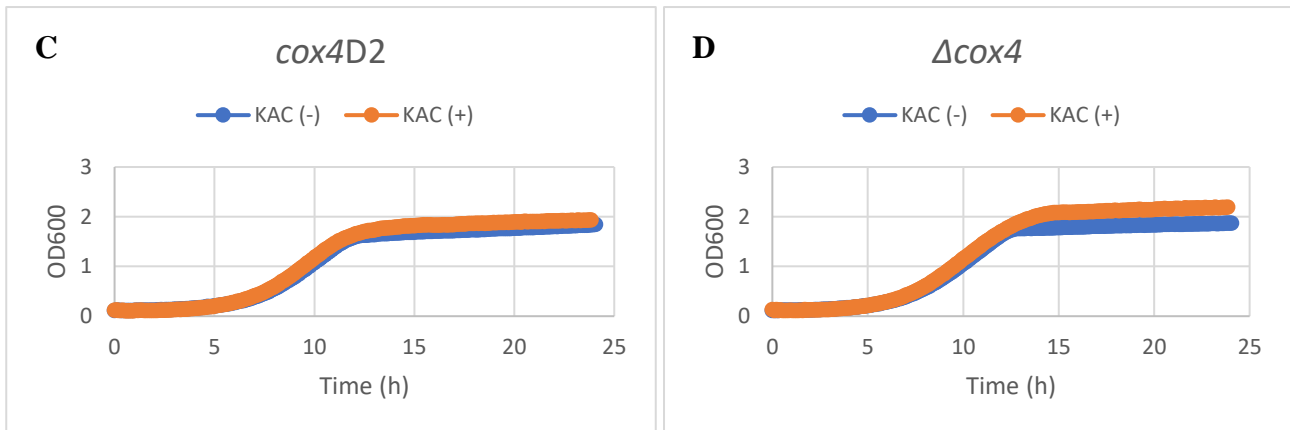


Figure 20: Growth analysis of *S. cerevisiae* strains over 24-hours, grown in YPD media and YPD media with KAc (as described in materials and methods). (A) Wild type cells, (B) *cox4D1* cells, (C) *cox4D2* cells, and (D) Δ *cox4* cells. The data represents the average of three biological replicates and three technical replicates, while error bars represent the standard deviation of the data set. (Orange) KAc supplemented cells, (Blue) Untreated cells.

Comparing the growth data of the wild type and *cox4* mutants individually, with and without KAc supplementation (Figure 20), suggested that there were minor alterations to the growth rates and growth capacities within the different strains following the addition of KAc. The growth capacity of the Δ *cox4* cells treated with KAc appeared to be increased compared to no supplementation, this seemed to also be observed in the *cox4D2* strain, however to a lesser extent. While the wild type and *cox4D1* strains appeared to display no considerable differences during the 24 hours of growth. The absence of change in the growth pattern of these cells, likely highlights that the cells are still able to withstand energy requirements and intracellular ROS levels, even with the 60% reduction of COX function. Contrastingly, in the strains with 96% and greater reduction in COX function, the energetic restraints and elevated levels of ROS are likely too great to prevent disruption to the growth rates and capacity in these strains, until the addition of KAc is provided to alleviate levels of intracellular ROS – which has been shown in other unpublished data from the Gourlay lab. Additional analysis would be required to confirm and determine the level of significance that the KAc supplementation has on the individual strains included in these growth assays.

3.1.4 Effects of KAc supplementation on the viability of *S. cerevisiae* cells with impaired or loss of COX function.

Following investigations into the growth rate of the wild type and *cox4* mutants, with and without the supplementation of KAc, we wished to determine if KAc supplementation influenced cell viability in any manner. To achieve this, cell viability assays were conducted, in which a total of 300 cells of each strain were assessed in their capabilities to form colony forming units, following 24 hours of growth, with or without KAc supplementation (Figure 21). Determining the viability of the different strains would prove to be beneficial in increase general understanding of the strains, while also indicating if the viability of the *cox4D2* and Δ *cox4* cells had any influence on the previous findings of this study.

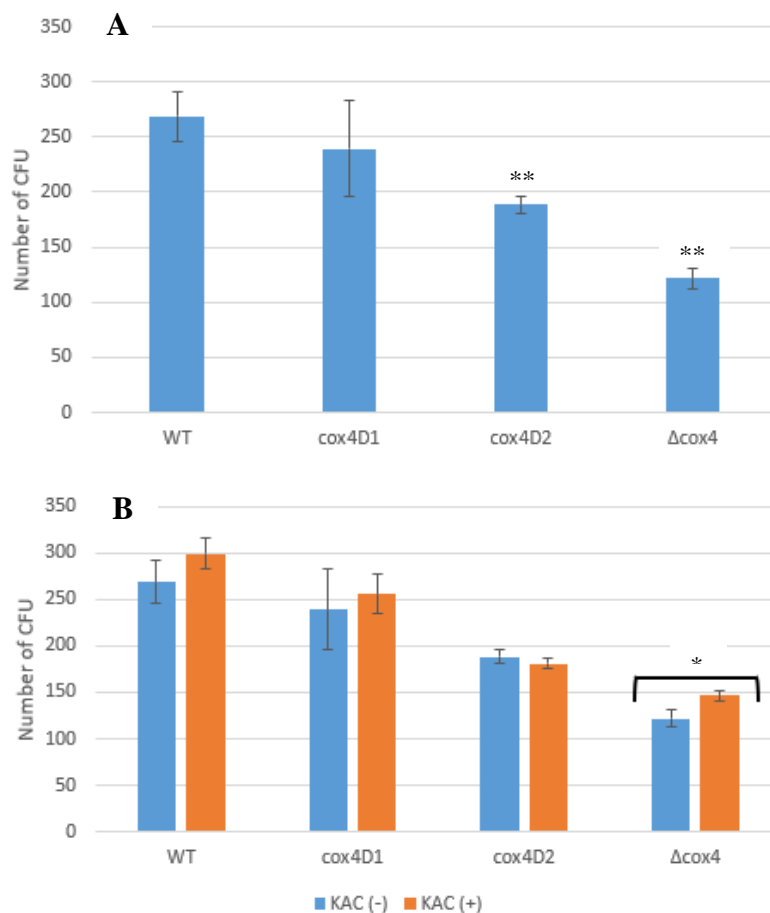


Figure 21: Graph showing the number of cell forming units (CFU) for the WT, *cox4D1*, *cox4D2* and Δ *cox4* cells, following a CFU assay. A total of 300 cells were streaked on YPD agar and grown for 24-48 hours, under standard growth conditions. (A) Strains without KAc (B) Comparison of the strains with and without KAc. Data are means \pm SEM of three biological replicates and three technical replicates. Error bars represent the standard deviation of the data set. A one-way ANOVA with a post hoc Tukey analysis was performed on the data set in Figure 21A, while a two-way ANOVA was used for the analysis of data in Figure 21B. *, $P > 0.05$. **, $P > 0.005$.

A significant loss of viability was observed as mitochondrial dysfunction increased above 96%, as in the *cox4D2* cells, relative to wild type cells. While levels of mitochondrial dysfunction below 95%, in the *cox4D1* strain, had negligible effect on cell viability. Following the KAc addition, the individual WT, *cox4D1* and *cox4D2* cells strains showed no significant changes in viability following the addition of KAc. However, the Δ *cox4* cells showed a significant increase in viability following KAc supplementation.

3.1.5 Conclusions

Findings from the initial investigations appeared to show that H4 acetylation was increased in strains with increased mitochondrial dysfunction, induced by 96% and greater reduction in COX function. This was concurrent with unpublished data from the Gourlay lab, however based on this data it was hypothesised that alterations to intracellular acetyl-CoA concentrations was the major driver in this change in acetylation. However, findings from this study indicated that alterations to intracellular acetyl-CoA concentration, via supplementation with KAc, have no significant effect on H4 acetylation when compared to the same untreated strains. This therefore suggests that the histone modification associated with the initiation of the Ras dependent ROS production by Yno1 was not driven by intracellular acetyl-CoA concentration directly, and instead another unknown mechanism is likely at play. Regarding the growth assay and cell viability data, as expected both were decreased in the *cox4* mutants with that had 96% reduction in COX function, relative to wild type – likely resulting from the increased intracellular ROS that is observed within these strains. Following the supplementation of KAc the only significant changes observed was in an increase in viability in the Δ *cox4* cells, which is to be expected as the supplementation of KAc is known to reduce intracellular ROS. Interestingly, no significant change was observed in in the *cox4D2* cells viability, while as expected no significant differences were observed in the wild type or *cox4D1* strains either. Similarly, no significant changes were observed in the growth assays due to lack of further statistical analysis, however the data appeared to suggest that KAc supplementation did increase the growth rate and capability of the *cox4D2* and Δ *cox4* cells.

3.2.1 Part 2: Introduction

Cellular health, adaptability and survival is coordinated by the function of the numerous organelles within eukaryotes, alongside the intricate interaction that occur between these organelles. An example of this, is the interactions shared between mitochondria and lipid droplets, with the lipid droplets providing the fatty acid (FA) substrate for β -oxidation and the mitochondria acting as the primary location of lipid degradation. In recent times, the interactions between the mitochondria and lipid droplets have been shown to be essential in coordinating the appropriate function of each of these organelles. With the lipid droplets being central in regulating lipid metabolism within the cell, the requirement for efficient interactions with the mitochondria are exemplified, with detrimental effects on cellular health being incurred if absent. Regulation of lipid metabolism has been shown to prevent cellular lipotoxicity [178], which in higher eukaryotes has been associated with the development of insulin resistance in skeletal muscle and heart dysfunction in obese and diabetic individuals.

Alongside the interactions between the mitochondria and lipid droplets, Ras signalling has been linked to the regulation and control of lipid droplets throughout the lifespan of the cell, through relatively unknown mechanisms [195-198]. Furthermore, considering that mitochondrial dysfunction, induced by loss of COX function, has been shown to induce an increase in intracellular ROS, resulting from aberrant Ras signalling, the wider perspective of the interactions between the mitochondria and lipid droplets, intertwined with Ras signalling becomes a major point of interest. Therefore, we wished to determine whether loss of COX function, of the mitochondria, and the consequential loss in Ras signalling regulation leads to changes in LD control and cell health.

3.2.2 Investigating the effect that increased levels of mitochondrial dysfunction have on the growth of *S. cerevisiae* cells, under standard growth conditions.

The state of lipid metabolism and homeostasis is constantly changing within the intracellular environment, to ensure cells can withstand and meet the nutritional and energetic requirements of growth, adaptability, and survival. So, prior to the investigations related to lipid droplet homeostasis, a general overview of growth in the WT, *cox4D1*, *cox4D2* and Δ *cox4* cells, under standard growth conditions, was conducted (Figure 22).

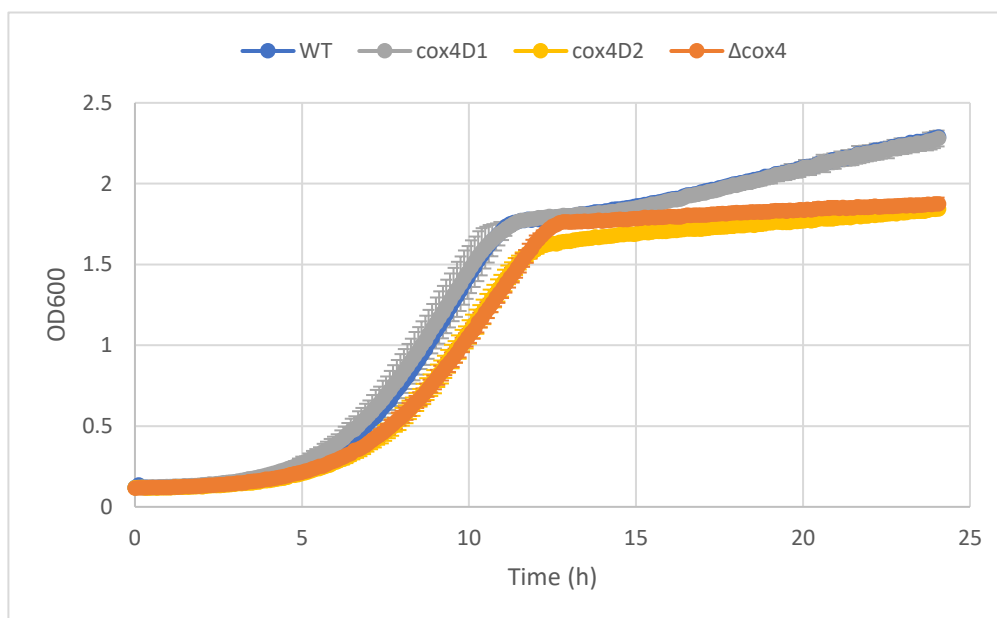


Figure 22: Growth analysis of *S. cerevisiae* strains over 24-hours, grown in YPD media, under standard growth conditions. The data represents the average of three biological replicates and three technical replicates, while error bars represent the standard deviation. (Blue) Wild Type, (Grey) *cox4D1*, (Yellow) *cox4D2*, and (Orange) Δ *cox4*.

Distinct phenotypes between the different mutants can be observed throughout the stages of growth across the 24-hour period. In cells with mitochondrial dysfunction, due to loss of $\geq 96\%$ *cox4* functionality and greater, the entry into the exponential growth phase was delayed, relative to wild type cells. Difference between the *cox4D2* and Δ *cox4* cells were negligible, however, the *cox4D2* strain seemed to exit the exponential phase of growth earlier than the *cox4* strain. The total growth capacity

of the *cox4D2* and Δ *cox4* cells was also reduced compared to wild type, highlighting the detrimental effect of the loss of mitochondrial function in these cells.

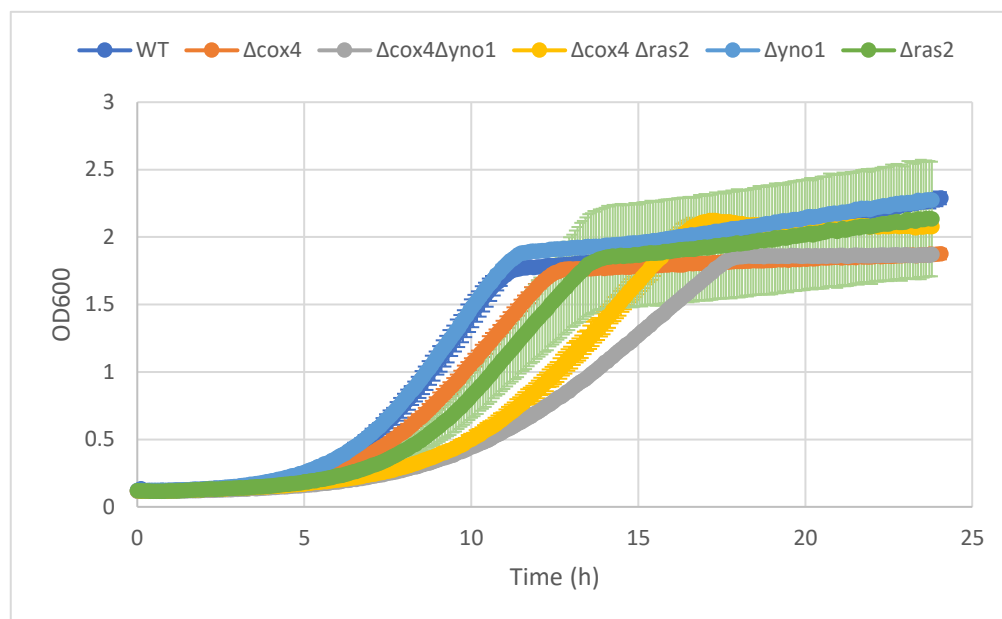


Figure 23: Growth analysis of *S. cerevisiae* strains over 24-hours, grown in YPD media, under standard growth conditions. The data represents the average of three biological replicates and three technical replicates, while error bars represent the standard deviation. (Dark Blue) Wild Type, (Orange) Δ *cox4*, (Grey) Δ *cox4* Δ *yno1*, (Yellow) Δ *cox4* Δ *ras2*, (Light Blue) Δ *yno1* and (Green) Δ *ras2*.

Additionally, the growth assays comparing the wild type, Δ *cox4*, Δ *cox4* Δ *yno1*, Δ *cox4* Δ *ras2*, Δ *yno1* and Δ *ras2* cells (Figure 23), appeared to show that the Δ *cox4* Δ *yno1* cells were delayed in their entry into the exponential phase of growth. Furthermore, the Δ *cox4* Δ *yno1* cells appeared to show a decreased rate of growth, when compared to the Δ *cox4* mutant, however the overall growth capacity remained similar. The Δ *cox4* Δ *ras2* cells also appeared to show entry into the exponential growth phase, however a longer duration of this growth phase, when compared to WT and Δ *cox4* cells, which is likely caused by the loss of *Δras2* which is instrumental in coordinating cell growth. However, the Δ *cox4* Δ *ras2* cells appeared to obtain a higher cell density compared to Δ *cox4* and Δ *cox4* Δ *yno1*, following the 24-hours of growth. Contrastingly, the Δ *yno1* and Δ *ras2* cells appeared to show a similar final cell density, relative to WT, alongside a similar trend of growth. This data therefore appears to also highlight the detrimental effects of mitochondrial dysfunction on the growth these strains. For the data of both growth assays (Figure 22/23), additional analysis would be required to confirm and determine the level of significance between the growth trends of the different strains.

3.2.3 Investigating the effect that increased levels of mitochondrial dysfunction have on the viability of *S. cerevisiae* cells, under standard growth conditions.

To finalise the overview of the wild type, *cox4D1*, *cox4D2*, Δ *cox4*, Δ *cox4* Δ *yno1*, Δ *cox4* Δ *ras2*, Δ *yno1* and Δ *ras2* cells, the viability of these cells was assessed (Figure 25). Based on identifying the number of cells that were able to form colonies, from a total of 300 cells, on YPD agar, following incubation of 24-48 hours, under standard growth conditions.

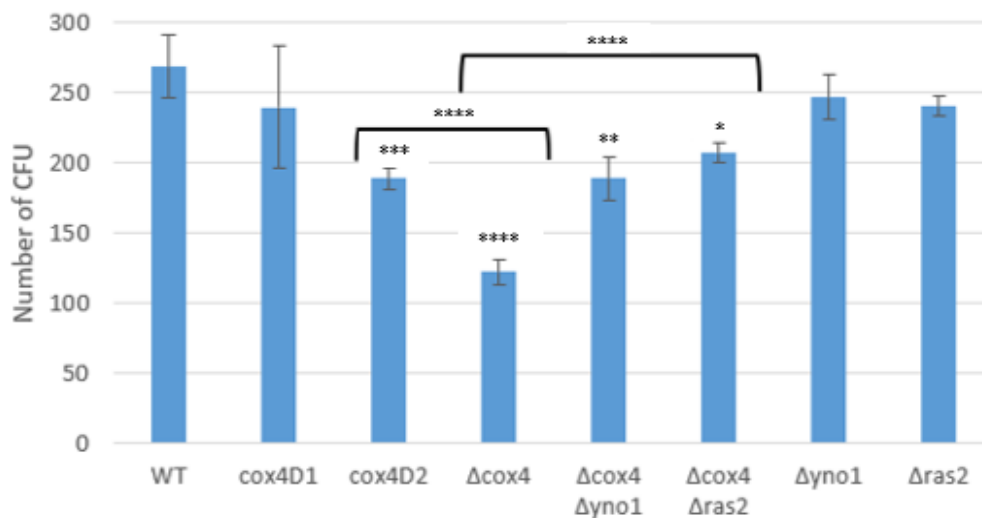


Figure 24: Graph showing the viability of cells, grown on YPD agar over a period of 24-48 hours, under standard growth conditions. The data are \pm SEM of three biological replicates and three technical replicates. A one-way ANOVA with a post hoc Tukey analysis was performed across the data set. *, $P \geq 0.05$ **, $P \geq 0.01$ ***, $P \geq 0.005$ **** $P \geq 0.001$.

Notably, the data highlights a significant reduction in viability of cells with mitochondrial dysfunction, with a trend of decline observed across the *cox4* single mutants, relative to wild type. This viability is partially rescued following the deletion of *yno1* and *ras2* in the *cox4* mutant cells, however these cells still display reduced viability, relative to wild type. Notably, a greater reduction in viability is observed in the Δ *cox4* cells, compared to *cox4D2* cells, even though *cox4D2* is a 96% reduction in COX function. While the Δ *yno1* and Δ *ras2* cells both had no significant changes in viability, relative to wild type. These findings were to be expected as the *cox4* mutants have increased intracellular ROS compared to wild type, which can be detrimental to cellular health.

3.2.4 Investigating the effects of partial and full loss of COX function on levels of intracellular lipid droplets.

Upon gaining a better understanding of the strains being used, we wished to determine the state of lipid metabolism within the cells, via the observation of lipid droplets. So, therefore initial investigations were centred around determining the LD number or distribution was altered in the wild type, *cox4D1*, *cox4D2*, Δ *cox4*, Δ *cox4* Δ *yno1*, Δ *cox4* Δ *aras2*, *yno1* and *aras2* cells. Intracellular lipid droplets were visualised by staining cells with LD540, which is a lipophilic dye that binds to neutral lipids, and then visualised using fluorescent microscopy. The number of lipid droplets were then quantified by counting. A representative selection of cells is shown Figure 26 and the lipid droplet count is shown in Figure 27.

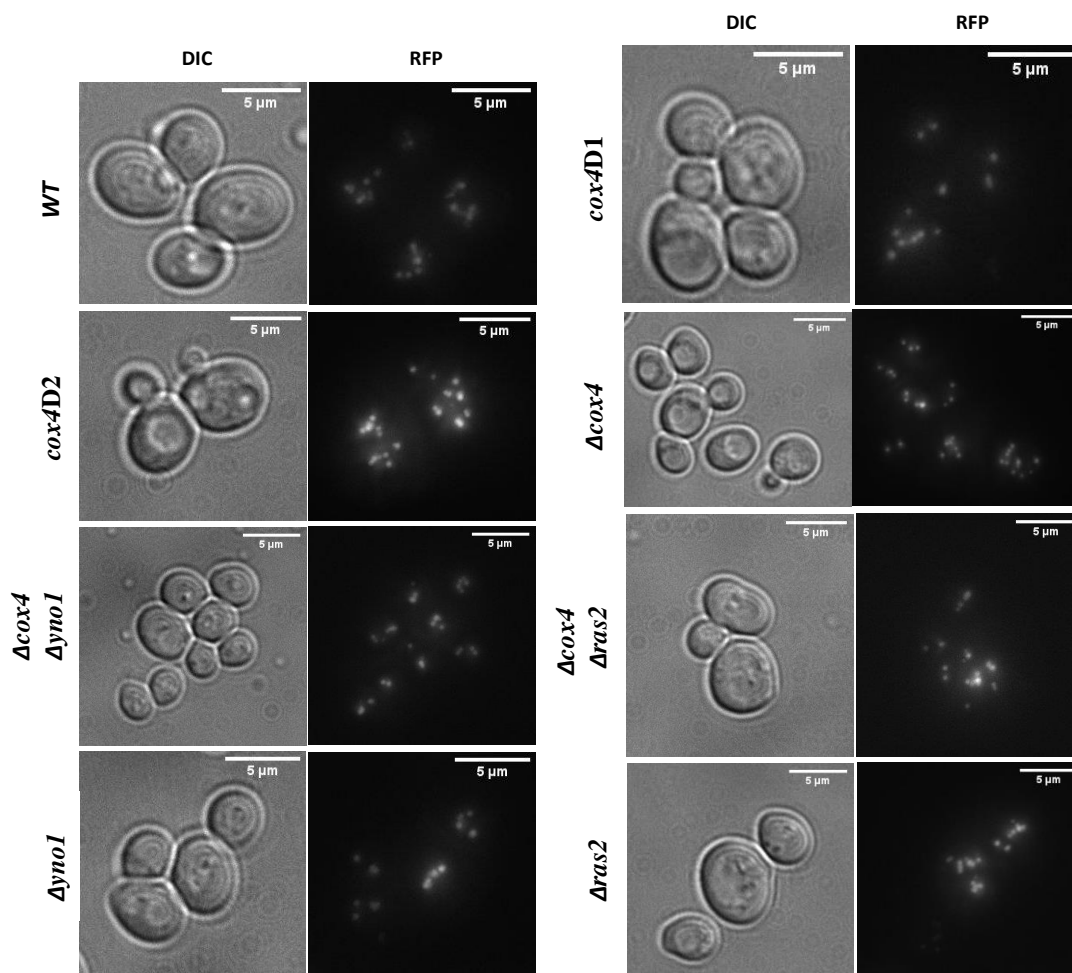


Figure 25: Fluorescence microscopy images of wild type, *cox4D1*, *cox4D2*, Δ *cox4*, Δ *cox4* Δ *yno1*, Δ *cox4* Δ *aras2*, *yno1* and *aras2* cells. Cells were stained with LD540 which is a lipophilic dye that binds to neutral lipids, following 24-hours of growth, under standard growth conditions. Three biological replicates and five technical replicates were utilised. Images were analysed using ImageJ. DIC images were provided as a control reference.

Relative to wild type, the *cox4D2* and Δ *cox4* cells showed increased levels of lipid droplets, alongside a brighter visible fluorescent signal. Comparatively, the *cox4D2* cells had relatively higher levels of lipid droplets, relative to the Δ *cox4* cells (Figure 26/27). Interestingly, the deletion of *yno1* in the Δ *cox4* mutant led to a reduction in lipid droplet content and fluorescent signal, displayed in the images. Similarly, the deletion of *ras2* in the Δ *cox4* cells also resulted in reduced intracellular lipid droplet content and fluorescent signal, within cells. The Δ *yno1* cells shared a similar phenotype with wild type and *cox4D1* cells, while the Δ *ras2* cells show an increased number of lipid droplets, relative to wild type – however, the fluorescent signal remains similar. A limitation of the microscopy images is that the analysis is primarily based on subjectivity, so to overcome this the average number of lipid droplets, across the biological replicates, was calculated to quantify the data (Figure 27).

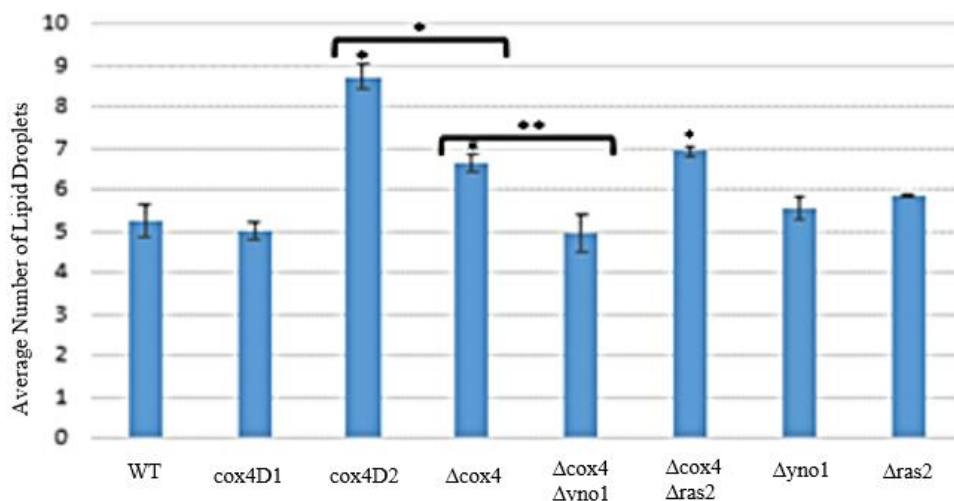


Figure 26: Graph showing the average number of intracellular lipid droplets, within wild type, *cox4D1*, *cox4D2*, Δ *cox4*, Δ *cox4* Δ *yno1*, Δ *cox4* Δ *ras2*, Δ *yno1* and Δ *ras2* cells. Lipid droplets were counted from images obtained after 24-hours of growth and following LD540 staining. The data are \pm SEM of three biological replicates and three technical replicates. A one-way ANOVA with a post hoc Tukey analysis was performed across the data set. *, $P < 0.005$. **, $P \leq 0.001$.

Quantification of the lipid droplets (Figure 27) highlighted a significant increase in the number of lipid droplets observed between the Δ *cox4* mutants, relative to wild type cells, with the most lipid droplets being observed in the *cox4D2* cells. The Δ *cox4* Δ *ras2* cells also show a similar number of lipid droplets to the Δ *cox4* cells. However, the deletion of *yno1* in the Δ *cox4* mutant shows a reduction of lipid droplets, as shown with the previous microscopy images, that restores numbers observed within wild type cells (Figure 26). The wild type, *cox4D1*, Δ *yno1* and Δ *ras2* cells, all showed similar numbers of

lipid droplets, indicating no significant difference induced by gene deletions. The quantification of lipid droplets represents half the story, as the images and number of lipid droplets fail to provide insight into the concentration of the neutral lipid content of cells. To obtain this data, cells stained with an LD540 dye, were analysed using flow cytometry, to determine the fluorescent intensity of the wild type, *cox4D1*, *cox4D2*, Δ *cox4*, Δ *cox4* Δ *yno1*, Δ *cox4* Δ *ras2*, *yno1* and Δ *ras2* cells (Figure 28).

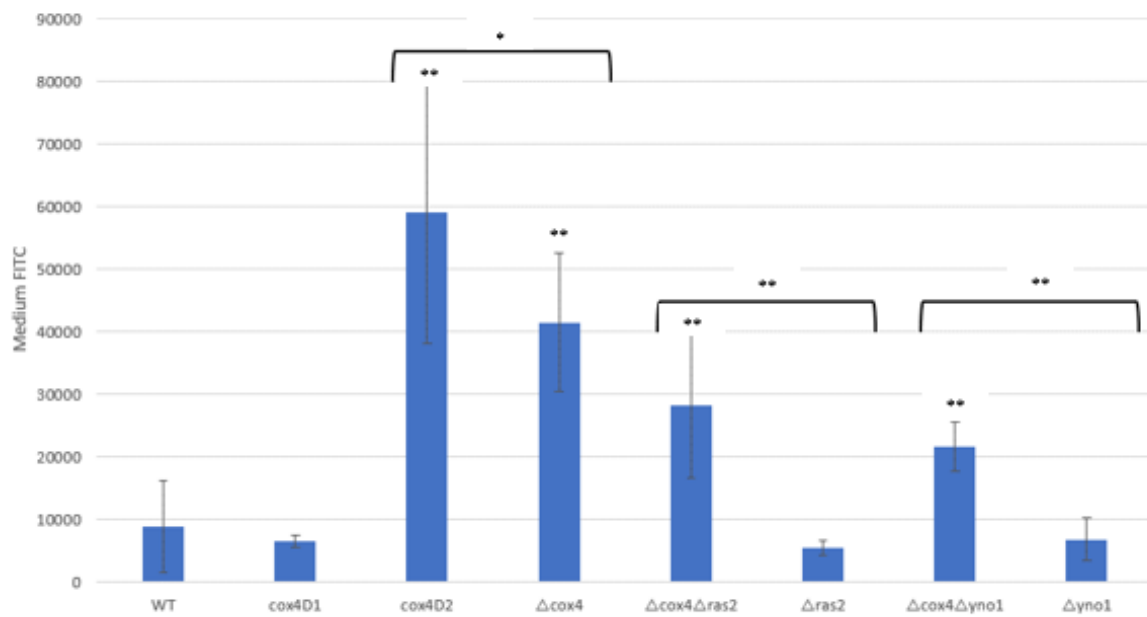


Figure 27: Average fluorescent intensity of stained intracellular neutral lipids in wild type, *cox4D1*, *cox4D2*, Δ *cox4*, Δ *cox4* Δ *yno1*, Δ *cox4* Δ *ras2*, *yno1* and Δ *ras2* cells. Lipid droplet fluorescent intensity was measured in live cells, grown for 24-hour under standard condition, utilising an LD540 stain, coupled with a BD Accuri™ C6 Plus flow cytometer. 10,000 cells per sample were analysed. The data are \pm SEM of five biological replicates and three technical replicate. A one-way ANOVA with a post hoc Tukey analysis was performed across the data set. *, $P < 0.01$. **, $P < 0.001$.

Concurrent with the previous findings, the *cox4D2* and Δ *cox4* cells had significantly higher concentration of neutral lipids, relative to wild type, with Δ *cox4* cells having reduce neutral lipid content, relative to *cox4D2*. Interestingly, as also shown by previous findings, the deletion of *ras2* reduced the levels of neutral lipids within cells relative to the single Δ *cox4* mutant, which was also shown in the Δ *cox4* Δ *yno1* double mutant. These findings suggest that *ras2* and/or *yno1* may be essential in coordinating lipid droplet biogenesis and/or regulating lipid droplet homeostasis.

3.2.5 Analysis of growth in WT and *ras2* mutants, under standard growth conditions.

With previous results suggesting that Ras2 signalling may have a role in lipid droplet biogenesis, this became a focal point of our investigation. To address the hypothesis that Ras2 signalling coordinates lipid droplet biogenesis, three new strains were utilised that consisted of a new wild type, $\Delta ras2$ and a *ras2-ala18, val19* strain (constitutively active Ras2), that possesses two point-mutation. As previously shown, establishing a general profile for the strains can be beneficial when interpreting future findings, by incorporating the wider perspective of cellular growth and viability. To ascertain data regarding the growth of these new strains, growth curves were generated from cells grown for 24-hours, under standard growth conditions (Figure 29).

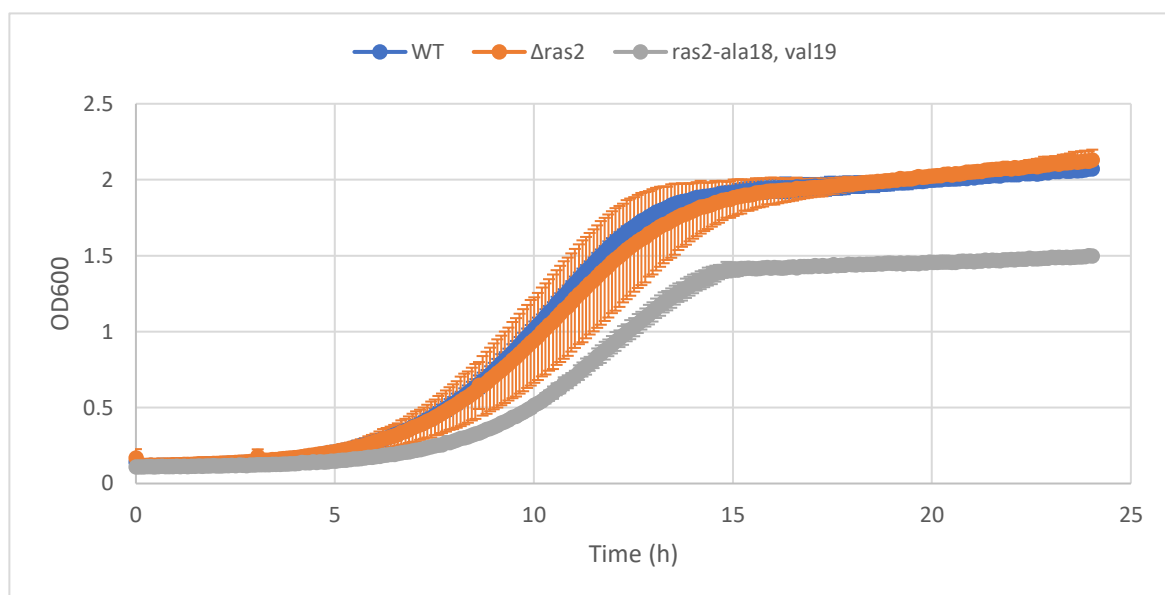


Figure 28: Growth analysis of *S. cerevisiae* strains over 24-hours, grown in YPD media, under standard growth conditions. The data represents the average of three biological replicates and three technical replicates per biological replicates, while error bars represent the standard deviation. (Blue) Wild Type, (Orange) $\Delta ras2$, and (Grey) *ras2-ala18, val19*.

As observed from the previous growth curves, with the previously used wild type and $\Delta ras2$ strains, there appeared to be no significant differences between the growth patterns of the wild type and $\Delta ras2$ cells. Contrastingly, it appeared that the *ras2-ala18, val19* cells showed a reduced rate and capacity of growth, relative to wild type. To confirm and determine if the altered growth trends were significant additional statistical analysis would need to be conducted.

To obtain a greater understanding of the individual level of growth in cells of the strain populations, the cell diameter of cells was measured, to provide further information for the overview of the new wild type and *ras2* mutant strains (Figure 30).

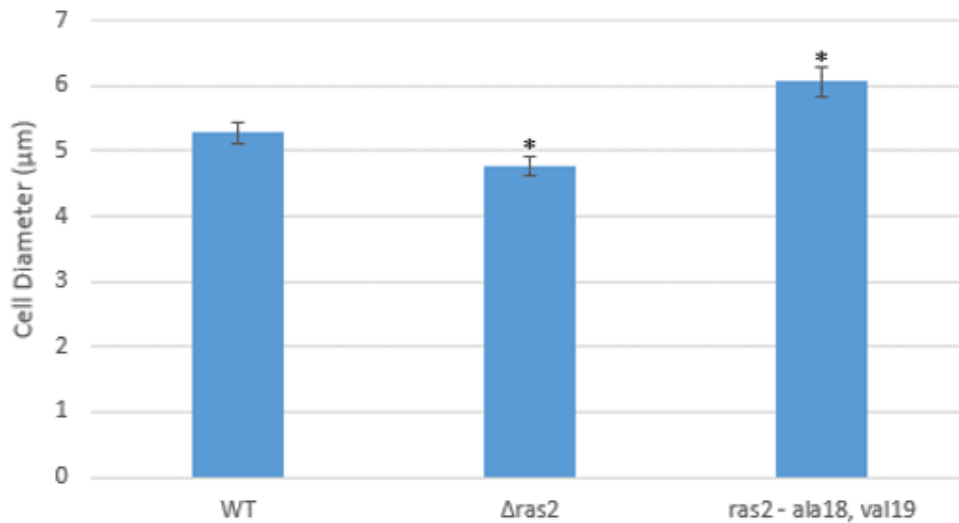


Figure 29: Graph showing the average diameter of wild type, *Δras2* and *ras2-ala18, val19* cells, after a 24-hour period of growth, under standard growth conditions. The data are \pm SEM of three biological replicates and three technical replicates per biological replicates. Error bars represent the standard deviation of the data set. A one-way ANOVA was performed across the data set. *, $P < 0.001$.

The diameters of the different strains cells varied across the wild type and *ras2* mutants (Figure 30). A marginal, yet statistically significant reduction in cell diameter is observed in the *Δras2* mutant, relative to wild type. This is not concurrent with the previous findings in this study; however, this can be explained by the use of a different *Δras2* mutant and wild type, which have a different background to the previously used *Δras2* strain, therefore meaning they would likely display altered phenotypes. Contrastingly, the constitutively active *ras2* mutant showed a significantly increased cellular diameter, relative to wild type. This decreased level of growth that appeared to be shown in Figure 29, alongside the increased cell diameters shown here suggests the overactivation of Ras2 signalling in the constitutively active *ras2* mutant is primarily driving cell growth, as opposed to cell proliferation. This could either be the result of direct or indirect Ras2 signalling, however further investigation would be required to determine this.

3.2.6 Analysis of viability in WT and *ras2* mutants, under standard growth conditions.

To complete the assessment of growth and viability of the new wild type and *ras2* mutant strains, only the viability of these cells was yet to be investigated. As previously conducted, a viability assay was used that determined how many colony forming units would be generated from a total of 300 cells, after 24-48 hours of growth on YPD agar, under standard growth conditions (Figure 31). Determining the viability/senescence of the strains may prove to be essential when interpreting findings in future experiments in this study.

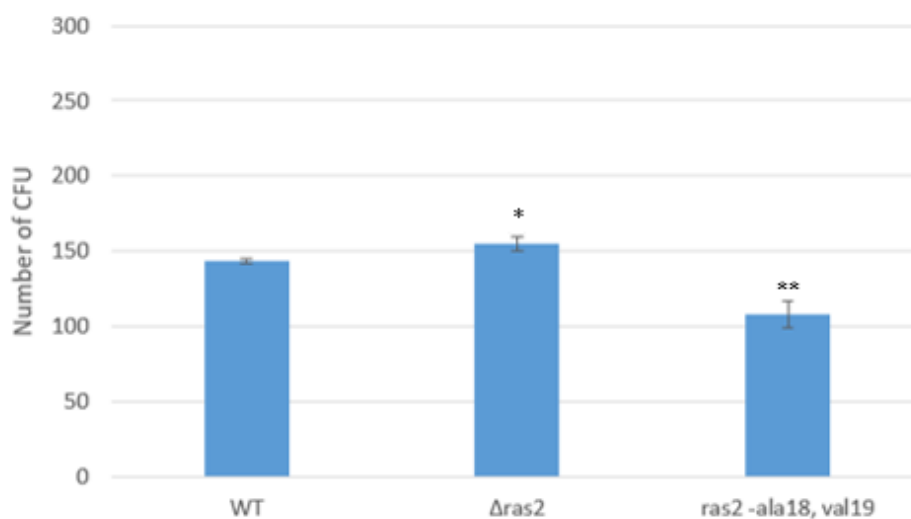


Figure 30: Graph showing the viability of wild type, $\Delta ras2$ and *ras2-ala18, val19* cells, grown on YPD agar over a period of 24-48 hours, under standard growth conditions. The data are \pm SEM of three biological replicates and three technical replicates. Error bars represent the standard deviation of the data set. A one-way ANOVA was performed across the data set with a post hoc tukey test. *, $P < 0.05$. **, $P < 0.001$.

The viability assay revealed that there is a significant increase in viability in the $\Delta ras2$ cells, relative to wild type, while a significant decrease in viability was observed in the constitutively active *ras2* cells, relative to wild type. Notably, the wild-type strain showed decreased viability compared to the previously utilised wild-type strain, which is likely a side effect of the different background of the strains. Interestingly, the $\Delta ras2$ cells showed increased viability compared to wild type, which could be the result of Ras2 signalling alleviating the metabolic burden that is associated with the background of this wild type, that is causing the wild type stains reduced viability, relative to the previous wild type.

3.2.7 Assessing level of intracellular Lipid Droplets in $\Delta ras2$ and $ras2$ -*ala18*, *val19* cells.

Having obtained a greater understanding of the growth and viability associated with these new wild type and *ras2* mutant strains, further investigations related to lipid metabolism and lipid droplet regulation could be conducted. The aim being to understand the role, if any, that Ras2 signalling has within the biogenesis of lipid droplets. Initial analysis of the lipid droplet content of the wild type, $\Delta ras2$ and *ras2*-*ala18*, *val19* cells was achieved through visualisation, coupling the use of the lipophilic LD540 stain and fluorescent microscopy (Figure 32). By investigating the lipid droplet content of these new *ras2* mutant strains, the specific intracellular effect associated with Ras2 signalling could be isolated and identified – thus eliciting the role that Ras2 signalling may have on lipid droplet biogenesis. Selections of cells in Figure 32 were chosen that best represented the cells observed across the three biological and five technical replicates utilised, for wild type and *ras2* mutant cells.

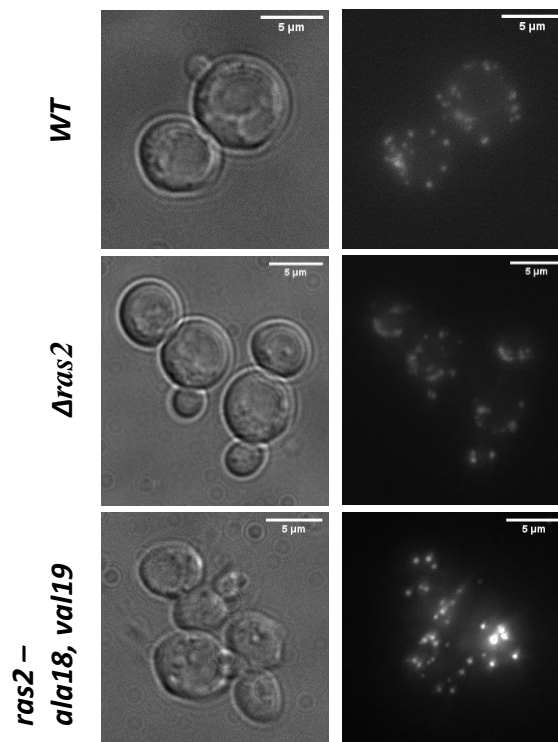


Figure 31: Fluorescent images of wild type, $\Delta ras2$ and *ras2*-*ala18*, *val19* cells, stained with LD540, following 24-hours of growth, under standard growth conditions. A total of three biological replicates were utilised and five technical replicates per biological replicate. Scale provided. Images analysed using ImageJ. DIC images are provided as a representative control.

The fluorescent images of the wild type and *ras2* mutant cells (Figure 32) highlighted a negligible reduction in lipid droplets for $\Delta ras2$ cells, relative to wild type. While the constitutively active Ras2-ala18, val19 cells displayed a significant increase in both number of lipid droplets and the visible fluorescent intensity, associated with the images, relative to wild type cells. Drawbacks of these images is the subjectivity that can be introduced during analysis and when cells are being selected for analysis. To overcome the initial subjectivity of selections, the best representatives, of the total biological and technical replicates, were selected. During analysis, subjectivity was overcome by randomly selecting cells to count the number of lipid droplets in cells (Figure 33).

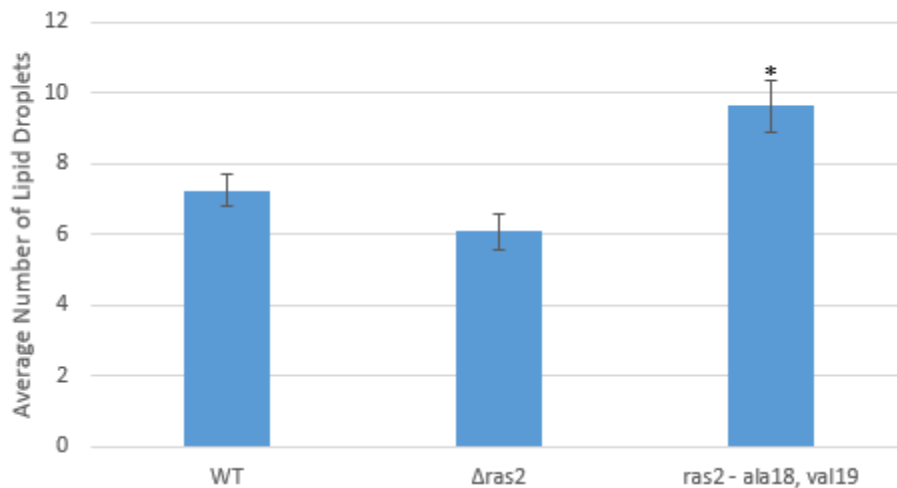


Figure 32: Graph showing the average number of intracellular lipid droplets, within wild type, $\Delta ras2$ and *ras2-ala18, val19* cells. Lipid droplets were counted from images obtained after 24-hours of growth and following LD540 staining. The data are \pm SEM of three biological replicates and five technical replicates. A one-way ANOVA was performed across the data set, with a post hoc tukey test. *, $P \leq 0.001$.

Quantification of the lipid droplets (Figure 33) highlighted the lack of significance difference between the lipid droplet content of wild type and $\Delta ras2$ cells. Alongside this, the lipid droplet count provided further evidence of the significant difference between the constitutively active *ras2-ala18, val19* cells and wild type. Although these results highlight the accumulation and localisation of lipid droplets, the neutral lipid content could still be extremely variable across lipid droplets. So, as conducted previously, the neutral lipid content of the different strains was analysed, by measuring the fluorescent intensity of the LD45 stain within cells (Figure 34).

Analysis of the neutral lipid content of cells was facilitated using flow cytometry, that measured the fluorescence of individual cells, stained with LD540 (Figure 34). The fluorescent intensity of cells was normalised based on an unstained negative control and data was isolated using specific gates that were set to identify the yeast cells based on side and forward scatter profiles, alongside a gate which removed doublets from analysis – ensuring the data was not unnecessarily altered.

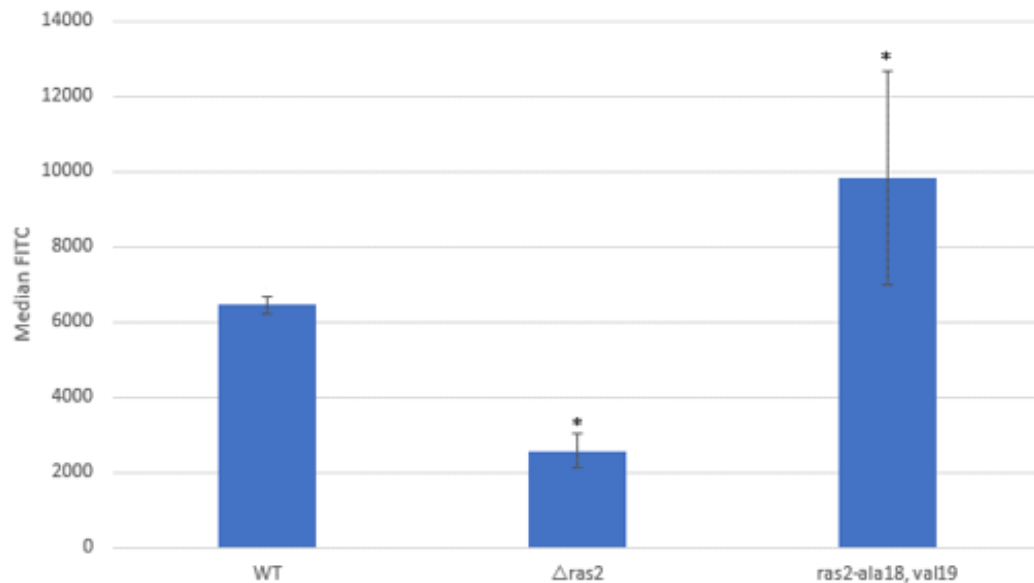


Figure 33: Average fluorescent intensity of stained intracellular neutral lipids in wild type, $\Delta ras2$ and *ras2-ala18, val19* cells. Lipid droplet fluorescent intensity was measured in live cells, grown for 24-hour under standard condition, using an LD540 stain, coupled with a BD Accuri™ C6 Plus flow cytometer. 10,000 cells per sample were analysed. The data are \pm SEM of five biological replicates and three technical replicates. A one-way ANOVA was performed across the data set with a post hoc tukey test. *, $P < 0.001$.

The fluorescent intensity, of the stained neutral lipids within cells, was extremely variable across the wild type and *ras2* mutant strains. A significant decrease in the neutral lipid content is observed in the $\Delta ras2$ cells, relative to wild type. Suggesting that the deletion of *ras2* reduces lipid droplet biogenesis, potentially indicating another regulatory role of Ras2 signalling. While the *ras2-ala18, val19* cells displayed a significantly greater fluorescent intensity, relative to wild type. This further supports the hypothesis that *ras2* signalling is essential in lipid droplet biogenesis, as neutral lipid concentrations were increased in cells with overactive *ras2* signalling. Unfortunately, this is not conclusive, as *ras2* signalling influences numerous cell processes, the observations could be the knock-on effect of this, as opposed to a direct link.

Also considering that growth and viability is affected in these *ras2* mutants, it is highly likely that lipid metabolism and therefore lipid droplet homeostasis would be altered to some degree. Therefore, from this point onwards the analysis of lipid droplets was conducted alongside necrotic assessment, using propidium iodide, to negate the effect of viability on these assessments. To facilitate this additional necrotic assessment, a Bodipy 493/503 stain replaced the LD540 stain, due to differing presence on the fluorescent spectrum, that would facilitate the use of the fluorescent propidium iodide stain.

3.2.8 Optimisation of Bodipy 493/503 Stain LD Staining Protocol.

For the Bodipy 493/502 stain to be effectively used the correct concentration of the stain for the proportion of cells being harvested had to be identified, to ensure appropriate staining and prevent overstaining. Preliminary investigations were conducted to determine the appropriate number of cells that could be stained with a 4 μ M concentration of Bodipy 493/503 (Figure 35/36). A range of 2×10^6 cells/ml to 1×10^7 cells/ml were used. The required time of staining was also assessed, ranging from 15 to 30 minutes.

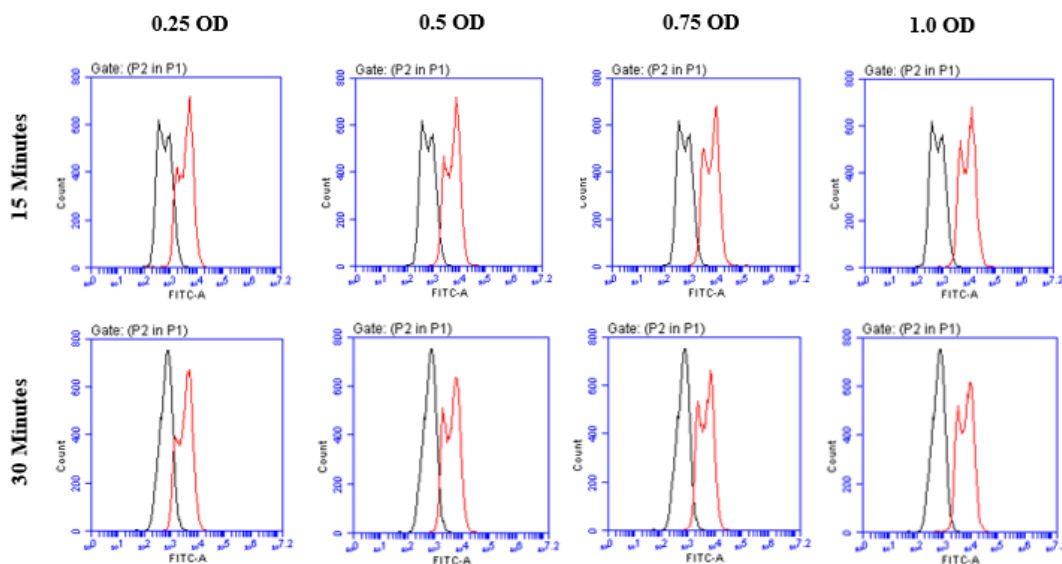


Figure 34: Histograms showing the fluorescent reading for the Bodipy 493/503 stain (Red), relative to an unstained control (Black), in wild type cells. Cells were analysed using a BD Accuri™ C6 Plus flow cytometer. 10,000 cells per sample were analysed. The histograms cover a range of OD readings correlated with a range of cell numbers. Cells were stained for 15 and 30 minutes, respectively. Overlap of the fluorescent signal was observed less significantly at an OD on 1.0, after 15 minutes of staining.

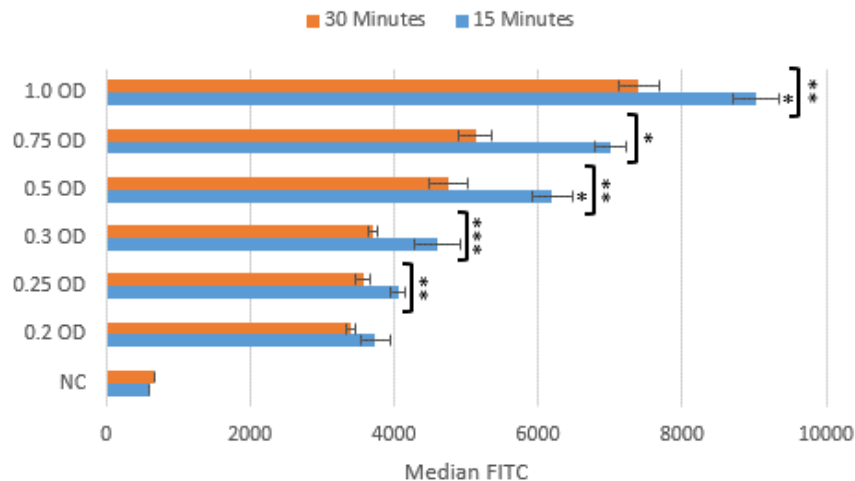


Figure 35: Graph showing the fluorescent intensity of wild type cells, stained with Bodipy 493/503. A range of OD readings correlated with a range of cell numbers were utilised. Cells were stained for 15 and 30 minutes, respectively. Cells were analysed using a BD Accuri™ C6 Plus flow cytometer. 10,000 cells per sample were analysed. The data are \pm SEM of three biological replicates and three technical replicates. A one-way ANOVA was performed across the data set, with a post hoc tukey test. *, $P \geq 0.01$. **, $P \geq 0.005$. ***, $P \geq 0.001$.

The most significant intensity in fluorescent was observed with cell number of 1×10^7 – correlated to an OD 1.0. A gradual decline was observed in intensity as OD of cells reduced. Notably, the greater fluorescent intensity was consistently observed in cells stained for 15 minutes, as opposed to 30 minutes. These results (Figure 35/36) indicated that a cell count of 1×10^7 cells was required for the staining of *S. cerevisiae*, with $4 \mu\text{M}$ of Bodipy 493/503. So, from this point onwards these were the parameters used to stain cells for both flow cytometry and microscopy.

3.2.9 Assessing level of intracellular Lipid Droplets in $\Delta ras2$ and *ras2-^{ala18}*, *val19* cells, following the addition of heat and oxidative stressors.

Having identified a significant decrease in intracellular lipid droplets following the deletion of *ras2*, alongside a significant increase in lipid droplets in the constitutively active *ras2-ala18*, *val19* cells. To conclude if the *ras2* signalling was involved in lipid droplet biogenesis, a variety of stressors (e.g., heat, H_2O_2 and CuSO_4) was introduced during the analysis of lipid droplets (Figure 37). The aim of these stressors was to promote the production of lipid droplets and subsequently identify if the same observations remained. The introduction of stressors would also allow any links between Ras2 signalling, the stress response of *S. cerevisiae*, and lipid droplet biogenesis to be elicited.

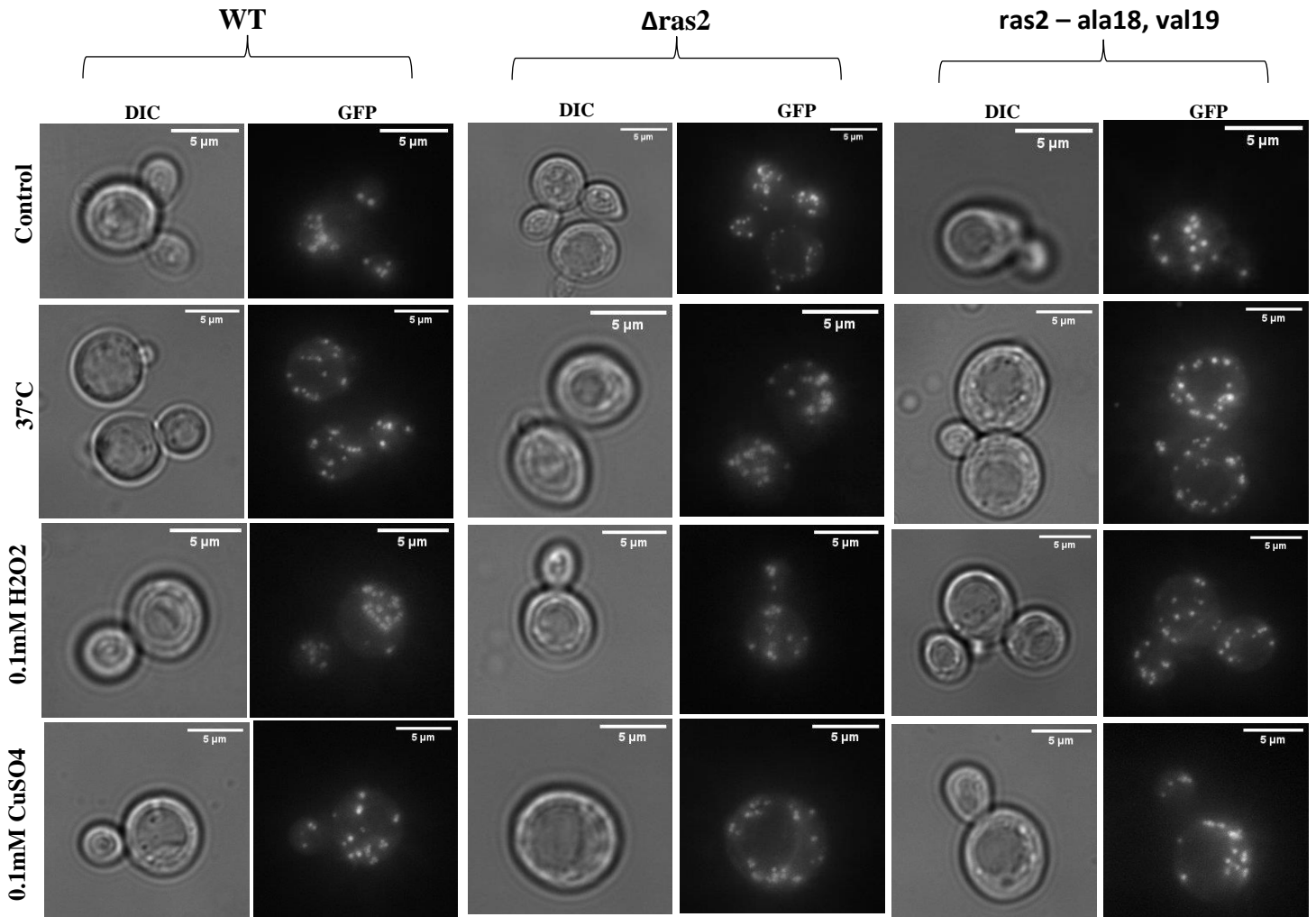


Figure 36: Representative fluorescent images of wild type, $\Delta ras2$ and $ras2$ -ala18, val19 cells, stained with Bodipy 493/503, following 24-hours of growth and 2-hours of exposure to a variety of stressors - 37°C, H₂O₂ and CuSO₄ at indicated concentrations. Scale provided. Images analysed using ImageJ. DIC images provided as a representative control.

Fluorescent images (Figure 37) of control cells highlight the same findings as previously observed, with wild type and $\Delta ras2$ cells showing negligible differences, which was maintained even following the introduction of various stressors (Figure 37). Contrastingly, the $ras2$ -ala18, val19 cells continued to show an increase in quantity of lipid droplets and increased fluorescent intensity, relative to wild type. The wild type cells remain relatively unaffected by the heat stress, while the introduction of an oxidative stress, H₂O₂, seemed to increase the quantity of lipid droplets within cells. When considering the stressors effect on the $\Delta ras2$ cells no significant changes were observed. Notably, the $ras2$ -ala18, val19 cells showed increases in lipid droplets following the addition of a heat stressor.

Similarly, to the previously presented fluorescent images, the subjectivity of the images could hinder analysis, therefore quantification the data was achieved by counting the intracellular lipid droplets, across biological/technical replicates (Figure 38).

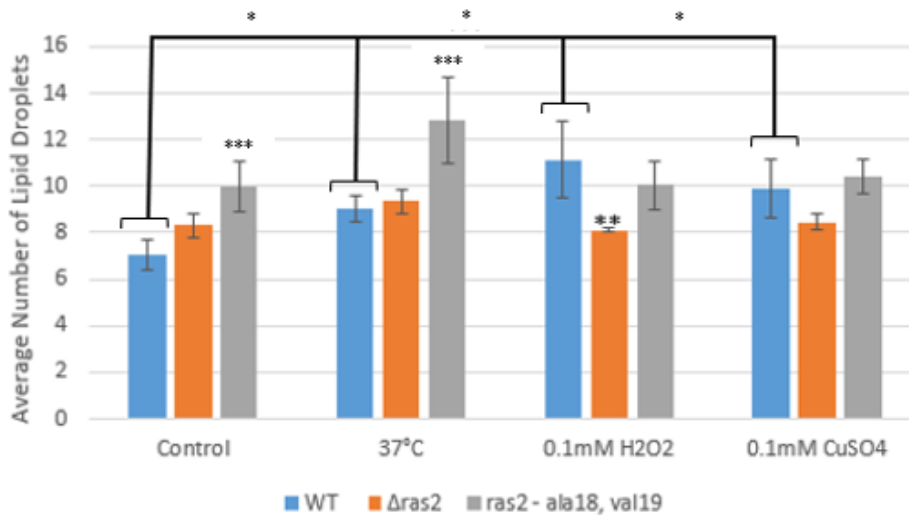


Figure 37: Graph showing the average number of intracellular lipid droplets, within wild type, *Δras2* and *ras2-ala18, val19* cells. Lipid droplets were counted from images obtained after 24-hours of growth and following 2-hours of stressing and Bodipy 493/503 staining. The data are \pm SEM of three biological replicates and three technical replicates. A one-way ANOVA was performed across the data set, with a post hoc tukey test. *, $P \leq 0.001$. **, $P \leq 0.005$. ***, $P \leq 0.05$.

The quantification of the lipid droplets (Figure 38) highlighted that only wild type cells displayed a significant change in the number of lipid droplets across the stressors, with the greatest change being observed with the introduction of an oxidative stress. Contrastingly, the *Δras2* and *ras2-ala18, val19* cells displayed no significant change in lipid droplets, across the stressors, relative to the *Δras2* control and *ras2-ala18, val19* control, respectively. For the individual stressor experiments, the data highlighted a significant increase in lipid droplets in the *ras2-ala18, val19* cells in the control and with the introduction of a heat stress, relative to wild type. While the deletion of *ras2* had no significant effect on the number of lipid droplets in the control or following the introduction of a heat stress, relative to wild type. Interestingly, the introduction of oxidative stress failed to induce a significant change in lipid droplet number for the *ras2-ala18, val19* cells, relative to wild type. However, the *Δras2* cells showed a significant reduction in lipid droplets following the introduction of hydrogen peroxide, relative to wild type. Interestingly, the addition of copper sulphate, failed to elicit a similar response for the *Δras2* cells.

Although the subjectivity of the images was overcome, a new drawback of this analysis emerged as lipid droplet fluorescence, if too bright, could mask lipid droplets, making them more difficult to count. To avoid this, counting was conducted in cells that did not show over-fluorescence, alongside calculating the average of the counts. As with the analysis using LD540, the fluorescent intensity of the Bodipy 493/503 stain was measured, using flow cytometry (Figure 39).

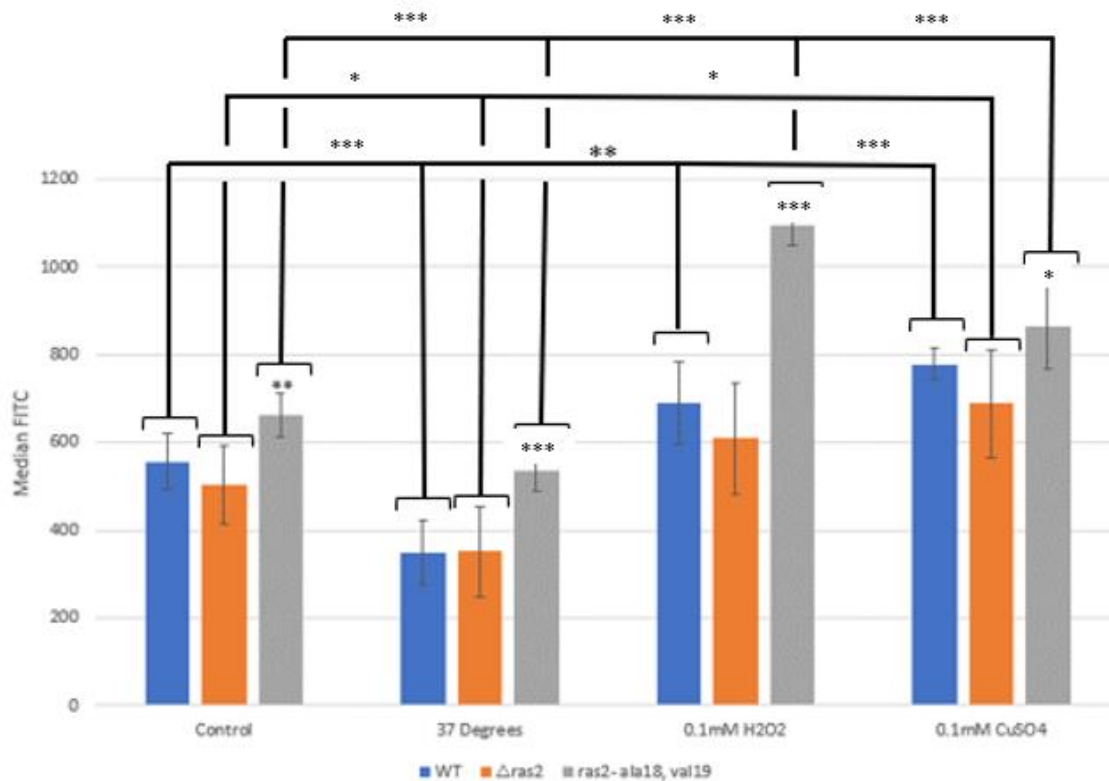


Figure 38: Average fluorescent intensity of stained intracellular neutral lipids in wild type, $\Delta ras2$ and *ras2-ala18, val19* cells, following 24-hours of growth and 2 hours exposure to stressors. Lipid droplet fluorescent intensity was measured in live cells, using an LD540 stain, coupled with a BD Accuri™ C6 Plus flow cytometer. 10,000 cells per sample were analysed. The data are \pm SEM of five biological replicates and three biological replicates. A one-way ANOVA was performed across the data set, with a post hoc tukey test. *, $P \leq 0.05$. **, $P < 0.005$. ***, $P < 0.001$.

The analysis of fluorescent intensity of the neutral lipid content of the cells (Figure 39) highlighted a significant increase in neutral lipids within the *ras2-ala18, val19* cells, relative to wild type, following the addition of oxidative and heat stressors, alongside in the control experiment. Contrastingly, there was no significant change in the neutral lipid content of $\Delta ras2$ cells, relative to wild type. When considering the effect of each stressor on the specific cells used it is revealed that the introduction of a heat stress consistently reduced the levels of neutral lipid within the wild type, $\Delta ras2$ cells and *ras2-*

ala18, val19 cells, relative to their controls. Regarding the level of significance observed, the wild type and the ras2-ala18, val19 cells displayed the greatest level statistically, while the $\Delta ras2$ cells were considerably less significant. Contrastingly, the introduction of an oxidative stress, via administration of copper sulphate, induced a significant increase in neutral lipid content of the cells, across all the strains, relative to their control. The greatest level of significance was observed between the wild type and ras2-ala18, val19 cells, while although still significant the increase of neutral lipid within the $\Delta ras2$ cells was relatively less statistically significant. Interestingly, the introduction of an oxidative stress, via the administration of hydrogen peroxide, also showed significant increases in the neutral lipid content of cells in the wild type and ras2-ala18, val19 cells, relative to their controls, with the greater level of significance observed in the ras2-ala18, val19 cells. However, the $\Delta ras2$ cells displayed no significant increase in neutral lipid, following the administration of hydrogen peroxide, relative to their control. Having analysed the ras2 mutant cells lipid droplet content, following the addition of stressors, the same experiment measuring lipid droplet content of cells with Bodipy 493/503 following the introduction of stressors, was implemented for the wild type, *cox4D1*, *cox4D2*, $\Delta cox4$, $\Delta cox4\Delta yno1$, $\Delta cox4\Delta ras2$, $\Delta yno1$ and $\Delta ras2$ cells.

3.2.10 Investigating the effects of partial and full loss of COX function on levels of intracellular lipid droplets, following the addition of heat and oxidative stressors.

Upon identifying that lipid droplet biogenesis was not dependent on *ras2* signalling, the previous assessment of lipid droplets was applied to the wild type, *cox4D1*, *cox4D2*, $\Delta cox4$, $\Delta cox4\Delta yno1$, $\Delta cox4\Delta ras2$, $\Delta yno1$ and $\Delta ras2$ cells (Figure 40/41). The aim of these experiments was to observe the effect of the range of stressors on intracellular lipid droplet content of these cells, while also investigating the role that *yno1* has in coordinating lipid droplet biogenesis, which was suggested in previous findings. The cells were visualised using fluorescent microscopy, coupled with the Bodipy 493/503 and propidium iodide stains (Figure 40/41). From these images' selection was made that represented the technical and biological replicates from a clear and fair format.

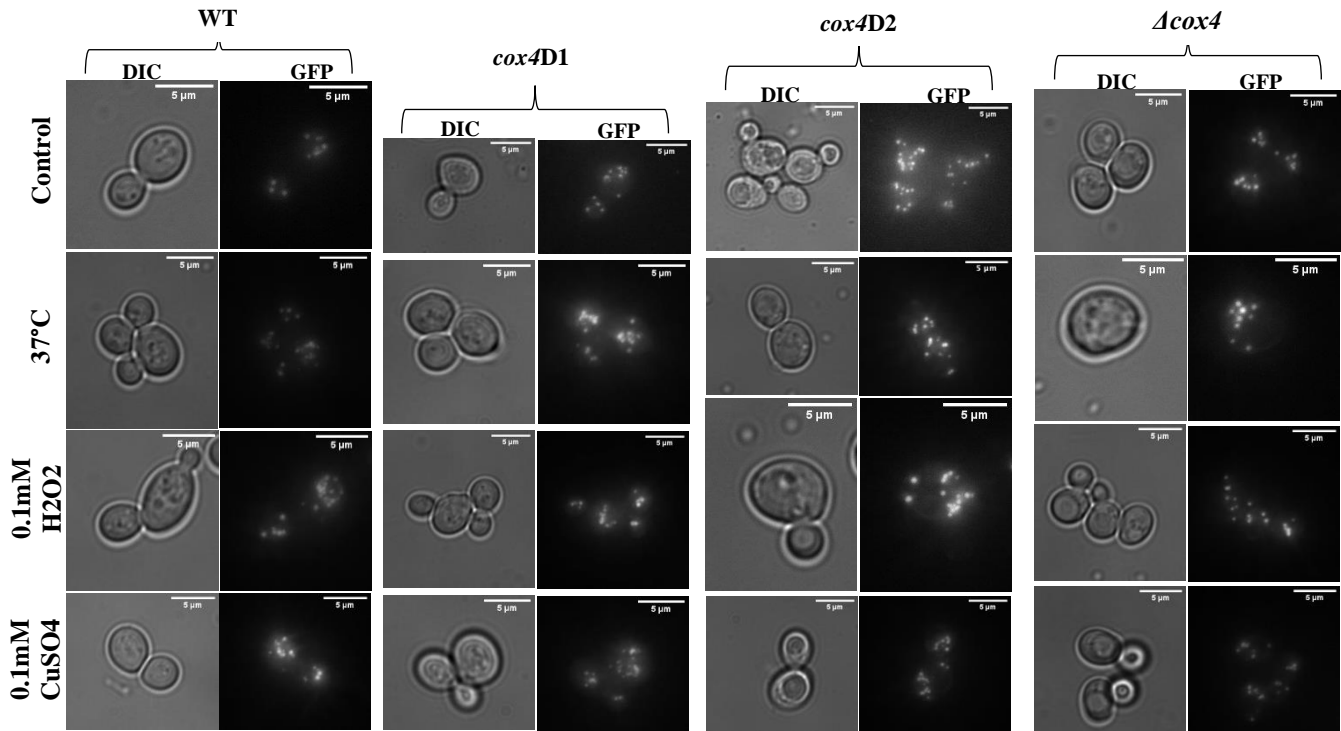


Figure 39: Fluorescent images of wild type, *cox4D1*, *cox4D2*, Δ *cox4* cells, stained with Bodipy 493/503, following 24-hours of growth and 2-hours of exposure to a variety of stressors - 37°C, H₂O₂ and CuSO₄. Scale provided. Images analysed using ImageJ. DIC images were provided as a representative control.

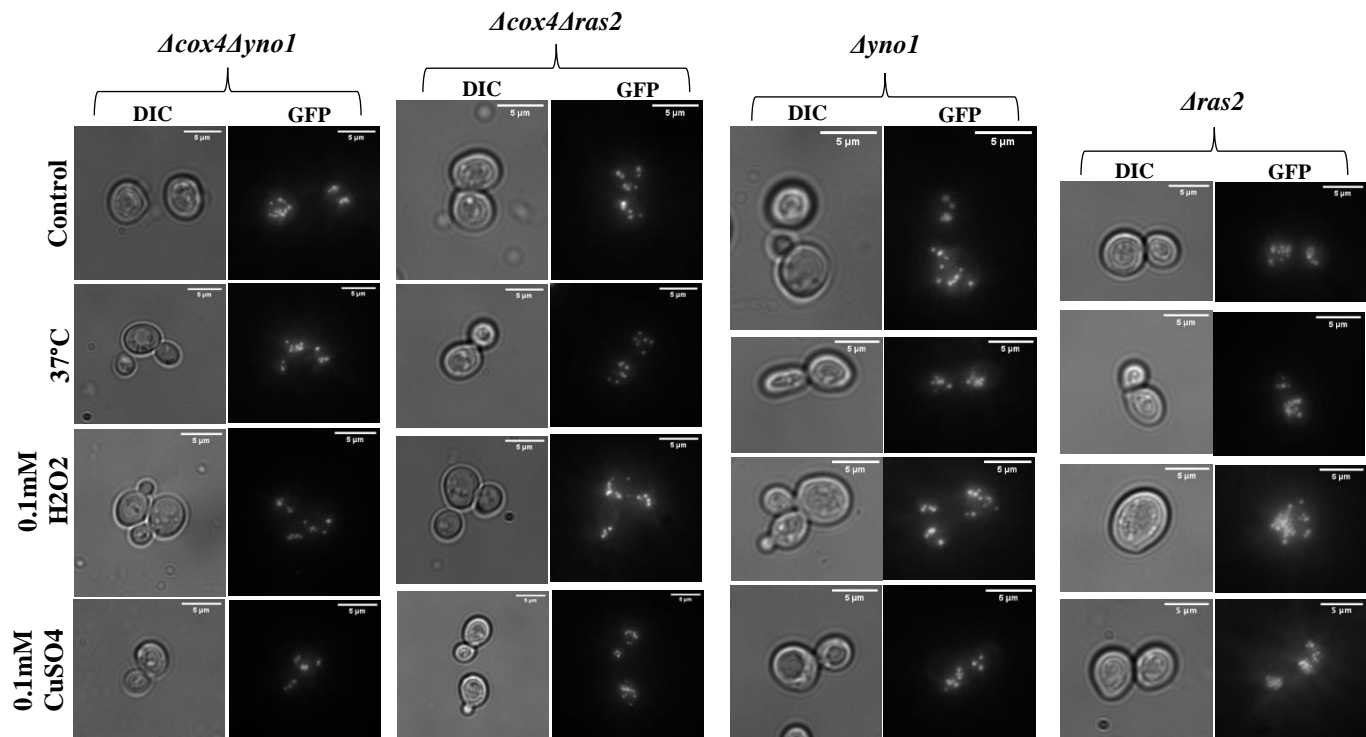


Figure 40: Fluorescent images of Δ *cox4* Δ *yno1*, Δ *cox4* Δ *ras2*, Δ *yno1* and Δ *ras2* cells, stained with Bodipy 493/503, following 24-hours of growth and 2-hours of exposure to a variety of stressors - 37°C, H₂O₂ and CuSO₄. Scale provided. Images analysed using ImageJ. DIC images were provided as a representative control.

Visualisation of the wild type, *cox4D1*, *cox4D2*, Δ *cox4*, Δ *cox4* Δ *yno1*, Δ *cox4* Δ *ras2*, Δ *yno1* and Δ *ras2* cells (Figure 40/41) highlighted similar findings to previously, specifically that increased mitochondrial dysfunction is correlated with an increase in intracellular lipid droplets, relative to wild type. Notably, in the *cox4D2* and Δ *cox4* cells the introduction of a CuSO_4 oxidative stress appeared to reduce the levels of lipid droplets in these cells, relative to the control for these strains. Interestingly, the deletion of *yno1* in the Δ *cox4* mutant led to a reduction in the lipid droplet content of the cells, relative to the Δ *cox4* cells, while the deletion of *ras2* in the Δ *cox4* mutant displayed no significant reduction in lipid droplets, across any stressor. As conducted in the previous analysis of the florescent images, the data was quantified by counting the lipid droplets for the different strains against across the technical and biological replicates (Figure 42).

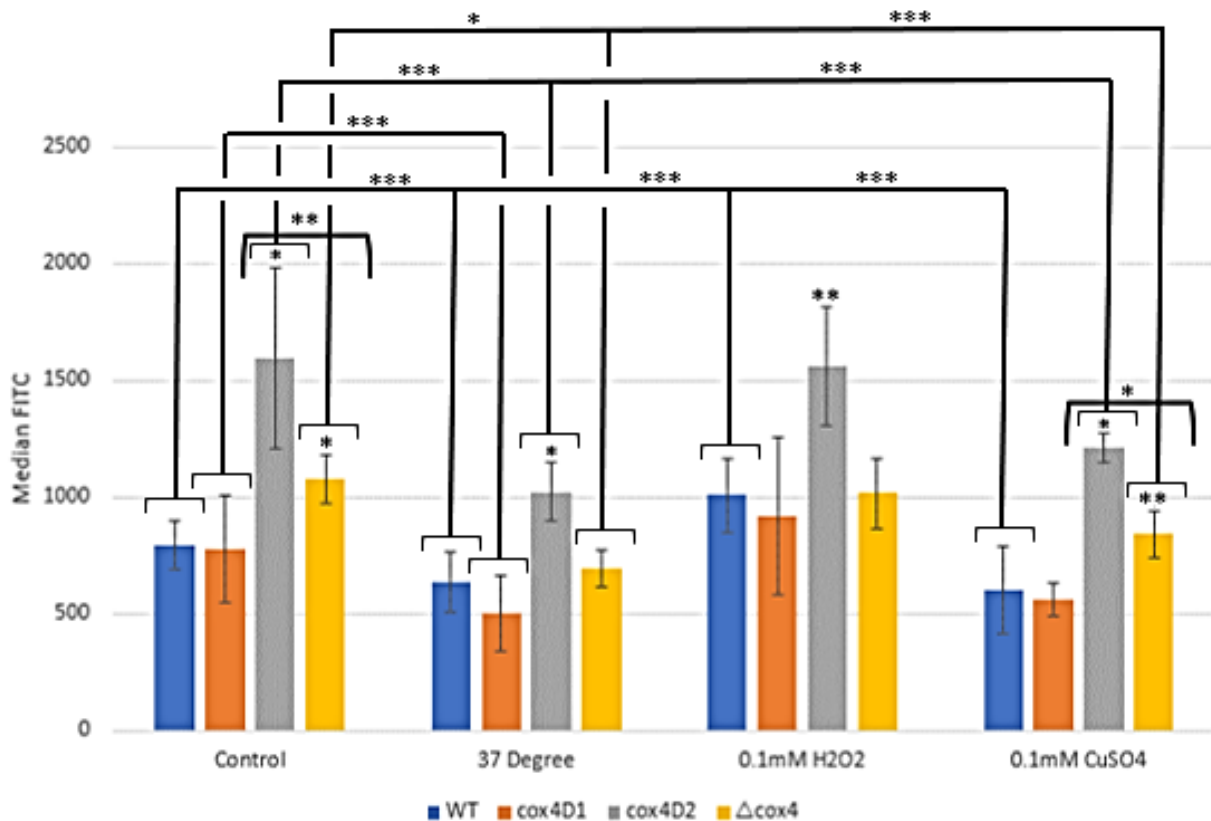


Figure 41: Graph showing the average number of intracellular lipid droplets, wild type, *cox4D1*, *cox4D2*, Δ *cox4*, Δ *cox4* Δ *yno1*, Δ *cox4* Δ *ras2*, Δ *yno1* and Δ *ras2* cells. Lipid droplets were counted from images obtained after 24-hours of growth and following 2-hours of stressing and Bodipy 493/503 staining, in addition with propidium iodide stain to assess cell necrosis. The data are \pm SEM of three biological replicates and three technical replicates. A one-way ANOVA was performed across the data set, with a post hoc tukey test. *, $P \leq 0.005$. **, $P \leq 0.001$.

Quantification of lipid droplets (Figure 42) highlighted no significant changes in the *cox4D1*, Δ *cox4*, Δ *cox4/\Delta**yno1*, Δ *cox4/\Delta**ras2*, Δ *yno1* across the stressors. Contrastingly, the wild type, *cox4D2* and the Δ *ras2* cells displayed a level of significance with the introduction of oxidative stressors and the heat stress, respectively. Comparing the different strains, the *cox4D2* and the Δ *ras2* cells displayed a greater amount of lipid droplet within cells, relative to wild type. To overcome the variance in the data set and to complete the assessment of lipid droplet content within the cell, the stained cells were analysed using flow cytometry (Figure 43).

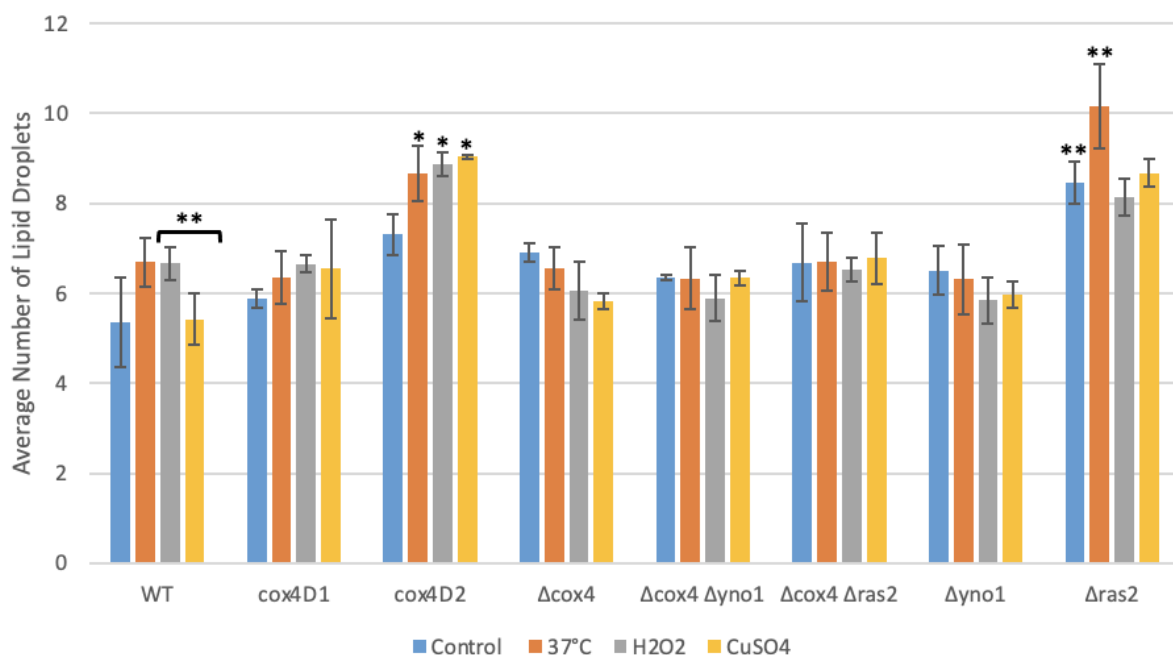


Figure 42: Lipid droplet fluorescent intensity in WT cells and *cox4* mutants (Table 1), following temperature and oxidative stress exposure. Lipid Droplet fluorescent intensity was measured in live cells using an Bodipy 493/503 stain, in addition with propidium iodide stain to assess cell necrosis. These stained cells were analysed using a BD Accuri™ C6 Plus flow cytometer. 10,000 cells per sample were analysed. The data are \pm SEM of six biological replicates and three biological replicates. A one-way ANOVA was performed across the data set. *, $P \leq 0.05$. **, $P \leq 0.005$. ***, $P \leq 0.001$.

Assessment of the neutral lipid content of the cells (Figure 43), highlighted a consistent significant increase in the neutral lipid content of cell for the *cox4D2* strain, relative to wild type, in the control and stressor experiments. In both the control experiment and following the introduction of an oxidative stress in the form of copper sulphate, neutral lipid content was significantly increase in the Δ *cox4* cells, relative to wild type.

Notably this increase was not observed following the introduction of a heat stress and oxidative stress, via hydrogen peroxide. Concurrent with previous findings, the *cox4D1* cells showed no significant increase in neutral lipid content, in the control and stressor experiments, relative to wild type. When considering the effect of each stressor on the specific cells used it is revealed that a significant increase in the neutral lipid content of the cell is observed for wild type cells following the introduction of oxidative stressors, relative to the control, with the most significant increase being observed following the introduction of hydrogen peroxide. While the introduction of a heat stress to the wild type cells induced a reduction in the neutral lipid content of the cells, relative to the wild-type control. Contrastingly, the *cox4D1* cells only showed a significant decline in neutral lipid following the introduction of a heat stress, relative to the *cox4D1* control, while no significant changes were observed following the introduction of oxidative stressors, relative to the control. For the *cox4D2* and Δ *cox4* cells, a significant reduction in the neutral lipid content of cells was observed following the introduction of a heat stress, relative to the control. While the administration of copper sulphate, as an oxidative stress, induced a significant increase in the neutral lipid content of these cells, relative to the control. For both of the *cox4D2* and Δ *cox4* cells, the addition of hydrogen peroxide had no significant effect of the neutral lipid content of cells, relative to the control, which may be caused by the already high levels reported within the cells. Significant differences were also identified between the *cox4D2* and Δ *cox4* cells, which may have previously been linked with the loss of viability between the *cox4D2* and Δ *cox4* cells, however the introduction of a propidium iodide stain alongside the Bodipy 493/502 stain allowed for this factor to be minimised, by implementing an additional gate during flow cytometry that removed necrotic cells from analysis.

Chapter 4:

Discussion

Understanding and detailing the roles that lipid droplets have within cells will be essential in shedding new light on the coordinated intracellular events that contribute to cellular processes, associated with maintaining cellular health, adaptability, and survival. At the base of understanding the functionality and dynamic nature of these organelles is the requirement to gain a greater understanding of the coordinated events that induce lipid droplet biogenesis. Although lipid droplets have been studied for many decades, the process of lipid droplet biogenesis and the regulatory signalling pathways in place that coordinate this process still remain poorly understood [131]. Gaining an understanding of these mechanisms and signalling pathways may be critical in elucidating the parallel processes within higher eukaryotes. By developing this understanding, new avenues for treatment of diseases associated with mitochondrial dysfunction and lipid droplet dysregulation – including neurodegeneration – may become explorable, offering new hope to affected individuals [179][180].

Recent studies, centred around investigating the intricate interactions between the mitochondria and lipid droplets, have shed light on the intertwined dependence that exists between the two organelles. Such dependences seem to be essential in the regulation of lipid droplet biogenesis, which then dictates the size of lipid droplet populations within the intracellular environment [181]. Studies have previously shown that an increase in intracellular lipid droplets can be observed in cells with dysfunctional mitochondria [182][183]. So, to build on these findings the level of lipid droplets were examined in cells with mitochondrial dysfunction, induced by loss of COX function, to see if the same observations of other studies were shown. Following on from this, the role of Ras2 in this regulation of lipid droplets was investigated. Before observing the effect that the introduction of heat and oxidative stressors have on the regulation of lipid droplet. This together would aid the investigation of the interaction between the mitochondria and lipid droplets with regards to the coordination of lipid droplet biogenesis, the underlying signalling pathways associated with lipid droplet regulation, and finally how different stressors alter the regulation of lipid droplet biogenesis. The hypothesis was: 1) that mitochondrial dysfunction would induce lipid droplet dysregulation, 2) Ras2 signalling was involved in the regulation of lipid droplet biogenesis and 3) the introduction of oxidative stressors would lead to greater increase in intracellular lipid droplet concentration.

Data presented in this study, suggested that the onset of mitochondrial dysfunction, induced by the loss of COX function, leads to lipid droplet dysregulation. Previous studies have shown similar finding, with greater levels of lipid droplets being observed in cells with dysfunctional mitochondria, however in these studies the mitochondrial dysfunction was induced by loss of mtDNA [184]. Considering the intricate interactions that exist between the mitochondria and lipid droplets, the greater number of lipid droplets may be the result of two main causative events. The first being a reduction in the physical contact points between the dysfunctional mitochondria and lipid droplets, relative to functioning mitochondria, as a result of altered mitochondrial morphology – indirectly induced by the altered metabolic state of the mitochondria, associated with the dysfunction. This alteration in morphology and mass has been described in diseases associated with mitochondrial dysfunction (e.g., metabolic syndrome, type II diabetes and neurodegeneration), so it is plausible that physical contacts with other organelles would also be significantly affected, as in this case with lipid droplets [185][186].

Alternatively, the disrupted metabolic activity of the mitochondria, which reduces the mitochondria's ability to partake in the β -oxidation of fatty acids, may lead to the increased lipid levels within the mammalian mitochondria [182][183]. As previously mentioned, with the primary interaction between the mitochondria and lipid droplets being based around the exchange of fatty acids, disrupted metabolic activity could result in a reduced exchange of lipids from the lipid droplets to the mitochondria [181][187]. This would then lead to increased lipid storage and a larger population of lipid droplets. Notably, yeast mitochondria do not participate in β -oxidation and instead these reactions that utilise lipids take place within intracellular peroxisomes [172]. These peroxisomes have been shown to display increased activity in yeast cells upon loss of COX function – a phenomenon induced by retrograde signalling. Considering the increase in local acetyl-CoA induced by the onset of mitochondrial dysfunction and the increased activity of the peroxisomes, the acetyl-CoA may itself be promoting the increase of lipid droplets and causing the production of more densely packed droplets – thus resulting in increased fluorescence [189].

As the lipid droplet dysregulation displayed an increase in lipid droplets relative to wild type cells, both theories are plausible. Reduced physical contacts points could lead to reduced levels of lipid consumptions, resulting in lipid droplet accumulation. Alternatively, if contact points are maintained then the higher levels of lipids within the mitochondria may lead to an increased transfer of lipids to the lipid droplets, from the mitochondria, to compensate for the lack of reduction usually associated with the activity of β -oxidation in the mitochondria of mammalian cell, or the activity of peroxisomes in yeast. The recently theorised bidirectional transport of lipids between the mitochondria and lipid droplets may be instrumental in this process [188].

A consideration that should be made is that the reduction of COX function is directly associated with oxidative phosphorylation and not β -oxidation within the mitochondria. However, it can be assumed that this reduction in function would generate more demand for energy production via β -oxidation of fatty acids, to which only certain levels of lipids can be utilised. Interestingly, another function that has been attributed to lipid droplets is acting as a ROS sink. With increases in intracellular ROS levels being shown to induce increased levels of lipid droplets [189]. Considering that mitochondrial dysfunction has separately been shown to increase intracellular ROS levels, it can be assumed that the mitochondrial dysfunction induced in this study contributed in some capacity to the significant increase in intracellular lipid droplet. It is likely that all of these potential causes play a part in inducing lipid droplet dysregulation. However, further investigations would be required to pinpoint the primary inducers of lipid droplet dysregulation and to what extent each factor plays a role. Notably, an alternative approach to this question would be to introduce lipid droplet-based mutations to observe and detail if/how the knock-on effects of disrupting lipid droplets influences mitochondrial function – however in this study these investigations were not conducted.

Notably, the dysregulation of lipid droplets was only observed following the reduction of COX function greater than 96%, while reduction of 60% had no significant effect. This could be the result of reduced dependence on oxidative phosphorylation throughout the early stages of the lifespan of cells, while when requirements are increased the remaining 40% of COX function in the mitochondria may be sufficient. Growth assays supported this theory with the most significant difference observed between the *cox4* mutants being displayed within the stationary phase – following diauxic shift – when the cells are more reliant on aerobic respiration - highlighted by the shift in the mitochondrial proteome, from the production of amino acid, sterols and phospholipids to respiratory metabolism [190]. Additionally, viability assays further highlighted this with greater reduction of COX function resulting in more significant reductions in viability. Which is concurrent with other studies that have observed reduced viability in cells with mitochondrial dysfunction [191][192]. This reduction in viability is likely the result of the reduced ability to fulfil energy requirements of the cell, due to the impaired mitochondria, alongside the significant increase in intracellular ROS, which leads to excessive oxidative damage. The reduced level of lipid droplets observed in the Δ *cox4* cells, compared to the *cox4D2* cells, could be the result of this reduced viability.

Regarding the investigations related to Ras2 signalling, the findings in this study indicated a regulatory role for Ras2 signalling in lipid droplet regulation, which supports the findings of other research studies [193]. This is highlighted in the Δ *ras2* cells which displayed less responsive changes to the introduction of stressors, relative to wild type, thus indicating the Δ *ras2* cells are inefficient at responding to their environment through changes in accumulation and distribution of lipid droplets. This study's findings built on previous work by introducing a variety of stressors, highlighting how this effected lipid droplet accumulation in Ras mutants. This can then be applied to the previously hypothesised model of Ras-dependent ROS production via Yno1 to gain a better understanding of Ras in this process. The result from this study suggests that lipid droplet biogenesis is not Ras2-dependent as no significant decline in lipid droplets were observed following the deletion of Ras2, relative to wild type. So, this highlights that Ras2 isn't the driving force behind lipid droplet biogenesis in this model and another protein is more likely the facilitator. Notably, a compensatory role of Ras1, that has been described in other yeast

models like *Cryptococcus neoformans*, which may be distorting these results to camouflage the true role of Ras2 signalling in lipid droplet biogenesis, however a more significant decline in lipid droplet content would still be expected [194]. When considering the finding associated with the *ras2-ala18, val19* cells a more significant regulatory role can be observed, with the lipid droplet content of cells being significantly increased in these cells throughout the addition of stressors, relative to wild type. So, in some capacity Ras signalling appears to be able to promote lipid droplet biogenesis.

Interestingly, in recent studies investigating the regulatory role of Ras2, the *ras2-val19* mutant cells failed to significantly alter the lipid droplet content of cells, relative to wild type. Instead, the expression of cAMP and phosphodiesterase 2, aimed at detailing the effects of diminishing Ras2-PKA signalling, led to a significant increase lipid droplet content, relative to wild type [195]. Further investigation identified that a reduction of glucose led to a suppression of PKA and a subsequent transient increase in lipid droplet content to ensure that the cell had a fuel source for energy. The difference in observation between the *ras2-ala18, val19* cells and the *ras2-val19* mutant cells are likely caused by the second point mutation which is having a significant effect on the specific function and/or localisation of the Ras2 protein and thus leading to an altered signalling pathway and associated phenotype. The study utilising the *ras2-val19* mutants, also implicated the target of Rapamycin complex 1 (TORC1) and the cytosolic regulation of pH – via plasma membrane-associated H⁺ ATPases and vacuole-associated ATPases – in the regulation of lipid droplets [195]. With TORC1 acting as a protein kinase that couples intracellular levels of amino acids fluctuations and glucose with the transcriptional metabolic reprogramming, via downstream effectors including Sch9/S6K kinase, Tap42/PP2A and Sit4/PP6 protein phosphatases [196-198]. These fluctuations in glucose and amino acids within the intracellular environment also influence the cytosolic pH through the action of the plasma membrane H⁺ ATPase and vacuole ATPase. Notably, the vacuole ATPase has been shown to modulate the Ras-PKA signalling pathway and the TORC1-Sch9 pathways via GTPases – Arf1 and Gtr1, respectively [199-202]. The primary link between the coupling changes to the intracellular environment, Ras2 signalling, and regulation of lipid droplets is observed through TORC1 which can regulate lipid droplet formation by altering the transcription of *DGA1*, which is essential in the regulation of lipid droplet biogenesis [195].

It is yet to be defined whether the TORC1-Sch9 works in parallel or upstream of Ras-PKA signalling, alternatively TORC1 and PKA may act independently of Sch9, regarding the regulation of lipid droplet metabolism [195].

Early findings in this research study also suggested that the NADPH oxidase, Yno1, may be essential in the regulation of lipid droplet biogenesis, having observed a significant reduction in lipid droplets following the deletion of *yno1* in cells within the *cox4D1*, *cox4D2*, and Δ *cox4* cells. Yno1 has separately been associated with the regulation of a variety of proteins including Ras2 and Yck1/Yck2, through the production of superoxide, which is subsequently converted into hydrogen peroxide by Sod1 [203]. Localisation of Yno1 to the ER places the protein in close proximity to the plasma membrane to facilitate the interaction with these proteins, while also being at the location of lipid droplet biogenesis – the ER membrane. When considering the previous discussion of Ras2 signalling indirectly regulating lipid droplet metabolism, introducing the additional level of regulation of the Ras protein via Yno1 could explain the finding from this study. The hydrogen peroxide produced by Yno1 has also been associated with the MAPK pathways within *S. cerevisiae*, which separately has been linked with coordinating stress response in cells (Figure 44) [203]. Considering that the increase in intracellular levels of ROS is considered an oxidative stress that occurs within cells with loss of COX function, Yno1 may be detecting these increases and coordinating the increase in lipid droplets as a response to stress. Furthermore, Ras2 signalling has been associated with MAPK kinase signalling pathway, suggesting further layers of regulation between Ras proteins and Yno1 may exist [204].

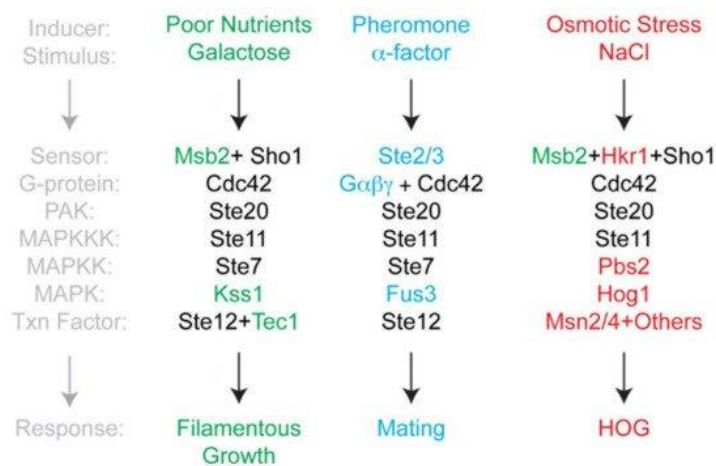


Figure 43: Diagram detailing specific changes in the intracellular environment, the sensors and signalling components that work in unison to elicit a response to the stressor – Figure taken from Devare.M.N., Kim.Y.H., et al 2020.

Notably, as previously mentioned the Ras2 is influenced by the hydrogen peroxide produced by Yno1. Considering that Ras2 is involved in the extracellular glucose sensing and modulation of the mitochondrial respiration, alongside the induction of the Ras-dependent ROS production via Yno1, in cells with mitochondrial dysfunction (Figure 7), it begins to become clear the true number of intricate interactions that exist to coordinate these cellular events. With the ROS production being in close proximity to the plasma membrane, a range of diverse signalling pathways can be generated by local signalling proteins. One of these signalling pathways has been associated with the polymerisation of F-actin cables [205]. Although this intracellular event has been associated with the formation of pseudo hyphae in *S. cerevisiae* in response to changes in the intracellular/extracellular environment [206][203], the effect that Yno1 has in coordinating the actin cytoskeleton could be associated with a greater variety of cellular processes than simply being associated with pseudohyphal formation. In this case it could be responsible for aiding the localisation of certain signalling proteins to coordinate specific signaling pathways.

Returning to the model detailing the Ras-dependent ROS production via NADPH oxidase, Yno1, in cells with loss of COX function (Figure 7), the findings of this study may shed light on some of the details of this model. Yno1 regulation of actin cytoskeleton dynamics, via the regulation of F-actin polymerisation, alongside the regulatory role that cyclase-associated proteins – associated with the function of adenylate cyclase – have with Ras signalling, alongside also influencing the actin cytoskeleton further suggests a crucial role of cytoskeletal manipulation to facilitate this process [207][208]. Considering that both Ras2 signalling and levels of Yno1 are increased in cells with mitochondrial dysfunction, it is likely that the actin cytoskeleton significantly influences the ROS production via Yno1. This may manifest by aiding the translocation of Ras2 to the endomembrane of the mitochondria and/or the indirect suppression of the ERAD pathways – that leads to an increase in intracellular levels of Yno1 – by determining the localisation of proteomes in the cytosol and the ER. However, It is difficult to determine the specific events coordinated by the actin cytoskeleton in this model (Figure 7). Notably, what the results do suggest is that the loss of COX function may be increasing the Ras2 activity, which in turn signals to generate more lipid droplet content. However, the

suppression of ERAD, which has been described in regulating lipid droplets, could be leading to lipid droplet accumulation, that then contributes to loss of viability. This would also provide an insight into what could be occurring when *ras2* is deleted – facilitating the restoration of the ERAD pathway and reducing the number of intracellular lipid droplets. In addition, the subsequent increased peroxisome activity in yeast, due to the increased lipid droplet content, can provide acetyl-CoA as a substrate for the growth of lipid droplets via retrograde signalling pathways – thus contributing to the increase in the number of dysfunctional organelles [189].

Insights into the state of lipid metabolism and lipid droplet homeostasis within cells with mitochondrial dysfunction, induced by loss of COX function, highlight the disruption that is caused by the mitochondrial dysfunction, which is to be expected as the mitochondria has such an integral role in coordinating cellular health, adaptability, and survival. As previously mentioned, the change in lipid droplets may be associated with altered interactions with the mitochondria, however additional factors may also be associated with the rise in intracellular ROS levels. The findings of this study highlight the important role of lipid metabolism and lipid droplet regulation, alongside indirectly highlighting the intricate interaction between organelles of cell (i.e., mitochondria, ER and lipid droplets). However, much is still unknown about the function, regulation, and dynamic nature of lipid droplets, for which future research will have to investigate to develop a greater understanding of numerous intracellular processes.

Future Work

At a fundamental level, findings of this research highlight how beneficial understanding lipid droplets could be in understand the wider perspective of cellular health, adaptability, and survival. For this reason, any prospect of future work would benefit investigating both the biogenesis and regulation of lipid droplets, alongside detailing the interactions shared with other organelles. Not only would this shed light on cellular processes that are relatively unknown, but this would also provide a valuable insight into the link between lipid droplets and lipid metabolism, alongside the wider perspective of how lipid metabolism and lipid droplet homeostasis contribute to cellular health.

Regarding the more specific findings of this study, with data suggesting an essential role for the Yno1 NADPH oxidase in the regulation of lipid droplet biogenesis, it would be worthwhile investigating to what extent and what roles the Yno1 NADPH oxidase enzyme has in this essential process. The findings in this research study and recent literature also suggests a significant role for Ras2 signalling in the regulation of lipid droplets, so further investigations to identify the specific signalling pathway would also be beneficial. In general, besides developing an understanding of the process of lipid droplet biogenesis, it would be useful to develop an understanding of the key intracellular signalling pathways associated with lipid droplet biogenesis, as this would shed light on the mechanisms associated with cellular adaptability to stressors, further detailing and advancing our understanding of the rules of life.

Regarding the model detailing the Ras-dependent ROS production via Yno1 (Figure 7), the findings in this study have already contributed to setting the scene for the wider perspective of the intracellular environment, within the pro-ROS environment. However, the exact role that these lipid droplets have in this pro-ROS environment are yet to be fully explained, whether it be acting as a ROS sink and/or protecting against lipotoxicity, induced by the mitochondrial dysfunction. Similarly, it will be important to understand what role the poorly defined aberrant Ras2 signalling pathway has in coordinating lipid droplet regulation, as both this study and previous studies have described regulatory roles for ras signalling with regards to lipid droplets. In general, it will be beneficial to continue to detail the overall

signalling networks of this model in order to firstly understand the metabolic state of the cell (e.g., lipid metabolism) and secondly to elucidate if the cellular processes are transferable to higher eukaryotes, in order to better understand and manipulate the process in these higher eukaryotes. Notably, in the early parts of this study the effect that KAc has on cells, in which the ras-dependent ROS production is occurring, was investigated to identify the role that it has within these cells. As the role remains a mystery, it would be beneficial to identify how KAc reduces intracellular ROS levels and whether or not it is this reduction in ROS that improves growth and viability of cells with loss of COX function, or if the KAc directly influences these processes.

References

- [1] Botstein.D., Fin.K.G.R.. Yeast: an experimental organism for 21st Century biology. *Genetics*. 2011; 189(3):695–704.
- [2] Murakami.C., Kaeberlein.M. Quantifying yeast chronological life span by outgrowth of aged cells. *J Vis Exp*, 27, p.e1156.
- [3] DeRisi.J.L., Iyer.V.R., Brown.P.O. Exploring the metabolic and genetic control of gene expression on a genomic scale. *Science (New York, N.Y.)* 1997; 278(5338):680–6.
- [4] Nasheuer.H.P., Smith.R., Bauerschmidt.C., Grosse.F., Weisshart.K. Initiation of eukaryotic DNA replication: regulation and mechanisms. *Prog Nucleic Acid Res Mol Biol*. 2002;72:41–94.
- [5] Cho.R.J., Campbell.M.J., Winzeler.E.A., Steinmetz.L., Conway.A., Wodicka.L., et al. A genome-wide transcriptional analysis of the mitotic cell cycle. *Molecular cell*. 1998; 2(1):65–73.
- [6] Villas-Bôas.S.G., Moxley.J.F., Akesson.M., Stephanopoulos.G., Nielsen.J. High-throughput metabolic state analysis: the missing link in integrated functional genomics of yeasts. *Biochem J*. 2005; 388(Pt 2):669–77.
- [7] Jewett.M.C., Hofmann.G., Nielsen.J. Fungal metabolite analysis in genomics and phenomics. *Curr Opin Biotechnol*. 2006; 17(2):191–7.
- [8] Owsianowski.E., Walter.D., Fahrenkrog.B. Negative regulation of apoptosis in yeast. *Biochem Biophys Acta*. 2008; 1783:1303–1310.
- [9] Foury.F., et al. Human genetic diseases: A crosstalk between man and yeast. *Gene* 1997, 195, 1–10.

- [10] Heinicke.S., Livstone.M.S., Lu.C., Oughtred.R., Kang.F., Angiuoli.S.V., White.O., Botstein.D., Dolinski.K. The Princeton Protein Orthology Database (P-POD): A comparative genomics analysis tool for biologists. PLoS ONE 2007, 2, e766.
- [11] Goffeau.A., Barrell.B.G., Bussey.H., Davis.R.W., Dujon.B., et al. (1996) Life with 6000 genes. Science 274: 546–567.
- [12] Engel.S.R., Dietrich.F.S., Fisk.D.G., Binkley.G., Balakrishnan.R., Costanzo.M.C., Dwight.S.S., Hitz.B.C., Karra.K., Nash.R.S., et al. The reference genome sequence of *Saccharomyces cerevisiae*: Then and now. G3 2014, 4, 389–398.
- [13] Winzeler.E.A., Shoemaker.D.D., Astromoff.A., Liang.H., Anderson.K., Andre.B., Bangham.R., Benito.R., Boeke.J.D., Bussey.H., et al. Functional characterization of the *Saccharomyces cerevisiae* genome by gene deletion and parallel analysis. Science 1999, 285, 901–906.
- [14] Jones.G.M., Stalker.J., Humphray.S., West.A., Cox.T., Rogers.J., et al. A systematic library for comprehensive overexpression screens in *Saccharomyces cerevisiae*. Nature methods. 2008; 5(3):239–41.
- [15] Giaever.G., Chu.A.M., Ni.L., Connelly.C., Riles.L., Veronneau.S., Dow.S., Lucau-Danila.A., Anderson.K., Andre.B., et al. Functional profiling of the *Saccharomyces cerevisiae* genome. Nature 2002, 418, 387–391.
- [16] Guaragnella.N., Coyne.L.P., Chen.X.J., Giannattasio.S. Mitochondria-cytosol-nucleus crosstalk: Learning from *Saccharomyces cerevisiae*. 2018 FEMS Yeast Research 18, 1–15.

- [17] Wu.Y., Chen.M., Jiang.J. 2019. Mitochondrial dysfunction in neurodegenerative diseases and drug targets via apoptotic signalling. *Mitochondrion*, 49, 35-45.
- [18] Pieczenik.S.R., Neustadt.J. 2006. Mitochondrial dysfunction and molecular pathways of disease. *Experimental and Molecular Pathology*, Volume 83, Issue 1, Pages 84-92.
- [19] Gorman.G.S., Chinnery.P.F., DiMauro.S., Hirano.M., Koga.Y., McFarland.R., Suomalainen.A., Thorburn.D.R., Zeviani.M., Turnbull.D.M., 2016. Mitochondrial diseases. *Nature Reviews Disease Primers* 2, 16080.
- [20] Strub.S.P., Stiller.S.B., et al. 2016. Dynamic organisation of the mitochondrial protein import machinery. *Biological Chemistry*, 397(11), pp. 1097-1114.
- [21] Foury.F., Roganti.T., Lecrenier.N., Purnelle.B. 1998. The complete sequence of the mitochondrial genome of *Saccharomyces cerevisiae*. *FEBS letters*, 440(3), 325-331.
- [22] Rhee.H.-W., Zou.P., Udeshi.N.D., Martell.J.D., Mootha.V.K., Carr.S.A., Ting.A. Y. (2013). Proteomic mapping of mitochondria in living cells via spatially restricted enzymatic tagging. *Science* 339, 1328-1331.
- [23] Reinders.J., Zahedi.R.P., Pfanner.N., Meisinger.C., Sickmann.A. 2006. Toward the complete yeast mitochondrial proteome: multidimensional separation techniques for mitochondrial proteomics. *J. ProteomeRes.*5, 1543-1554.
- [24] Pagliarini.D.J., Calvo.S.E., Chang.B., Sheth.S.A., Vafai.S.B., Ong.S.E., Walford.G.A., Sugiana.C., Boneh.A., Chen.W.K., et al. A mitochondrial protein compendium elucidates complex I disease biology. *Cell*. 2008; 134:112–123.

- [25] Johnson.D.T., Harris.R.A., French.S., Blair.P.V., You.J., Bemis.K.G., Wang.M., Balaban.R.S. 2007. Tissue heterogeneity of the mammalian mitochondrial proteome. *American Journal of Physiology-Cell Physiology* 2007, 292:2, 689-697.
- [26] Palade.G.E., et al. 1952. The Fine Structure of Mitochondria. *The Anatomical Record*. Vol 114, 427-451.
- [27] Zinser.E., Sperka-Gottlieb.C.D.M., Fasch.E.V., Kohlwein.S.D., Paltauf.F., Daum.G. 1991. Phospholipid synthesis and lipid composition of subcellular membranes in the unicellular eukaryote *Saccharomyces cerevisiae*. *Journal of Bacteriology*, 173, 6, 2026–2034.
- [28] Zinser.E., Daum.G. Isolation and biochemical characterization of organelles from the yeast, *Saccharomyces cerevisiae*. *Yeast*, vol. 11, no. 6, pp. 493–536, 1995.
- [29] Houtkooper.R.H., Vaz.F.M. Cardiolipin, the heart of mitochondrial metabolism. *Cellular and Molecular Life Sciences*, vol. 65, no. 16, pp. 2493–2506, 2008.
- [30] Fawcett.D.W., et al. 1966. *The Cell, Its Organelles, and Inclusion: An Atlas of fine structures*.
- [31] Hoppins.S., et al. 2014. The regulation of mitochondrial dynamics. *Cell Biology*, vol 29, 143.
- [32] Losón.O.C., Song.Z., Chen.H., Chan.D.C. 2013. Fis1, Mff, MiD49, and MiD51 mediate Drp1 recruitment in mitochondrial fission. *Mol Biol Cell*. 2013 Mar; 24(5):659-67.
- [33] Chen.H., Chomyn.A., Chan.D.C. 2005. Disruption of fusion results in mitochondrial heterogeneity and dysfunction.. *J Biol Chem*, 280(28):26185-92.

- [34] Williamson.D. 2002. The curious history of yeast mitochondrial DNA. *Nature Reviews Genetics*, 3, 475-481.
- [35] Anderson.S., Bankier.A.T., Barrell.B.G., de Bruijn.M.H.L., Coulson.A.R., Drouin.J., Eperon.I.C., Nierlich.D.P., Roe.B.A., Sanger.F., Schreier.P.H., Smith.A.J.H., Staden.R., Young.I.G. 1981. Sequence and organisation of the human mitochondrial genome. *Nature*, 290, 457-465.
- [36] Thorsness.P.E., Fox.T.D. 1990. Escape of DNA from mitochondria to the nucleus in *Saccharomyces cerevisiae*. *Nature*, 346, 376-379.
- [37] Thorsness.P.E., Fox.T.D. 1993. Nuclear mutations in *Saccharomyces cerevisiae* that affect the escape of DNA from mitochondria to the nucleus. *Genetics*, 134, 1, 21-28.
- [38] Taanman.J.W. 1999 The mitochondrial genome: structure, transcription, translation, and replication. *BBA Vol 1410;2;103-123*
- [39] Gonczarowska-Jorge.H., Zahedi.R.P., Sickmann.A. The proteome of baker's yeast mitochondria. *Mitochondrion*. 2017;33:15–21.
- [40] Sickmann.A., Reinders.J., Wagner.Y., et al. The proteome of *Saccharomyces cerevisiae* mitochondria. *Proc Natl Acad Sci USA*. 2003;100:13207–12.
- [41] Reinders.J., Zahedi.R.P., Pfanner.N., et al. 2006. Toward the complete yeast mitochondrial proteome: multidimensional separation techniques for mitochondrial proteomics. *J Proteome Res* 2006;5:1543–54.
- [42] Cherry.C., Thompson.B., et al. 2016. A ‘Mitochondria’ Odyssey. *Trends in Molecular Medicine*, 22, 5, 391-403.

- [43] Schmidt.O., Pfanner.N., Meisinger.C. 2010. Mitochondrial protein import: from proteomics to functional mechanisms. *Nature Reviews Molecular Cell Biology*, 11, 655-667.
- [44] Fox.T.D. Mitochondrial protein synthesis, import, and assembly. *Genetics* 2012;192:1203–34.
- [45] Vögtle.F.N., Burkhardt.J.M., Gonczarowska-Jorge.H., et al. 2009. Landscape of submitochondrial protein distribution. *Nat Commun* 2017;8:290.
- [46] Herrmann.J.M., Neupert.W. Protein import into mitochondria. In: Lennarz.W.J., Lane MD (eds). *Encyclopaedia of Biological Chemistry*. 2nd edn. Waltham, MA: Elsevier Inc., 2013;632–6.
- [47] Yamamoto.H., Itoh.N., Kawano.S., et al. Dual role of the receptor Tom20 in specificity and efficiency of protein import into mitochondria. *Proc Natl Acad Sci USA* 2011;108:91–6.
- [48] Martin.J., Mahlke.K., Pfanner.N. Role of an energized inner membrane in mitochondrial protein import. *J Biol Chem* 1991;266:18051–7.
- [49] Gakh.O., Cavadini.P., Isaya.G. Mitochondrial processing peptidases. *BBA-Mol Cell Res* 2002;1592:63–77.
- [50] Bonnefoy.N., Fiumera.H.L., Dujardin.G., et al. Roles of Oxa1-related inner-membrane translocases in assembly of respiratory chain complexes. *BBA-Mol Cell Res* 2009;1793:60–70.
- [51] Chacinska.A., Koehler.C.M., Milenkovic.D., et al. 2009. Importing Mitochondrial Proteins: Machineries and Mechanisms. *Cell*, 138, 4, 628-644.
- [52] Nisoli.E., Cozzi.V., & Carruba.M.O. (2008). Amino acids and mitochondrial biogenesis. *The American journal of cardiology*, 101(11A), 22E–25E.

- [53] Mayr.J.A., et al. 2015. Lipid metabolism in mitochondrial membranes. *J Inherit Metab Dis* 38, 137–144.
- [54] Williams.G.S., Boyman.L., Lederer.W.J. 2015. Mitochondrial calcium and the regulation of metabolism in the heart. *Journal of molecular and cellular cardiology*, 78, 35–45.
- [55] Willems.P.H., Rossignol.R., Dieteren.C.E., Murphy.M.P., Koopman.W.J. 2015. Redox Homeostasis and Mitochondrial Dynamics. *Cell metabolism*, 22(2), 207–218.
- [56] Lill.R., Hoffmann.B., Molik.S., Pierik.A.J., Rietzschel.N., Stehling.O., Uzarska.M.A., Webert.H., Wilbrecht.C., Mühlhoff.U. 2012. The role of mitochondria in cellular iron-sulphur protein biogenesis and iron metabolism. *Biochimica et biophysica acta*, 1823(9), 1491–1508.
- [57] Laura.D., Thomas.S., et al. 2012. Cellular and molecular mechanisms of mitochondrial function. *Best Practice & Research Clinical Endocrinology & Metabolism*, 26, 6, 711-723.
- [58] Chance.B., Schoener.B., Oshino.R., et al. 1979. Oxidation-reduction ratio studies of mitochondria in freeze-trapped samples. NADH and flavoprotein fluorescence signals. *Journal of Biological Chemistry*, 254, 11, 4764-4771.
- [59] Hill.G.E., et al. 2014. Cellular Respiration: The Nexus of Stress, Condition, and Ornamentation, *Integrative and Comparative Biology*, 54, 4, 645–657.
- [60] Wallace.D.C. 2005. A Mitochondrial Paradigm of Metabolic and Degenerative Diseases, Aging, and Cancer: A Dawn for Evolutionary Medicine. *Annual Review of Genetics*, 39:1, 359-407.
- [61] Zhao.R.Z., Jiang.S., Zhang.L., Yu.Z.B. 2019. Mitochondrial electron transport chain, ROS generation and uncoupling. *International Journal of Molecular Medicine*, Vol 44;1;3-15.

- [62] Zelenaya-Troitskaya.O., Perlman.P.S., Butow.R.A. 1995. An enzyme in yeast mitochondria that catalyses a step in branched-chain amino acid biosynthesis also functions in mitochondrial DNA stability. *The EMBO Journal*, Vol 14;13;3268-3276.
- [63] Mayr.J.A., et al. 2015. Lipid metabolism in mitochondrial membranes. *J Inherit Metab Dis* 38, 137–144.
- [64] Brancaccio.D., Gallo.A., Mikolajczyk.M. et al. 2014. Formation of [4Fe-4S] Clusters in the Mitochondrial Iron-Sulphur Cluster Assembly Machinery. *J. AM. Chem. Soc*; 136; 46; 16240-16250.
- [65] Swenson.S.A., Moore.C.M., Marcero.J.R., Medlock.A.E., Reddi.A.R., Khalimonchuk.O. 2020. From Synthesis to Utilization: The Ins and Outs of Mitochondrial Heme. *Cells*. 2020; 9(3):579.
- [66] Rinnerthaler.M., Buttner.S., Laun.P., et al. (2012) Yno1p/Aim14p, a NADPH-oxidase ortholog, controls extramitochondrial reactive oxygen species generation, apoptosis, and actin cable formation in yeast. *P Natl Acad Sci USA*109: 8658–8663.
- [67] Ayer.A., Gourlay.C.W., Dawes.I.W., et al (2014) Cellular redox homeostasis, reactive oxygen species and replicative ageing in *Saccharomyces cerevisiae*. *FEMS Yeast Research*; Vol 14;1;60-72.
- [68] Chiu.J., Dawes.I.W. (2012) Redox control of cell proliferation. *Trends Cell Biol*; Vol 22; 11; P592-601.
- [69] Kwon.Y.W., Masutani.H., Nakamura.H., Ishii.Y., Yodo.J. 2003. Redox Regulation of Cell Growth and Cell Death. *Biol Chem*; Vol 364; P991-996.
- [70] Santos.M.A., Pires.K.M.P., et al. 2012. Redox Imbalance and Pulmonary Function in Bleomycin-induced Fibrosis in C57BL/6, DBA/2 and BALB/c Mice. *Sage Journals*; Vol 40; 5; 731-741.

- [71] Ristow.M., Schmeisser.S. 2011. Extending life span by increasing oxidative stress. *Free Radic Biol Med*; 51;2;327-36.
- [72] Madeo.F., Frohlich.E., Ligr.M., Grey.M., Sigrist.S.J., et al. 1999. Oxygen stress: a regulator of apoptosis in yeast. *J Cell Biol*145: 757–767.
- [73] D'Autreaux.B., Toledano.M.B., et al. 2007. ROS as signalling molecules: mechanisms that generate specificity in ROS homeostasis. *Nat Rev Mol Cell Biol*8: 813–824.
- [74] Zilbermann.I., Maimon.E., Cohen.H., Meyerstein.D. 2005. Redox chemistry of nickel complexes in aqueous solutions. *Chem Rev*; 105;6;2609-25.
- [75] Harman.D. 1956. Free radical theory of aging. *Mutation Research/DNAging*. Volume 275, Issues 3–6, Pages 257-266.
- [76] Balaban.R.S., Nemoto.S., Finkel.T. 2005. Mitochondria, Oxidants, and Aging. *Cell*. Volume 120, Issue 4, Pages 483-495.
- [77] Harman.D. 1972. The Biologic Clock: The Mitochondria? *Journal of the American Geriatrics Society*. Vol 20, Issue 4, 145-147.
- [78] Schriener.S.E., Linford.N.J., Martin.G.M., et al (2005) Extension of Murine Life Span by Overexpression of Catalase Targeted to Mitochondria. *Science*. Vol 308, Issue 5730, 1909-1911.
- [79] Perez.V.I., Remmen.H.V., Bokov.A., et al. 2009. The overexpression of major antioxidant enzymes does not extend the lifespan of mice. *Aging Cell*. Vol 8, Issue 1, 73-75.

- [80] Schaar.C.E., Dues.D.J., Spielbauer.K.K., et al. 2015. Mitochondrial and Cytoplasmic ROS Have Opposing Effects on Lifespan. *PLOS Genetics*. Vol 11, Issue 2, e1004972.
- [81] Leadsham.J.E., Sanders.G., Giannaki.S., Bastow.E.L., Hutton.R., Naeimi.W.R., Breitenbach.M., Gourlay.C.W. 2013. Loss of Cytochrome c Oxidase Promotes RAS-Dependent ROS Production from the ER Resident NADPH Oxidase, Yno1p, in Yeast. *Cell Metabolism*. Volume 18, Issue 2, Pages 279-286.
- [82] Weber.M., Basu.S., Gonzalez.B., et al. 2021. Actin Cytoskeleton Regulation by the Yeast NADPH Oxidase Yno1p impacts Processes Controlled by MAPK Pathways. *Antioxidants*. Vol 10, Issue 2, 322.
- [83] Reddi.A.R., Culotta.V.C. 2013. SOD1 Integrates Signals from Oxygen and Glucose to Repress Respiration. *Cell*. Volume 152, Issues 1–2, Pages 224-235.
- [84] Matangkasombut.O., Buratowski.R.M., et al. 2000. Bromodomain factor 1 corresponds to a missing piece of yeast TFIID. *Genes and Development*. Vol 14, 951-962.
- [85] Bivona.T.G., Quatela.S.E., Bodemann.B.O., Ahearn.I.M., et al. 2006. PKC Regulates a Farnesyl-Electrostatic Switch on K-Ras that promotes its Association with Bcl-Xl on Mitochondria and Induces Apoptosis. *Molecular Cell*. Vol 21, Issue 4, 481-493.
- [86] Bodenmiller.B., Aebersold.R. 2010. Quantitative Analysis of Protein Phosphorylation on a System-Wide Scale by Mass Spectrometry-Based Proteomics. *Methods in Enzymology*. Vol 470, 317-334.
- [87] Vetter.I.R., Wittinghofer.A. 2001. The Guanine Nucleotide-Binding Switch in Three Dimensions. *Science*. Vol 294, Issue 5545, 1299-1304.

- [88] Schmidt, A. and Hall, A. 2002. Guanine nucleotide exchange factors for Rho GTPases: turning on the switch. *Genes & development*. Vol 16, Issue 13, pp.1587-1609.
- [89] Wennerberg K., Rossman.K.L., Der.C.J. 2005. The Ras Superfamily at a glance. *Cell Science at a Glance*. Vol 118, Issue 5.
- [90] Colicelli.J., et al. (2004) Human RAS superfamily proteins and related GTPases. *Science's STKE*, 2004(250), pp.re13-re13.
- [91] Biou.V., Cherfils.J., 2004. Structural principles for the multi-specificity of small GTP-binding proteins. *Biochemistry*, 43(22), pp.6833-6840.
- [92] Crespo.P., León.J. 2000. Ras proteins in the control of the cell cycle and cell differentiation. *Cellular and molecular life sciences : CMLS*, 57(11), 1613–1636.
- [93] Cazzanelli.G., Pereira.F., Alves.S., et al. 2018. The Yeast *Saccharomyces cerevisiae* as a model for understanding RAS proteins and their role in human tumorigenesis. *Cells*. Vol 7; Issue 2; 14.
- [94] Dever.T.E., Glynias.M.J., Merrick.W.C. 1987. GTP-binding domain: Three consensus sequence elements with distinct spacing. *Proc. Natl. Acad. Sci. U.S.A.* 1987;84:1814–1818.
- [95] Bourne.H.R., Sanders.D.A., McCormick.F. 1991. The GTPase superfamily: Conserved structure and molecular mechanism. *Nature*. 1991;349:117–127.
- [96] Walker.J.E., Saraste.M., Runswick.M.J., Gay.N.J. 1982. Distantly related sequences in the alpha- and beta-subunits of ATP synthase, myosin, kinases and other ATP-requiring enzymes and a common nucleotide binding fold. *EMBO J.* 1982;1:945–951.

- [97] Choy.E., Chiu.V.K., Silletti.J., Feoktistov.M., Morimoto.T., Michaelson.D., Ivanov.I.E., Philips.M.R. 1999. Endomembrane trafficking of ras: The CAAX motif targets proteins to the ER and Golgi. *Cell*. 1999;98:69–80.
- [98] Powers S, Kataoka T, Fasano O, et al. Genes in *S. cerevisiae* encoding proteins with domains homologous to the mammalian Ras proteins. *Cell*. 1984;36:607-12.
- [99] DeFeo-Jones.D., Scolnick.E.M., Koller.R., Dhar.R. 1983. Ras-Related gene sequences identified and isolated from *Saccharomyces cerevisiae* . *Nature*. 1983;306:707-9.
- [100] Tamanoi.F. 2011. Ras Signalling in Yeast. *Genes Cancer*. Vol 2; Issue 3; 210-215.
- [101] Kataoka.T., Powers.S., McGill.C., et al. 1984. Genetic analysis of yeast *RAS1* and *RAS2* genes. *Cell*. 1984;37:437-45.
- [102] Toda.T., Uno.I., Ishikawa.T., et al. 1985. In yeast, RAS proteins are controlling elements of adenylate cyclase. *Cell*. 1985;40:27-36.
- [103] Ahearn.I., Zhou.M., Philips.M.R. 2018. Posttranslational Modifications of Ras Proteins. *Cold Spring Harb Perspect Med*. Vol 8; Issue 11; a031484.
- [104] Fujiyama.A., Tamanoi.F. 1990. Ras2 Protein of *Saccharomyces cerevisiae* Undergoes Removal of Methionine at N Terminus and Removal of three amino acid at C Terminus. *J. Biol. Chem*. 1990, 265, 3362-3368.
- [105] L.E.Goodman., S.R.Judd., C.C.Farnsworth., S.Powers., M.H.Gelb., J.A.Glomset., F.Tamanoi. 1990. Mutants of *Saccharomyces cerevisiae* defective in the farnesylation of Ras proteins. *Proc Natl Acad Sci U S A*, 87(24), pp.9665-9669.

- [106] He.B., Chen.P., Chen.S.Y., Vancura.K.L, Michaelis.S., Powers.S. 1991. *RAM2*, and essential gene of yeast, and *RAM1*, encode the two polypeptide components of the farnesyltransferase that prenylates a-factor and Ras proteins. *Proc Natl Acad Sci USA*; 88:11373-7.
- [107] Finegold.A.A., Johnson.D.I., Farnsworth.C.C., 1991. Protein geranylgeranyltransferase of *Saccharomyces cerevisiae* is specific for Cys-Xaa-Xaa-Leu motif proteins and requires the *CDC43* gene product but not the *DPR1* gene product. *Proc Natl Acad Sci USA*; 88:4448-52.
- [108] Cox.A.D., Der.C.J. 2010. Ras history: The saga continues. *Small GTPases* 2010, 1, 2–27.
- [109] Choy.E., Chiu.V.K., Silletti.J., Feoktistov.M., Morimoto.T., Michaelson.D., Ivanov.I.E., Philips.M.R. 1999. Endomembrane trafficking of Ras: The CAAX motif targets proteins to the ER and Golgi. *Cell* 98: 69-80.
- [110] Clark.S.G., McGrath.J.P., Levinson.A.D. 1985. Expression of normal and activated human Ha-ras cDNAs in *Saccharomyces cerevisiae*. *Mol. Cell. Biol.* 1985, 5, 2746–2752.
- [111] Simanshu.D.K., Nissley.D.V., McCormick.F. 2017. RAS Proteins and their Regulators in Human Disease. *Cell*. Vol 170; Issue 1; 17-33.
- [112] Hunter.J.C., Manandhar.A., Carrasco.M.A., Gurbani.D., Gondi.S., Westover.K.D. 2015. Biochemical and structural analysis of common cancer associated K-RAS mutations. *Mol. Cancer Res.* 2015;13:1325–1335.
- [113] Bos.J.L., Rehmann.H., Wittinghofer.A. 2007. GEFs and GAPs: critical elements in the control of small G proteins. *Cell*. 2007;129:865–877.

- [114] Scheffzek.K., Ahmadian.M.R., Kabsch.W., Wiesmüller.L., Lautwein.A., Schmitz.F., Wittinghofer.A. 1997. The Ras-RasGAP complex: structural basis for GTPase activation and its loss in oncogenic Ras mutants. *Science*. 1997;277:333–338.
- [115] Robertson.L.S., Fink.G.R. 1998. The three yeast A Kinases have specific signalling functions in pseudohyphal growth. *Proc Natl Acad Sci USA*. Vol 95; Issue 23; 13783-13787.
- [116] Nikawa.J., Sass.P., Wigler.M. 1987. Cloning and characterization of the low-affinity cyclic AMP phosphodiesterase gene of *Saccharomyces cerevisiae*. *Mol Cell Biol*. 1987;7:3629-36.
- [117] Scaltriti.M., Baselga.J. 2006. The Epidermal Growth Factor Receptor Pathway: A Model for Targeted Therapy. *Clinical Cancer Research*. Vol 12; Issue 18.
- [118] Wee.P., Wang.Z. 2017. Epidermal Growth Factor Receptor Cell Proliferation Signalling pathway. *Cancers (Basel)*. Vol 9; Issue 5; 52.
- [119] Dhanasekaran.N., Premkumar.R.E. 1998. Signaling by dual specificity kinases. *Oncogene*. 1998;17:1447–1455. doi: 10.1038/sj.onc.1202251.
- [120] Fahy.E., Subramaniam.S., Murphy.R.C., Nishijima.M., Raetz.C.R., Shimizu.T., Spener.F., van Meer.G., Wakelam.M.J., Dennis.E.A. 2009. Update of the LIPID MAPS comprehensive classification system for lipids¹. *Journal of lipid research*, 50, pp.S9-S14.
- [121] Fahy.E., Cotter.D., Sud.M., Subramaniam.S. 2011. Lipid classification, structures and tools. *Biochimica et Biophysica Acta (BBA)-Molecular and Cell Biology of Lipids*, 1811(11), pp.637-647.
- [122] Fagone.P., Jackowski.S. 2009. Membrane phospholipid synthesis and endoplasmic reticulum function. *Journal of lipid research*, 50, pp.S311-S316.

- [123] Osman.C., Haag.M., Wieland.F.T., Brügger.B., Langer.T. 2010. A mitochondrial phosphatase required for cardiolipin biosynthesis: the PGP phosphatase Gep4. *The EMBO journal*, 29(12), pp.1976-1987.
- [124] Tamura.Y., Kawano.S., Endo.T. 2020. Lipid homeostasis in mitochondria. *Biological chemistry*, 401(6-7), pp.821-833.
- [125] Achleitner.G., Gaigg.B., Krasser.A., Kainersdorfer.E., Kohlwein.S.D., Perktold.A., Zellnig.G., Daum.G., 1999. Association between the endoplasmic reticulum and mitochondria of yeast facilitates inter-organelle transport of phospholipids through membrane contact. *European journal of biochemistry*, 264(2), pp.545-553.
- [126] Peretti.D., Dahan.N., Shimoni.E., Hirschberg.K., Lev.S. 2008. Coordinated lipid transfer between the endoplasmic reticulum and the Golgi complex requires the VAP proteins and is essential for Golgi-mediated transport. *Molecular biology of the cell*, 19(9), pp.3871-3884.
- [127] Klug.L., Daum.G. 2014. Yeast lipid metabolism at a glance. *FEMS yeast research*, 14(3), pp.369-388.
- [128] Manivannan.S., Metya.S.K., Sadaf.S., Kumar.S., Schwudke.D., Hasan.G. 2013. Altered lipid homeostasis in *Drosophila* *InsP3* receptor mutants leads to obesity and hyperphagia. *Disease models & mechanisms* 6, no. 3 (2013): 734-744.
- [129] Prabhu.A.V., Krycer,J.R., Brown.A.J. 2013. Overexpression of a key regulator of lipid homeostasis, *Scap*, promotes respiration in prostate cancer cells. *FEBS letters*, 587(7), pp.983-988.
- [130] Zweytick.D., Athenstaedt.K., Daum.G. 2000. Intracellular lipid particles of eukaryotic cells. *Biochimica et Biophysica Acta (BBA)-Reviews on Biomembranes*, 1469(2), pp.101-120.

- [131] Wilfling.F., Haas.J.T., Walther.T.C. et al. 2014. Lipid Droplet Biogenesis. *Current Opinions in Cell Biology*. Vol 29; 39-45.
- [132] Wang.C.W. 2015. Lipid droplet dynamics in budding yeast. *Cell. Mol. Life Sci.* 72, 2677-2695.
- [133] Leber.R., Zinser.E., Zellnig.G., Paltauf.F., Daum.G. 1994. Characterization of lipid particles of the yeast, *Saccharomyces cerevisiae*. *Yeast*, 10, pp. 1421-1428.
- [134] Kraemer.N., Guo.Y., Wilfling.F., Hilger.M., Lingrell.S., Heger.K., Newman.H.W., Schmidt-Supprian.M., Vance.D.E., Mann.M., Farese Jr.R.V., Walther.T.C. Phosphatidylcholine synthesis for lipid droplet expansion is mediated by localized activation of CTP:phosphocholine cytidyltransferase. *Cell metabolism*, 14(4), pp.504-515.
- [135] Fei.W., et al. 2011. A role for phosphatidic acid in the formation of supersized. Lipid droplets. *PLoS Genet*, 7.
- [136] Jacquier.N., et al. 2011. Lipid droplets are functionally connected to the endoplasmic reticulum in *Saccharomyces cerevisiae*. *J. Cell Sci.* 124, 2424-2437.
- [137] Choudhary.V., Jacquier.N., Schneider.R. 2011. The topology of the triacylglycerol synthesizing enzyme Lro1 indicates that neutral lipids can be produced within the luminal compartment of the endoplasmic reticulum: Implications for the biogenesis of lipid droplets. *Commun. Integr. Biol.* 4, 781-784 (2011).
- [138] Zanghellini.J., Wodlei.F., von Grenberg.H.H. 2010. Phospholipid demixing and the birth of a lipid droplet. *J. Theor. Biol.* 264, 952-961 (2010).

- [139] Yen.C.L., Stone.S.J., Koliwad.S., Harris.C., Farese Jr.R.V. 2008. Thematic review series: glycolipids DGAT enzymes and triacylglycerol biosynthesis *J Lipid Res*, 49 (2008), pp. 2283-2301.
- [140] Markgraf.D.F., et al. An ER protein functionally couples neutral lipid metabolism on lipid droplets to membrane lipid synthesis in the ER. *Cell. Rep.* 6, 44ñ55 (2014).
- [141] Sorger.D., Daum.G. 2002. Synthesis of triacylglycerols by the acyl-coenzyme A:diacyl-glycerol acyltransferase Dga1p in lipid particles of the yeast, *Saccharomyces cerevisiae*. *J. Bacteriol.* 184, 519ñ524 (2002).
- [142] Thiam.A.R., Forêt.L. 2016. The physics of lipid droplet nucleation, growth and budding. *Biochimica Et Biophysica Acta (BBA)-Molecular and Cell Biology of Lipids*, 1861(8), pp.715-722.
- [143] Gross.D.A., Zhan.C., Silver.D.L. 2011. Direct binding of triglyceride to fat storage-inducing transmembrane proteins 1 and 2 is important for lipid droplet formation. *Proceedings of the National Academy of Sciences*, 108(49), pp.19581-19586.
- [144] Chung.J., Wu.X., Lambert.T.J., Lai.Z.W., Walther.T.C., Farese Jr.R.V. 2019. LDAF1 and seipin form a lipid droplet assembly complex. *Developmental cell*, 51(5), pp.551-563.
- [145] Thoms.S., Debelyy.M.O., Connerth.M., Daum.G., Erdmann.R. 2011. The putative *Saccharomyces cerevisiae* hydrolase Ldh1p is localized to lipid droplets. *Eukaryotic cell*, 10(6), pp.770-775.
- [146] Wilfling.F., Wang.H., Haas.J.T., Krahmer.N., Gould.T.J., Uchida.A., Cheng.J.X., Graham.M., Christiano.R., Fröhlich.F., Liu.X. 2013. Triacylglycerol synthesis enzymes mediate lipid droplet growth by relocalizing from the ER to lipid droplets. *Developmental cell*, 24(4), pp.384-399.

- [147] Listenberger.L.L., Han.X., Lewis.S.E., Cases.S., Farese.R.V., Ory.D.S., Schaffer.J.E. 2003. Triglyceride accumulation protects against fatty acid-induced lipotoxicity. *Proceedings of the National Academy of Sciences*, 100(6), pp.3077-3082.
- [148] Kurat.C.F., Wolinski.H., Petschnigg.J., Kaluarachchi.S., Andrews.B., Natter.K., Kohlwein.S.D. 2009. Cdk1/Cdc28-dependent activation of the major triacylglycerol lipase Tgl4 in yeast links lipolysis to cell-cycle progression. *Molecular cell*, 33(1), pp.53-63.
- [149] Nakamura.N., Banno.Y., Tamiya-Koizumi,K. 2005. Arf1-dependent PLD1 is localized to oleic acid-induced lipid droplets in NIH3T3 cells. *Biochemical and biophysical research communications*, 335(1), pp.117-123.
- [150] Schulz.H. 1991. Beta oxidation of fatty acids. *Biochimica et Biophysica Acta (BBA)-Lipids and Lipid Metabolism*, 1081(2), pp.109-120.
- [151] Bishop.W.R., Bell.R.M. 1988. Assembly of phospholipids into cellular membranes: biosynthesis, transmembrane movement and intracellular translocation. *Annual review of cell biology*, 4(1), pp.579-606.
- [152] Jarc.E., Petan.T. 2019. Focus: Organelles: Lipid droplets and the management of cellular stress. *The Yale journal of biology and medicine*, 92(3), p.435.
- [153] Reggiori.F., Canivenc-Gansel.E., Conzelmann.A. 1997. Lipid remodelling leads to the introduction and exchange of defined ceramides on GPI proteins in the ER and Golgi of *Saccharomyces cerevisiae*. *The EMBO journal*, 16(12), pp.3506-3518.
- [154] Lee.S.J., Zhang.J., Choi.A.M., Kim.H.P. 2013. Mitochondrial dysfunction induces formation of lipid droplets as a generalized response to stress. *Oxidative medicine and cellular longevity*.

- [155] Petan.T., Jarc.E., Jusović.M. 2018. Lipid droplets in cancer: guardians of fat in a stressful world. *Molecules*, 23(8), p.1941.
- [156] Olzmann.J.A., Carvalho.P. 2019. Dynamics and functions of lipid droplets. *Nature reviews Molecular cell biology*, 20(3), pp.137-155.
- [157] Velázquez.A.P., Graef.M. 2016. Autophagy regulation depends on ER homeostasis controlled by lipid droplets. *Autophagy*, 12(8), pp.1409-1410.
- [158] Helle.S.C., Kanfer.G., Kolar.K., Lang.A., Michel.A.H., Kornmann.B. 2013. Organization and function of membrane contact sites. *Biochimica et Biophysica Acta (BBA)-Molecular Cell Research*, 1833(11), pp.2526-2541.
- [159] Novikoff.A.B., Novikoff.P.M., Rosen.O.M., Rubin.C.S. 1980. Organelle relationships in cultured 3T3-L1 preadipocytes. *The Journal of cell biology*, 87(1), pp.180-196.
- [160] Szymanski.K.M., Binn.D., Bartz.R., Grishin.N.V., Li.W.P., Agarwal.A.K., Garg.A., Anderson.R.G., Goodman.J.M. 2007. The lipodystrophy protein seipin is found at endoplasmic reticulum lipid droplet junctions and is important for droplet morphology. *Proceedings of the National Academy of Sciences*, 104(52), pp.20890-20895.
- [161] Wilfling.F., Wang.H., Haas.J.T., Kraemer.N., Gould.T.J., Uchida.A., Cheng.J.X., Graham.M., Christiano.R., Fröhlich.F., Liu.X. 2013. Triacylglycerol synthesis enzymes mediate lipid droplet growth by relocalizing from the ER to lipid droplets. *Developmental cell*, 24(4), pp.384-399.
- [162] Jacquier.N., Choudhary.V., Mari.M., Toulmay.A., Reggiori.F., Schneider.R. 2011. Lipid droplets are functionally connected to the endoplasmic reticulum in *Saccharomyces cerevisiae*. *Journal of cell science*, 124(14), pp.2424-2437.

- [163] Markgraf.D.F., Klemm.R.W., Junker.M., Hannibal-Bach.H.K., Ejsing.C.S., Rapoport.T.A. 2014. An ER protein functionally couples neutral lipid metabolism on lipid droplets to membrane lipid synthesis in the ER. *Cell reports*, 6(1), pp.44-55.
- [164] Fei.W., Wang.H., Fu.X., Bielby.C., Yang.H. 2009. Conditions of endoplasmic reticulum stress stimulate lipid droplet formation in *Saccharomyces cerevisiae*. *Biochemical Journal*, 424(1), pp.61-67.
- [165] Welte.M.A. 2007. Proteins under new management: lipid droplets deliver. *Trends in cell biology*, 17(8), pp.363-369.
- [166] Suzuki.M., Otsuka.T., Ohsaki.Y., Cheng.J., Taniguchi.T., Hashimoto.H., Taniguchi.H., Fujimoto.T. 2012. Derlin-1 and UBXD8 are engaged in dislocation and degradation of lipidated ApoB-100 at lipid droplets. *Molecular biology of the cell*, 23(5), pp.800-810.
- [167] Olzmann.J.A., Richter.C.M., Kopito.R.R. 2013. Spatial regulation of UBXD8 and p97/VCP controls ATGL-mediated lipid droplet turnover. *Proceedings of the National Academy of Sciences*, 110(4), pp.1345-1350.
- [168] Stevanovic,A., Thiele.C. 2013. Monotopic topology is required for lipid droplet targeting of ancient ubiquitous protein 1 [S]. *Journal of lipid research*, 54(2), pp.503-513.
- [169] Ohsaki.Y., Cheng.J., Fujita.A., Tokumoto.T., Fujimoto.T. 2006. Cytoplasmic lipid droplets are sites of convergence of proteasomal and autophagic degradation of apolipoprotein B. *Molecular biology of the cell*, 17(6), pp.2674-2683.
- [170] Zhang.Z., Lanza.E., Kris-Etherton.P.M., Colburn.N.H., Bagshaw.D., Rovine.M.J., Ulbrecht.J.S., Bobe.G., Chapkin.R.S., Hartman.T.J. 2010. A high legume low glycaemic index diet improves serum lipid profiles in men. *Lipids*, 45(9), pp.765-775.

- [171] Klemm.E.J., Spooner.E., Ploegh.H.L. 2011. Dual role of ancient ubiquitous protein 1 (AUP1) in lipid droplet accumulation and endoplasmic reticulum (ER) protein quality control. *Journal of Biological Chemistry*, 286(43), pp.37602-37614.
- [172] Gao.Q., Goodman.J.M. 2015. The lipid droplet—a well-connected organelle. *Frontiers in cell and developmental biology*, 3, p.49.
- [173] Wang.H., Sreenivasan.U., Hu.H., Saladino.A., Polster.B.M., Lund.L.M., Gong.D.W., Stanley.W.C., Sztalryd,C. 2011. Perilipin 5, a lipid droplet-associated protein, provides physical and metabolic linkage to mitochondria [S]. *Journal of lipid research*, 52(12), pp.2159-2168.
- [174] Mason.R.R., Watt.M.J. 2015. Unravelling the roles of PLIN5: linking cell biology to physiology. *Trends in Endocrinology & Metabolism*, 26(3), pp.144-152.
- [175] Goodman.J.M., et al. 2008. The gregarious lipid droplet. *Journal of Biological Chemistry*, 283(42), pp.28005-28009.
- [176] Bosma.M., Minnaard.R., Sparks.L.M., Schaart.G., Losen.M., De Baets.M.H., Duimel.H., Kersten.S., Bickel.P.E., Schrauwen.P., Hesselink.M.K. 2012. The lipid droplet coat protein perilipin 5 also localizes to muscle mitochondria. *Histochemistry and cell biology*, 137(2), pp.205-216.
- [177] Henne.W.M., Reese.M.L., Goodman.J.M. 2018. The assembly of lipid droplets and their roles in challenged cells. *The EMBO journal*, 37(12), p.e98947.
- [178] Tsushima.K., Bugger.H., Wende.A.R., Schaffer.J.E., Abel.E.D. 2012. Lipid Overload in Cardiomyocytes Impairs Mitochondrial Energetics by Altering Mitochondrial Dynamics.

- [179] Picone.P., Nuzzo.D., Caruana.L., Scafidi.V., Di Carlo.M. 2014. Mitochondrial dysfunction: different routes to Alzheimer's disease therapy. *Oxidative medicine and cellular longevity*, 2014.
- [180] Kunkle.B.W., Grenier-Boley.B., Sims.R., Bis.J.C., Damotte.V., Naj.A.C., Boland.A., Vronskaya,M., Van Der Lee.S.J., Amlie-Wolf.A., Bellenguez.C. 2019. Genetic meta-analysis of diagnosed Alzheimer's disease identifies new risk loci and implicates A β , tau, immunity and lipid processing. *Nature genetics*, 51(3), pp.414-430.
- [181] Benador.I.Y., Veliova.M., Liesa.M., Shirihai.O.S. 2019. Mitochondria bound to lipid droplets: where mitochondrial dynamics regulate lipid storage and utilization. *Cell metabolism*, 29(4), pp.827-835.
- [182] Guo.C., Sun.L., Chen.X., Zhang.D. 2013. Oxidative stress, mitochondrial damage and neurodegenerative diseases. *Neural regeneration research*, 8(21), p.2003.
- [183] Boren.J., Brindle.K.M. 2012. Apoptosis-induced mitochondrial dysfunction causes cytoplasmic lipid droplet formation. *Cell Death & Differentiation*, 19(9), pp.1561-1570.
- [184] Lee.S.J., Zhang.J., Choi.A.M., Kim.H.P. 2013. Mitochondrial dysfunction induces formation of lipid droplets as a generalized response to stress. *Oxidative medicine and cellular longevity*, 2013.
- [185] Kelley.D.E., He.J., Menshikova.E.V., Ritov.V.B. 2002. Dysfunction of mitochondria in human skeletal muscle in type 2 diabetes. *Diabetes*, 51(10), pp.2944-2950.
- [186] Civitarese.A.E., MacLean.P.S., Carling.S., Kerr-Bayles.L., McMillan.R.P., Pierce.A., Becker.T.C., Moro.C., Finlayson.J., Lefort.N., Newgard.C.B. 2010. Regulation of skeletal muscle oxidative capacity and insulin signaling by the mitochondrial rhomboid protease PARL. *Cell metabolism*, 11(5), pp.412-426.

- [187] Jarc.E., Petan.T. 2019. Focus: Organelles: Lipid droplets and the management of cellular stress. *The Yale journal of biology and medicine*, 92(3), p.435.
- [188] Schuldiner.M., Bohnert.M. 2017. A different kind of love–lipid droplet contact sites. *Biochimica et Biophysica Acta (BBA)-Molecular and Cell Biology of Lipids*, 1862(10), pp.1188-1196.
- [189] Trendeleva.T.A., Zvyagilskaya.R.A. 2018. Retrograde Signaling as a Mechanism of Yeast Adaptation to Unfavourable Factors. *Biochemistry Moscow* 83, 98–106 (2018).
- [190] Jin.Y., Tan.Y., Chen.L., Liu.Y., Ren.Z. 2018. Reactive oxygen species induces lipid droplet accumulation in HepG2 cells by increasing perilipin 2 expression. *International journal of molecular sciences*, 19(11), p.3445.
- [191] Di Bartolomeo.F., Malina.C., Campbell.K., Mormino.M., Fuchs.J., Vorontsov.E., Gustafsson.C.M., Nielsen.J. 2020. Absolute yeast mitochondrial proteome quantification reveals trade-off between biosynthesis and energy generation during diauxic shift. *Proceedings of the National Academy of Sciences*, 117(13), pp.7524-7535.
- [192] Lasserre.J.P., Dautant.A., Aiyar.R.S., Kucharczyk.R., Glatigny.A., Tribouillard-Tanvier.D., Rytka.J., Blondel.M., Skoczen.N., Reynier.P., Pitayu.L. 2015. Yeast as a system for modelling mitochondrial disease mechanisms and discovering therapies. *Disease models & mechanisms*, 8(6), pp.509-526.
- [193] de Oliveira.G.P., Cortez.E., Araujo.G.J., de Carvalho Sabino.K.C., Neves.F.A., Bernardo.A.F., de Carvalho.S.N., Moura.A.S., Carvalho.L., Thole.A.A. 2014. Impaired mitochondrial function and reduced viability in bone marrow cells of obese mice. *Cell and tissue research*, 357(1), pp.185-194.

- [194] Onal.G., Kutlu.O., Gozuacik.D., Emre.S.D. 2017. Lipid droplets in health and disease. *Lipids in health and disease*, 16(1), pp.1-15.
- [195] Waugh.M.S., Nichols.C.B., DeCesare.C.M., Cox.G.M., Heitman.J., Alspaugh.J.A. 2002. Ras1 and Ras2 contribute shared and unique roles in physiology and virulence of *Cryptococcus neoformans*. The GenBank accession number for the RAS2 sequence of *C. neoformans* H99 is AF294349. *Microbiology*, 148(1), pp.191-201.
- [196] Teixeira.V., Martins.T.S., Prinz.W.A., Costa.V. 2021. Target of Rapamycin Complex 1 (TORC1), Protein Kinase A (PKA) and Cytosolic pH Regulate a Transcriptional Circuit for Lipid Droplet Formation. *International Journal of Molecular Sciences*, 22(16), p.9017.
- [197] Gonzalez.S., Rallis.C. 2017. The TOR signaling pathway in spatial and temporal control of cell size and growth. *Frontiers in cell and developmental biology*, 5, p.61.
- [198] Larabee.R.N., Weisman.R. 2020. Nuclear functions of TOR: Impact on transcription and the epigenome. *Genes*, 11(6), p.641.
- [199] Loewith.R., Hall.M.N. 2011. Target of rapamycin (TOR) in nutrient signaling and growth control. *Genetics*, 189(4), pp.1177-1201.
- [200] Dechant.R., Binda.M., Lee.S.S., Pelet.S., Winderickx.J., Peter.M. 2010. Cytosolic pH is a second messenger for glucose and regulates the PKA pathway through V-ATPase. *The EMBO journal*, 29(15), pp.2515-2526.
- [201] Koch.L.M., Birkeland.E.S., Battaglioni.S., Helle.X., Meerang.M., Hiltbrunner.S., Ibáñez.A.J., Peter.M., Curioni-Fontecedro.A., Opitz.I., Dechant.R. 2020. Cytosolic pH regulates proliferation and tumour growth by promoting expression of cyclin D1. *Nature Metabolism*, 2(11), pp.1212-1222.

- [202] Dechant.R., Saad.S., Ibáñez.A.J., Peter.M. 2014. Cytosolic pH regulates cell growth through distinct GTPases, Arf1 and Gtr1, to promote Ras/PKA and TORC1 activity. *Molecular cell*, 55(3), pp.409-421.
- [203] Devare.M.N., Kim.Y.H., Jung.J., Kang.W.K., Kwon.K.S., Kim.J.Y. 2020. TORC1 signaling regulates cytoplasmic pH through Sir2 in yeast. *Aging Cell*, 19(6), p.e13151.
- [204] Weber.M., Basu.S., González.B., Greslehner.G.P., Singer.S., Haskova.D., Hasek.J., Breitenbach.M., Gourlay.C.W., Cullen.P.J., Rinnerthaler.M. 2021. Actin Cytoskeleton Regulation by the Yeast NADPH Oxidase Yno1p Impacts Processes Controlled by MAPK Pathways. *Antioxidants*, 10(2), p.322.
- [205] Slack, C. 2017. Ras signaling in aging and metabolic regulation. *Nutrition and healthy aging*, 4(3), pp.195-205.
- [206] Rinnerthaler.M., Büttner.S., Laun.P., Heeren.G., Felder.T.K., Klinger.H., Weinberger.M., Stolze.K., Grousl.T., Hasek.J., Benada.O. 2012. Yno1p/Aim14p, a NADPH-oxidase ortholog, controls extramitochondrial reactive oxygen species generation, apoptosis, and actin cable formation in yeast. *Proceedings of the National Academy of Sciences*, 109(22), pp.8658-8663.
- [207] Gimeno.C.J., Ljungdahl.P.O., Styles.C.A., Fink.G.R. 1992. Unipolar cell divisions in the yeast *S. cerevisiae* led to filamentous growth: regulation by starvation and RAS. *Cell*, 68(6), pp.1077-1090.
- [208] Ono.S. 2013. The role of cyclase-associated protein in regulating actin filament dynamics—more than a monomer-sequestration factor. *Journal of cell science*, 126(15), pp.3249-3258.

[209] Zhang.H., Ghai.P., Wu.H., Wang.C., Field.J., Zhou.G.L. 2013. Mammalian adenylyl cyclase-associated protein 1 (CAP1) regulates cofilin function, the actin cytoskeleton, and cell adhesion. *Journal of biological chemistry*, 288(29), pp.20966-20977.

[210] Welte.M.A. 2015. Expanding roles for lipid droplets. *Current biology*, 25(11), pp.R470-R481.